THE PROCEEDINGS OF
THE PHYSICAL SOCIETY

VOL. 57, PART 4 1 July 1945 No. 322

DEFINITIVE EQUATIONS FOR THE FLUID RESISTANCE OF SPHERES

BY C. N. DAVIES,

Industrial Health Research Board, Medical Research Council, London

MS. received 22 January 1945

ABSTRACT. For calculation of terminal velocities it is convenient to express the Reynolds' number, Re, of a moving sphere as a function of the dimensionless group ψRe^2, where ψ is the drag coefficient. The following equations have been fitted by the method of least squares to critically selected data from a number of experimenters :

$$1.\quad Re=\frac{\psi Re^2}{24}-0\cdot00023363(\psi Re^2)^2+0\cdot0000020154(\psi Re^2)^3-0\cdot0000000069105(\psi Re^2)^4$$

for $Re<4$ or $\psi Re^2<140$. This tends to Stokes' law for low values of Re. It is specially suited to calculation of the sedimentation of air-borne particles. The upper limit corresponds to a sphere weighing $1\cdot5$ μg. falling in the normal atmosphere, that is, one having a diameter of 142 μ for unit density.

$$2.\quad \log Re=-1\cdot29536+0\cdot986\,(\log\psi Re^2)-0\cdot046677\,(\log\psi Re^2)^2+0\cdot0011235\,(\log\psi Re^2)^3$$

for $3<Re<10{,}000$ or $100<\psi Re^2<4\cdot5\,.\,10^7$.

Correction for slip in gases should be applied to Stokes' law by the following expression, based on the best results available :

$$1+\frac{l}{a}[1\cdot257+0\cdot400\exp(-1\cdot10a/l)],$$

where the mean free path l is given by $\eta/0\cdot499\sigma\bar{c}$.

This conveniently transforms to the following for the sedimentation of particles in air at pressure p cm. mercury :

$$1+\frac{1}{pa}[6\cdot32\,.\,10^{-4}+2\cdot01\,.\,10^{-4}\exp(-2190ap)].$$

§ 1. INTRODUCTION

A COMMON requirement in the interpretation of experiments is a knowledge of the fluid resistance offered to the motion of spheres; work on viscosity, or involving the sedimentation of dusts or liquid suspensions, can be cited, and there are many other applications. Experiments on this subject have been carried out since the time of Newton and there exists a large bulk of material upon which various empirical equations have been based. None of these, however, is derived quantitatively from selected data, and most suffer from the disadvantage that explicit solution for the terminal velocity of a falling sphere is impossible.

The present attempt provides equations which do not exhibit this defect. It is not possible to deduce a single formula, covering all sizes and speeds, without overburdening it with constants; the wide range which must be covered, for practical reasons, has, therefore, been split into two. The equation covering the lower section tends to Stokes' law, in the limit, and at the same time is accurate for spheres of any size, large compared with the mean free path, and weighing less than 1·5 μg. (diameter 142 μ for unit density) falling freely in normal air; hence it is useful for most problems concerned with air-borne particles and also provides the best available assessment of viscosity experiments. The other equation continues, using logarithms on account of the large range, up to a Reynolds' number equal to 10,000, above which value the interest becomes purely aerodynamical. This region covers all spheres falling through normal air which have masses betwen 1·1 μg. and 0·48 g.

Finally, the effect of slip for motion through gases in the Stokes' law region is discussed in the light of the best available experimental data.

§ 2. THEORETICAL BASIS

A sphere of diameter d moving steadily through a medium of density σ and viscosity η, with velocity v, experiences a resistance force W. Hence, if no other variables are concerned, the problem is summarized by the equation

$$f(d, v, \sigma, \eta, W)=0. \qquad \text{......(1)}$$

By Buckingham's theorem (1914) this can be reduced to

$$f\left(\frac{vd}{\nu}, \frac{8W}{\pi d^2\sigma v^2}\right)=0, \qquad \text{......(2)}$$

where $\nu=\eta/\sigma$ is the kinematic viscosity of the fluid and the factor $8/\pi$ is inserted for conventional reasons. vd/ν is the Reynolds' number, Re, and $8W/\pi d^2\sigma v^2$ is the drag coefficient, ψ. The latter can be regarded as a variable coefficient which must multiply the product of cross-section ($\pi d^2/4$) and dynamic pressure ($\frac{1}{2}\sigma v^2$) in order to yield the resistance: hence the numerical factor.

Convention has established the practice of exhibiting experimental results as graphs of Re against ψ. This is more convenient than plotting the actual measurements, such as velocity and diameter, since, by equation (2), a single curve must be obtained for all possible variations of fluid and sphere, providing the conditions of equation (1) are not transgressed. Also, because Re and ψ are dimensionless, any consistent system of units may be used in the measured quantities without altering their magnitudes. However, if it is desired to use such a curve to derive velocities, indirect procedure is necessary since v occurs in both variables.

This obstacle is avoided by arranging equation (2) thus:

$$f(Re, \psi Re^2)=0, \qquad \text{......(3)}$$

since $\psi Re^2=8W/\pi\sigma\nu^2$, which contains only properties of the fluid. In the case of a sphere rising or falling freely at its terminal velocity we have

$$W=(m-m')g,$$

m being its mass and m' the mass of fluid displaced. Hence if Re is expressed by an equation in ψRe^2, the independent variable involves only the mass of the sphere and the nature of the fluid, so that direct solution for v is possible.

Stokes' law of resistance can be reduced to

$$Re=\psi Re^2/24. \qquad \text{......(4)}$$

This is well established for very small values of *Re*, but it forecasts too low a resistance as *Re* increases. Hydrodynamical equations due to Oseen and Goldstein are valid a little further than that of Stokes, but then yield resistances which are too great. The precise determination of a point at which experiments show these equations to be in error by a definite amount is a matter of difficulty. The equation of Goldstein is cumbersome and apparently little better than that of Oseen, while the latter's suffers from the disadvantage that it leads to a quadratic in *Re* when ψRe^2 is made the independent variable. It is therefore inconvenient to fit an empirical polynomial in ψRe^2 to the experimental results which would tend, as *Re* diminished, to Oseen's expression. For this reason the procedure adopted has been to fit selected observations, by the method of least squares, with a polynomial in ψRe^2 which passes through the origin of a plot of *Re* against ψRe^2 and which has, at the origin, the slope given by equation (4). In other words it tends to Stokes' law as *Re* tends to zero. In order to give a satisfactory fit for *Re* less than 4, a quartic in ψRe^2 has been found necessary; this leaves three coefficients to be determined by least squares, since there is no absolute term and the coefficient of the first-power term is 1/24.

For $Re>4$ a cubic, using the logarithms of the same variables, has been deduced. This contains four numerical constants. It is thus not possible to make it tend to Stokes' law, in the limit, and it must not be used for lower Reynolds' numbers. The upper limit of validity is $Re=10^4$, which is a little beyond the point at which the drag coefficient passes through a minimum. Experimental data at higher Reynolds' numbers are not discussed.

§3. OBSERVATIONS WITH REYNOLDS' NUMBERS LESS THAN 4

The latest determinations are due to Möller (1938) and cover the range $0{\cdot}0507<Re<1{\cdot}603$. His results are corrected for wall effect by Faxén's method, and he was at pains to keep the correction small; it ranges from 0·02% to 0·81%, and the ratio of sphere diameter to the diameter of the vessel is always below 0·02. Schmiedel (1928) covers the range $0{\cdot}053<Re<1{\cdot}493$ and uses the Faxén correction, which varies between 1·1% and 7·7%, the ratio of sphere to tube diameter being between 0·018 and 0·074. Liebster (1927) has results for $0{\cdot}1355<Re<1{\cdot}927$, also evaluated by Faxén's formula. The maximum wall correction is 2·68% and the least 0·21%, with diameter ratios up to 0·0525. Seven results for $2{\cdot}32<Re<4{\cdot}16$ have been used from a series of experiments extending to higher Reynolds' numbers. The diameter ratios were all below 0·0353, and no correction has been applied for wall effect.

The Faxén correction is based upon Oseen's equation, which is increasingly erroneous as *Re* exceeds unity. However, with increasing *Re*, the correction diminishes and is probably quite negligible in this instance. There is no experimental work on wall effect from $Re\gtrsim 2$ until we come to determinations by Lunnon in the region of $Re\gtrsim 10^4$. For a diameter ratio 0·02 at $Re=0{\cdot}4$ the Faxén correction to the drag coefficient is $1\frac{1}{2}$%; at $Re=10^4$ an equation given by Lunnon yields a 1% correction for diameter ratio 0·022. It appears, therefore, that over a very wide region the wall effect may be small and approximately constant.

Use of the Ladenburg formula for wall effect gives a correction which is independent of Reynolds' number. Thus, as the Reynolds' number increases, too great an allowance is made for the increased resistance due to wall effect; experimental data are thereby shifted to show specious agreement with Stokes' law, though coincidence at lower values, which would be genuine, may be impaired. The data of Arnold (1911) show this defect. Many of his determinations involved a large wall correction. Lemin (1931) covered the range $0{\cdot}00028 < Re < 0{\cdot}0053$; he showed, in this region of very low Reynolds' numbers, that the Stokes-Ladenburg formula was valid if the diameter ratio was below 0·06. We are not concerned with Lemin's figures in the present discussion, since their function is the confirmation of Stokes' law, but Arnold has results for $0{\cdot}002 < Re < 1{\cdot}9$. These have been recalculated by Schiller (1932) with the Faxén correction, and we have adopted for use in this paper those having a diameter ratio below 0·06, following Lemin, and within the range $0{\cdot}05 < Re < 0{\cdot}19$.

There remains for consideration the work of Allen (1900). Timing the ascent of air bubbles in aniline and water, he covered a range from $Re = 0{\cdot}009$ up to 25. The results are scattered, relative to modern measurements, and, while of historical importance, do not merit inclusion in our analysis. Some measurements were also done with spheres of paraffin wax rising through aniline for $0{\cdot}554 < Re < 20{\cdot}2$. Drag coefficients calculated from these are consistently high relative to those from the workers previously mentioned, so these figures are likewise ignored.

We are left with determinations due to Möller, Schmiedel, Liebster and Arnold. Computed values of ψRe^2 written in order of Reynolds' number are given in table 1 and number 68 in all. The lower limit of Reynolds' number was selected as 0·05, since below this the failure of Stokes' law is negligible. Möller's figures deviate progressively from those of Schmiedel for $Re > 0{\cdot}2$ in the direction of low resistance. Consistent error of 1% in viscosity determinations, a possibility which Möller states may exist in his own work, could not account for this. Liebster's points, on the whole, lie nearer to Möller's than to those of Schmiedel. The latter has been criticized because of the magnitude of the wall correction applied in some cases (8%), but these individual experiments do not fall out of the general sequence which is established by many having only a 2% correction. Liebster's correction exceeded 2% in only one instance. Möller was careful to keep the correction small because he wished to demonstrate whether experiments conformed more closely to Oseen's law than to Stokes'. His conclusion would have been unconvincing if the correction had been larger than the small difference in question.

There seems to be no reason for weighting the determinations of these four workers unequally; accordingly their observations have been fitted by the method of least squares with the following equation:

$$Re = \psi Re^2/24 - 0{\cdot}00023363\,(\psi Re^2)^2 + 0{\cdot}0000020154\,(\psi Re^2)^3 - 0{\cdot}0000000069105\,(\psi Re^2)^4. \quad \ldots\ldots(5)$$

This, therefore, represents the best available means of calculating terminal velocities for $Re < 4$ or $\psi Re^2 < 140$.

The fit of this equation and the scatter of the observations can be judged by the residuals, shown in table 1, and by the quantities in table 2. Owing to the wide range of Re values (eighty-fold) the residuals would be greater for the higher

Table 1

Author	Re	ψRe^2	Calculated Re	Residuals, v Exp. − Calc.	v^2
1 M	0·0507	1·235	0·0531	$-4 . 10^{-4}$	$16 . 10^{-8}$
2 S	0·0531	1·296	0·0536	−5	25
3 A	0·0538	1·288	0·0533	5	25
4 A	0·0624	1·472	0·0608	16	256
5 A	0·0771	1·873	0·0772	−1	1
6 M	0·0865	2·107	0·0868	−3	9
7 M	0·0882	2·130	0·0877	5	25
8 M	0·1000	2·431	0·0999	1	1
9 M	0·1008	2·453	0·1008	0	0
10 S	0·1008	2·503	0·1029	−21	441
11 S	0·1059	2·610	0·1072	−13	169
12 A	0·1090	2·613	0·1073	17	289
13 L	0·1355	3·292	0·1347	8	64
14 A	0·1450	3·575	0·1461	−11	121
15 A	0·1510	3·625	0·1481	29	841
16 S	0·1515	3·801	0·1551	−36	1296
17 S	0·1537	3·855	0·1573	−36	1296
18 A	0·1570	3·870	0·1579	− 9	81
19 L	0·1600	4·024	0·1640	−40	1600
20 S	0·1636	4·084	0·1664	−28	784
21 M	0·1703	4·213	0·1715	−12	144
22 M	0·1730	4·256	0·1733	− 3	9
23 A	0·1900	4·658	0·1892	8	64
24 M	0·2016	5·004	0·2029	−13	169
25 M	0·2038	5·054	0·2049	−11	121
26 S	0·2437	6·242	0·2515	−78	6084
27 M	0·2687	6·723	0·2702	−15	225
28 M	0·2751	6·776	0·2722	29	841
29 L	0·3160	7·719	0·3086	−26	676
30 S	0·3287	8·470	0·3373	−86	7396
31 M	0·3847	9·779	0·3869	−22	484
32 M	0·3914	9·848	0·3895	19	361
33 S	0·4755	12·490	0·4877	−122	14884
34 S	0·4924	12·933	0·5040	−116	13456
35 S	0·4953	13·043	0·5080	−127	16129
36 L	0·5110	12·663	0·4942	168	28224
37 S	0·5157	13·702	0·5320	−163	26569
38 M	0·5547	14·328	0·5547	0	0
39 M	0·5592	14·416	0·5579	13	169
40 L	0·5660	15·443	0·5948	−288	82944
41 L	0·5680	14·646	0·5662	18	324
42 M	0·6464	16·910	0·6470	− 6	36
43 M	0·6491	17·013	0·6506	− 15	225
44 S	0·6693	18·377	0·6985	−292	85264

Table 1—*continued*

Author	Re	ψRe^2	Calculated Re	Residuals, v Exp. − Calc.	v^2
45 L	0·6810	17·810	0·6787	23	529
46 S	0·7277	20·275	0·7644	−367	134689
47 S	0·7489	19·570	0·7400	89	7921
48 S	0·7640	19·620	0·7418	222	49284
49 M	0·8389	21·996	0·8233	156	24336
50 S	0·9241	26·08	0·9615	−374	139876
51 S	1·005	27·79	1·017	−120	14400
52 S	1·042	28·95	1·055	−150	22500
53 S	1·087	31·13	1·125	−380	144400
54 M	1·169	31·29	1·130	390	152100
55 L	1·242	35·64	1·268	−260	67600
56 L	1·492	40·67	1·425	670	448900
57 S	1·493	42·93	1·494	−10	100
58 M	1·501	41·30	1·444	570	324900
59 L	1·530	42·18	1·471	590	348100
60 M	1·603	45·04	1·551	520	270400
61 L	1·927	56·33	1·896	310	96100
62 L	2·32	70·61	2·315	0	0
63 L	2·53	79·05	2·560	−300	90000
64 L	3·005	96·35	3·053	−480	230400
65 L	3·94	132·54	3·978	−400	160000
66 L	3·94	129·75	3·918	200	40000
67 L	4·07	138·28	4·097	−300	90000
68 L	4·16	139·35	4·118	400	160000

Table 2. Analysis of residuals. Equation (5). $0{\cdot}0507 < Re < 4{\cdot}16$

Author	Number of observations	Σv	Σv^2	Standard error σ	$\overline{Re}$	$\sigma/\overline{Re}$
Möller	21	0·1599	0·00774571	0·0192	0·478	0·040
Schmiedel	21	−0·2213	0·00686963	0·0194	0·559	0·035
Arnold	8	0·0054	0·00001678	0·00145	0·118	0·012
Liebster	18	0·0293	0·01845461	0·031	1·836	0·017
All	68	−0·0267	0·03308673	0·022	0·822	0·027

Reynolds' numbers, although the percentage error in the experiments remained nearly constant. For this reason the standard error for each experimenter is given both alone and also after division by the mean of his Reynolds' numbers.

The curve defined by equation (5) can be seen from the sums of the residuals to lie between the data of Möller and Schmiedel, but a little nearer to those of the former. Liebster's results govern its course at the upper end of the range.

In using this equation it may be noted that the fourth-power term is negligible, as far as the fourth decimal place, for Reynolds' numbers below 0·35. Below 0·11 the cube can be neglected. For the third decimal place the figures are, respectively, 0·6 and 0·25.

In table 3 the differences between Reynolds' numbers from the equation and those calculated by Stokes' law are given. The latter predicts numbers which are too great.

Table 3. The difference between Stokes' law and equation (5)

Re	0·82	0·38	0·15	0·074	0·037
% difference in *Re* (Stokes' law is high)	10%	5%	2%	1%	0·5%

For use in viscosity determinations it would be best on physical grounds, as well as convenient, to work at low Reynolds' numbers so that the cubic and fourth-power terms are negligible. A cubic equation in the kinematic viscosity then results which leads to a solution in which this quantity is given explicitly in terms of the experimentally determined variables.

§ 4. REYNOLDS' NUMBERS BETWEEN 4 AND 10^4

Experiments within this range have been carried out by Liebster (1927), Davies (1939), Wieselsberger (1922, 1923), Lunnon (1928) and Allen (1900). Results due to the last-named are not included. Those obtained with amber spheres, having Reynolds' numbers below 204, yield drag coefficients which are above the general trend of other workers' values and some with steel spheres, with $2304 < Re < 8247$, as computed by Castleman (1926), Wieselsberger (1922, 1923) and the present writer, come out too low. Liebster (1927), however, has obtained different values in some way and shows them well in line with the determinations of Wieselsberger and Lunnon. Schiller (1932) reproduces his figures.

Liebster's own figures for Reynolds' numbers exceeding 1000 have been abandoned since the scatter is great and the trend doubtful, for reasons explained by the author. Seven observations for Reynolds' numbers down to 2·32 are included to provide an overlap with the previous equation. From 1·927 up to 32·6 only Liebster's experiments have been used.

The author's own work was carried out in air with spheres of paraffin wax and small liquid drops; these fall like rigid spheres if not too large. A paper will be published in due course.

The experiments of Wieselsberger consisted of direct drag measurements on spheres suspended in a wind tunnel. All falling within our upper limit have been considered. The same applies to Lunnon's accurate data on spheres falling in water.

Values of log *Re* and log ψRe^2 computed from these various sources are given in table 4. No wall corrections have been attempted since in all cases they would

Table 4

Author	log Re	log ψRe^2	Calculated log Re	Residuals, v Exp. − Calc.	v^2
1 L	0·366	1·849	0·375	−9	81
2 L	0·403	1·898	0·416	−13	169
3 L	0·478	1·984	0·486	−8	64
4 L	0·596	2·122	0·597	−1	1
5 L	0·596	2·113	0·590	6	36
6 L	0·610	2·141	0·613	−3	9
7 L	0·619	2·144	0·615	4	16
8 L	0·669	2·195	0·657	12	144
9 L	0·849	2·452	0·858	−11	121
10 L	0·886	2·485	0·884	2	4
11 L	1·004	2·644	1·006	−2	4
12 L	1·083	2·723	1·066	17	289
13 L	1·106	2·788	1·115	−9	81
14 L	1·165	2·852	1·163	2	4
15 L	1·283	3·027	1·293	−10	100
16 L	1·383	3·150	1·382	1	1
17 L	1·513	3·325	1·508	5	25
18 D	1·591	3·404	1·564	27	729
19 L	1·744	3·659	1·743	1	1
20 D	1·887	3·869	1·886	1	1
21 L	1·918	3·913	1·915	3	9
22 D	2·097	4·196	2·103	−6	36
23 L	2·159	4·274	2·154	5	25
24 D	2·200	4·350	2·203	−3	9
25 D	2·209	4·337	2·195	14	196
26 D	2·213	4·369	2·215	−2	4
27 D	2·263	4·442	2·262	1	1
28 D	2·268	4·449	2·266	2	4
29 L	2·398	4·658	2·398	0	0
30 D	2·515	4·844	2·513	2	4
31 L	2·528	4·850	2·517	11	121
32 L	2·707	5·164	2·706	1	1
33 L	2·786	5·343	2·812	−26	676
34 L	2·843	5·407	2·849	−6	36
35 W	2·898	5·466	2·883	15	225
36 L	2·926	5·535	2·923	3	9
37 D	2·935	5·558	2·936	−1	1
38 W	3·061	5·813	3·080	−19	361
39 D	3·086	5·835	3·092	−6	36
40 Lun.	3·149	5·947	3·154	−5	25
41 W	3·170	5·973	3·168	2	4
42 W	3·267	6·167	3·274	−7	49
43 W	3·324	6·276	3·332	−8	64
44 Lun.	3·364	6·335	3·363	1	1

Table 4—*continued*

Author	$\log Re$	$\log \psi Re^2$	Calculated $\log Re$	Residuals, v Exp.−Calc.	v^2
45 W	3·373	6·386	3·390	−17	289
46 W	3·500	6·583	3·493	7	49
47 W	3·544	6·690	3·548	− 4	16
48 W	3·597	6·780	3·594	3	9
49 Lun.	3·645	6·873	3·641	4	16
50 W	3·721	7·024	3·717	4	16
51 Lun.	3·829	7·241	3·823	6	36
52 W	3·841	7·269	3·837	4	16
53 W	3·924	7·446	3·922	2	4
54 W	4·009	7·627	4·008	1	1
55 Lun.	4·037	7·671	4·029	8	64

probably have been negligible. There are thus 55 observations for $0{\cdot}366 < \log Re < 4{\cdot}037$. These have been fitted by the following polynomial:

$$\log Re = -1{\cdot}29536 + 0{\cdot}986\,(\log \psi Re^2) - 0{\cdot}046677\,(\log \psi Re^2)^2 + 0{\cdot}0011235\,(\log \psi Re^2)^3 \quad \ldots\ldots(6)$$

The residuals are shown in table 4 and the standard errors, etc., in table 5. They relate, in this case, to the logarithms of the Reynolds' numbers.

Table 5. Analysis of residuals (logs). Equation (6). $0{\cdot}366 < \log Re < 4{\cdot}037$

Author	Number of observations	Σv	Σv^2	Standard error
Liebster	26	−0·025	0·002027	0·0088
Davies	11	0·010	0·001021	0·0096
Wieselsberger	13	−0·017	0·001103	0·0091
Lunnon	5	0·014	0·000142	0·0053
All	55	−0·018	0·004293	0·0088

Table 6. Overlap of equations (5) and (6). Liebster's data

Experimental Re	Calculated Re (5)	(6)	Eq. (6)−Eq. (5)
2·32	2·315	2·371	0·056
2·53	2·560	2·606	0·046
3·005	3·053	3·062	0·009
3·94	3·978	3·954	−0·024
3·94	3·918	3·890	−0·028
4·07	4·097	4·102	0·005
4·16	4·118	4·121	0·003

The agreement between the two formulae in the region of overlap is demonstrated in table 6. It is clear that equation (6) can be used down to $Re = 3$ to give values of Re within 1% of those from equation (5).

§ 5. MOTION IN GASES: THE SLIP EQUATION

In the case of a sphere falling through a gas, the density of which is small in comparison, Stokes' law predicts that the terminal velocity will be independent of pressure as a result of the constancy of viscosity, which is accounted for by kinetic theory. When the gas is at a sufficiently low pressure it can no longer be regarded as a continuous medium with respect to the sphere, which then falls more rapidly than hydrodynamic theory would suggest. This is explained as due to slip of the gas at the surface, since the mean free path of its molecules has become comparable with the size of the sphere, and one of Stokes' basic assumptions is violated. Having considered the departure from his law with increasing Reynolds' number it is now proposed to examine results in the other direction.

Knudsen and Weber (1911) carried out experiments with glass spheres 0·389 cm. radius, fixed to a suspended beam, by observing the damping of torsional oscillations in air. They worked from atmospheric pressure down to 0·14 dynes/cm.^{2} and deduced an equation for slip correction the form of which has been retained by all subsequent experimenters:

$$F = 1 + \frac{l}{a}[A + B\exp(-ca/l)]. \qquad \ldots\ldots(7)$$

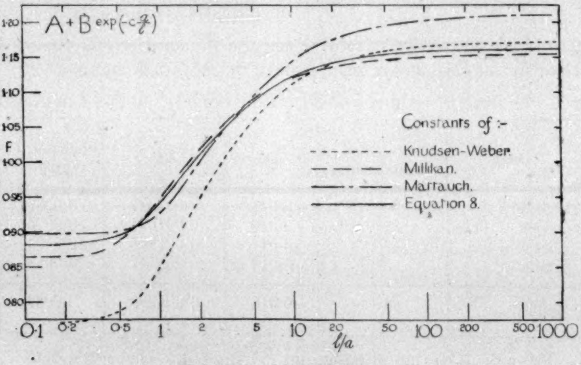

Slip correction for motion in gases.

Here l is the mean free path of the gas molecules, a the sphere radius and A, B and c are constants. The slip factor F multiplies the Stokes' law velocity to yield the true value. Their upper limit of l/a was 188.

Millikan (1920) published his final values for these constants after experimental work on the electronic charge which extended over ten years. His range of l/a was from 0·5 to 134 and the experiments were described in 1923 (b). His value for $A+B$ agreed with that of Knudsen and Weber within 1%, although derived from work with minute oil drops falling freely through air. When the pressure is low ($l/a > 20$) the slip factor becomes equal to

$$1 + \frac{l}{a}(A + B).$$

Millikan considered (1923 a), from a review of capillary-tube experiments by Warburg and by Knudsen, that the coefficient of slip between glass and air was exceedingly close to that between oil and air. At higher pressures, although the total correction diminishes, the exponential term becomes important; under these conditions Knudsen and Weber found a smaller slip correction than Millikan, that is better agreement with Stokes' law, and Millikan suggested this might be due to wall effect.

Mattauch (1925) carried out work on rather similar lines to Millikan, using oil drops in nitrogen. His experiments extended only up to $l/a = 5$ and down to 0·1. In the region immediately adjoining that in which Stokes' law is valid, the slip factor reduces to

$$l + A\,l/a.$$

Mönch (1933) experimented with tobacco smoke, in this region only, and found the same value for A as did Mattauch.

In table 7 the constants determined by these observers are summarized. They have been worked out for the following definition of the mean free path:

$$l = \frac{\eta}{0{\cdot}3502\sigma\bar{c}}.$$

In the figure the function $A + B \exp(-ca/l)$ is plotted for the constants of each experimenter.

Table 7

Author	A	B	c	$A+B$
Knudsen and Weber	0·772	0·400	1·63	1·172
Millikan	0·864	0·29	1·25	1·154
Mattauch	0·898	0·312	2·37	1·210
Mönch	0·90	—	—	—

The derivation of a working equation from these results will now be discussed. Consider first the constant A; this is important at low values of l/a. There is agreement within 4% between Millikan, Mattauch and Mönch, but Knudsen and Weber are very low. Millikan, as mentioned above, gave grounds for suspecting their figure. In addition (1923 a) he derived a relationship between the constant A and a slip coefficient which could be measured by rotating-cylinder experiments, using hydrodynamic theory, at pressures where slip was small. Such experiments, by his associates, provide a good check on his oil-drop figures. Next, there exists no confirmation that the slip coefficient for tobacco-smoke particles in air is the same as for oil in air or nitrogen, which is assumed in comparing the value of Mönch with those of the others. Thus it seems advisable to average the values of A given by Millikan, Mattauch and Mönch, giving double weight to that of the first-named. Knudsen and Weber's figure is rejected. This gives us $A = 0{\cdot}882$.

For high values of l/a we have only the data of Millikan and of Knudsen and Weber to consider, since Mattauch's observations do not extend beyond $l/a = 5$. These agree very well, and the average of their values of $A + B$ is 1·163, giving $B = 0{\cdot}281$.

It now remains to assign a value to the constant c, which is operative for intermediate values of l/a. A single point on the graph will serve to define this, and the point (2,1·010) has been selected, this being the mean of the values of Millikan and Mattauch, approximately in the middle of the latter's range of l/a. Calculation then gives $c=1{\cdot}57$.

Hence the following equation for the slip factor has been obtained:

$$F=1+l/a[0{\cdot}882+0{\cdot}281\exp(-1{\cdot}57\,a/l)]. \qquad \ldots\ldots(8)$$

The relevant part of this equation is shown on the graph for comparison with the figures of the workers from the results of whose labours it has been deduced.

If the latest definition of the mean free path, due to Chapman and Enskog, is used,

$$l=\frac{\eta}{0{\cdot}499\sigma\bar{c}};$$

this transforms to

$$F=1+(l/a)[1{\cdot}257+0{\cdot}400\exp(-1{\cdot}10\,a/l)]. \qquad \ldots\ldots(9)$$

For experiments in air, equation (8) can be put into a convenient form free from kinetic theory constants, since

$$pl=7{\cdot}16\,.\,10^{-4},$$

where p is the pressure in cm. mercury.

$$F=1+(10^{-4}/pa)[6{\cdot}32+2{\cdot}01\exp(-2190\,pa)]. \qquad \ldots\ldots(10)$$

In using these equations it must be remembered that differences in the constants may occur owing to the conditions of reflection of gas molecules being governed by their own nature and by that of the surface of the sphere. Millikan (1923 a) gives a list of values of A for various interfaces and Epstein (1924) discusses the question theoretically.

ACKNOWLEDGMENT

The author wishes to express his appreciation of the encouragement and advice which he has received from Dr. T. Bedford.

REFERENCES

ALLEN, H. S., 1900. *Phil. Mag.* **50**, 323, 519.
ARNOLD, H. D., 1911. *Phil. Mag.* **22**, 755.
BUCKINGHAM, E., 1914. *Phys. Rev.* **4**, 345.
CASTLEMAN, R. A., 1926. *N.A.C.A. Tech. Note*, no. 231.
DAVIES, C. N., 1939. *Thesis and Dissertation* (London).
EPSTEIN, P. S., 1924. *Phys. Rev.* **23**, 710.
KNUDSEN, M. and WEBER, S., 1911. *Ann. Phys., Lpz.*, **36**, 982.
LEMIN, C. E., 1931. *Phil. Mag.* **12**, 589.
LIEBSTER, H., 1927. *Ann. Phys., Lpz.*, **82**, 541.
LUNNON, R. G., 1928. *Proc. Roy. Soc.* A, **118**, 680.
MATTAUCH, J., 1925. *Z. Phys.* **32**, 439.
MILLIKAN R. A., 1920. *Phys. Rev.* **15**, 545; 1923 a. *Ibid.* **21**, 217, 223; 1923 b. *Ibid.* **22**, 1.
MÖLLER, W., 1938. *Phys. Z.* **39**, 57.
MÖNCH, G., 1933. *Phys. Z.* **34**, 77.
SCHILLER, L., 1932. *Handb. Exp. Phys.* **4**, 2 T. 339.
SCHMIEDEL, J., 1928. *Phys. Z.* **29**, 593.
WIESELSBERGER, C., 1922. *Phys. Z.* **23**, 219.
WIESELSBERGER, C., 1923. *Ergeb. Aerodynam. Versuchsanstalt, Göttingen*, **2**, 28.

A PHYSICAL THEORY OF THE SOLAR CORONA*

BY MEGHNAD SAHA, F.R.S.,
University of Allahabad

Lecture delivered 23 *November* 1944 ; *MS. received* 6 *April* 1945

§ 1. INTRODUCTION

NEARLY twenty-five years ago, when the present writer was preparing his paper "On a physical theory of stellar spectra" (Saha, 1921), he had the benefit of very sound advice from the late Professor Alfred Fowler, who allowed him to make free use of his (Fowler's) own unrivalled knowledge of spectroscopy and of stellar spectra. Fowler's remarks on this theory, which to my knowledge were never put in print, may now be disclosed. "The thermal ionization theory", he told me repeatedly, "accounts in a general way for the spectra of normal stars; but there are very important exceptions, e.g. the stars with peculiar spectra, the planetary nebulae ; even in the case of normal stars, the great strength of Balmer lines of hydrogen which persists throughout all stellar classes is a disquieting feature, and in the case of the sun, the peculiar behaviour of helium cannot, in my opinion, be accounted for by the thermal ionization theory at all".

During the past twenty-five years, many of these points raised by Fowler have been taken up by well-known workers : Darwin, R. H. Fowler and Milne, Zanstra, and others in this country, mostly on the theoretical side ; and by Russell, Bowen, Struve, Menzel, Payne, and their co-workers in the U.S.A., Unsöld, Pannekoek, and other workers on the Continent. But the helium problem appears to have remained very much as it was twenty-five years ago. Briefly the problem is as follows : The Fraunhofer spectrum of the sun shows only the lines of such elements as have excitation potentials (energy values of the lower state) between zero and 10 volts ; in the chromospheric spectrum, the lines of ionized elements are relatively stronger, but in no case, helium excepted, do we get lines of stronger excitation than 14 to 15 volts (energy value of upper state). The lines of He do not occur at all in the normal Fraunhofer spectrum, except over disturbed regions, like penumbra of sunspots, but occur prominently in the flash spectrum up to heights of 7500 km. These lines have an excitation potential exceeding 20 volts; but the line of ionized helium $\lambda\,4686$, $\nu=4R\left(\frac{1}{3^2}-\frac{1}{4^2}\right)$ occurs as a prominent but low-level chromospheric line scarcely exceeding 2000 km. in height. This line has an excitation potential of about 75 volts, and one fails to see how such high excitation can exist in the sun, and that too in the lower levels.

The points were repeatedly urged by Professor A. Fowler, and were repeated by myself later on many occasions. and have also received attention from others.

---

* For fuller details, see Saha (1942).

There are certain additional features regarding the occurrence of He lines. I think it was Evershed who first drew attention to the fact that the chromospheric He lines tend to get fainter and ultimately disappear towards the limb. The matter was confirmed by Pannekoek, and Minnaert (1928), and more fully by Perepelkin and Melnikov (1935). The findings of the later workers are represented in table 1 and figure 1, taken from their works.

Table 1

Height (km.)	*E* (erg/cm^3 sec.)	Height (km.)	*E* (erg/cm^3 sec.)
500	39×10^{-6}	4000	60×10^{-6}
1000	125	4500	29
1500	186	5000	12
2000	212	5500	4·3
2500	195	6000	1·3
3000	151	6500	0·3
3500	100	7000	0·1

These results are inexplicable on the ionization theory, or any modification of it. For some time past I have been thinking of another explanation, which I hesitated to put forward on account of its radically heterodox nature. Allowing that He exists in some quantity in the solar atmosphere, it is clear that neither the ultra-violet radiation from the sun nor the thermal conditions existing on the surface of the photosphere is capable of exciting it to luminescence in the way we obtain in the sun. The suggestion regarding their origin is as follows :—First, suppose that α-particles are constantly being produced throughout the solar surface, as a result of some nuclear reaction, and hurled forth through the solar atmosphere. As they pass through the solar gases (mostly hydrogen), they go on ionizing these atoms by collision (as in J. J. Thomson's theory of ionization by collision), and continuously losing energy. When their energy

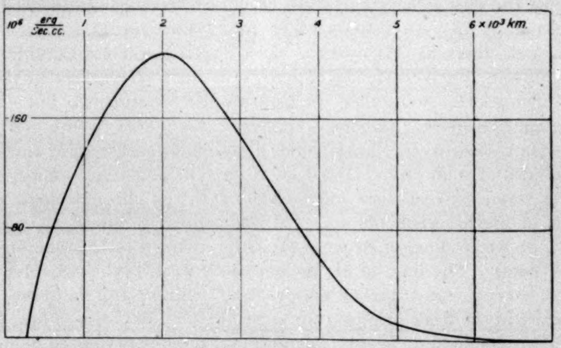

Figure 1.

has sufficiently diminished, they capture an electron in any orbit and become normal or excited He^+. The excited He^+ atom may radiate energy of which only $\lambda 4686$, and possibly the lines $\nu = 4\boldsymbol{R}\left(\frac{1}{4^2} - \frac{1}{m^2}\right)$, are within observable range. The He^+ atom moves forward along the original direction but it goes on losing energy, which is spent, as in the case of He^{++}, in releasing electrons from atoms by collision. When its velocity of motion has sufficiently diminished, it may capture a second electron, and become a normal or excited He atom. The excited He atom gives us the high-level chromospheric He lines.

This phenomenon of capture of electrons by α-particles to form He^+ and He was discovered by Rutherford and Henderson (1923) while studying α-tracks in the cloud-chamber. The capture of the first electron begins to take place when the velocity of the α-particle has fallen to $2\boldsymbol{c}\alpha$, where $\boldsymbol{c}$ is the velocity of light and α the Sommerfeld constant. It may be recalled that $\boldsymbol{c}\alpha$ is the velocity of the electron moving in the first orbit of the H atom. We have $\boldsymbol{c}\alpha = 2{\cdot}18 \times 10^5$ km./sec. We shall have frequently to express velocities in this paper in terms of $\boldsymbol{c}\alpha$ as unit in the form $V = s\boldsymbol{c}\alpha$, where s is a numerical coefficient. In the cloud-chamber, when the α-particle starts to move, it does so with a velocity of the order of $9\boldsymbol{c}\alpha$ (for α-particles of range 11 cm. from Th C″). It goes on producing electrons by collision, and thus gradually loses energy. When the last centimetre is reached, and its velocity has reached $2\boldsymbol{c}\alpha$, corresponding to an energy of 1×10^5 volts, and range of about 0·46 cm., the α-particle begins to capture electrons to an appreciable degree.

But He^+ which is formed by the capture of an electron may again lose this electron by collision with atoms, and again become He^{++} or α-particle. In fact Rutherford (1924) showed that this alternate loss and capture of electrons may occur thousands of times within the last millimetre of the range of the α-particle, but all the time the velocity of the α-particle or of He^+ is falling, and when it reaches $\simeq \boldsymbol{c}\alpha$, He^+ may capture a second electron from cloud-chamber gases and become He. But this may be again ionized to He^+, until ultimately we get He, and the track terminates.

A mathematical theory of this effect has been worked out by Oppenheimer (1928) and by Kramers and Brinkmann (1930), and applied by Jacobsen (1935) for explaining the velocity-range phenomenon in the experiments of Rutherford and Henderson, and also in his own experiments.

The suggestion regarding the occurrence of He^+ and He lines is equivalent to saying that the cloud-chamber phenomena described here occur on the sun on a gigantic scale, but the α-particles are due not to natural radioactive bodies but to some reaction taking place on the solar surface. In the cloud-chamber, some of the α-particles must be capturing electrons in excited orbits, but we cannot observe emission of the characteristic lines of He, owing to their feebleness. The same is true of the capture of electrons from atoms by He^+. But in the sun the captures are sufficiently numerous and the lines emitted are strong enough to be observed in the flash. The explanation accounts in a satisfactory manner, at least qualitatively, for the occurrence of $\lambda 4686$ in some strength in the lower chromosphere (up to a height of 2000 km.), and of the occurrence of He lines in the higher chromosphere up to heights of 7500 km., and also their tendency to disappear towards the limb.

There is only one apparent difficulty in this hypothesis of the origin of He$^+$ and He lines on the sun. According to laboratory observations so far available, the capture of the electron by He^{++} begins to take place when $V \simeq 2c\alpha$, and of the second electron by He$^+$ when $V \simeq c\alpha$. The He atoms in the sun ought therefore to be in motion with velocities of this order. But this is not apparently observed, though the He lines are actually found broad. The explanation is probably to be found in the fact that α-particles originate below the reversing layer, and by the time they come out of this region they have dissipated most of their energy in the process of ionizing other particles by collision.

If these suggestions stand criticism, it should be possible for us to calculate the intensity of ultra-violet emission from the sun due to He$^+$ and He, and estimate their relative importance in promoting ionization of the earth's upper atmosphere.

Alpha-particles are produced in many nuclear reactions, and at this stage it is needless to look for any particular reaction which may be mainly responsible for its production on the solar surface. The question is whether α-particles on such vast scales can be produced on the surface of the sun. If so, what is the subsequent fate of these particles ? Do they sink deep, get doubly ionized in the interior, and contribute to restoring the α-particle balance of the interior of the sun ? These questions may stand for the moment.

It is also worthy of notice that though the visible lines of He are not usually found in the Fraunhofer spectrum, Babcock (1934) records λ10830, which is $1s\,2s\,^3S - 1s\,2p\,^3P$ as a faint absorption line in the infra-red part of the Frauenhofer spectrum. This line requires for its production as absorption line some accumulation of He in the $1s\,2s$ state, which is metastable. This indicates that He exists in some strength in the reversing layer in the normal $1s^2$ and $1s\,2s$ states, but not in the $1s\,2p$ or any higher state. The finding is not, in my opinion, antagonistic to the hypothesis of formation of He in the solar atmosphere out of α-particles.

It is obvious that the hydrogen atmosphere of the sun may also originate, at least partly, in the same way, for the proton is also a most frequent product of nuclear reactions. But a hydrogen atom once formed by the capture of an electron by the proton in the first or, better, in the second orbit can be sustained by radiation pressure, so its career should be fundamentally different from that of the He atom.

It is the belief of the present author that many outstanding problems of the solar and stellar atmospheres, such as prominences, spots, flares giving rise to radio fade-outs, may find their explanation in nuclear reactions taking place more vigorously on limited parts of the surface. It is quite probable that nuclear reactions of the type considered take place more vigorously in the interior, as shown by Bethe (1939) and Gamow (1939), but the probability of their occurrence on the surface on a reduced scale cannot be excluded. For example, it has been found that the He line λ5876 occurs as an absorption line in the neighbourhood of disturbed areas, namely, penumbrae of spots. Probably nuclear reactions producing particles are the cause of formation of such disturbed regions, and reactions are much more vigorous than on the normal surface, and a temporary He atmosphere sufficient to give us D_3 in absorption may be formed in these regions.

§ 2. THE PROBLEM OF THE SOLAR CORONA

Extraordinary interest, in spite of the war, has been aroused in recent years in the problems of the outermost part of the solar atmosphere (inner and outer corona) by the work of Edlén (1942) on the identification of coronium lines. The story of this identification has been told by Russell (1941), by Swings (1943), and by Edlén himself in an exhaustive memoir (1942), and need not be repeated here. It appears to have been conclusively proved that most of the coronal lines are due to atoms of Fe, Ni and Ca which have lost a large number of their outer electrons, sometimes amounting to as many as fifteen or sixteen. The details of this identification, as far as required for our purpose, are given in table 2.

Table 2*

Wave-length (A.)	Intensity		Identification		Ionization potential (ev.)
	Grotrian	Lyot	Ion	Transition	
3328·1	1·0		Ca XII	${}^2P_{3/2}$–${}^2P_{1/2}$	589
3388·10	16		Fe XIII	${}^3P_2$–${}^1D_2$	325
3454·13	2·3				
3600·97	2·1		Ni XVI	${}^2P_{1/2}$–${}^2P_{3/2}$	455
3642·87			Ni XIII	${}^3P_1$–${}^1D_2$	350
3800·77					
3986·88	0·7		Fe XI	${}^3P_1$–${}^1D_2$	261
4086·29	1·0		Ca XIII	${}^3P_2$–${}^3P_1$	655
4231·4	2·6		Ni XII	${}^2P_{3/2}$–${}^2P_{1/2}$	318
4311·5					
4359					
4567	1·1				
5116·03	4·3	2·6	Ni XIII	${}^3P_2$–${}^3P_1$	350
5302·86	100	120	Fe XIV	${}^2P_{1/2}$–${}^2P_{3/2}$	355
5694·42		1·5			
6374·51	8·1	28	Fe X	${}^2P_{3/2}$–${}^2P_{1/2}$	233
6701·83	5·4	3·3	Ni XV	${}^3P_0$–${}^3P_1$	422
7059·62		4			
7891·94		29	Fe XI	${}^3P_2$–${}^3P_1$	261
8024·21		1·3	Ni XV	${}^3P_1$–${}^3P_2$	422
10746·80		240	Fe XIII	${}^3P_0$–${}^3P_1$	325
10797·95		150	Fe XIII	${}^3P_1$–${}^3P_2$	325

* Taken from an article by Swings (1943).

As there appears to be no way of denying the accuracy of the identification, the astrophysicist is faced with a number of problems of a unique type, which may be enumerated as follows :

(1) What is the physical process giving rise to such highly charged ions ?

(2) How can these highly charged ions, once produced, maintain their charge in the solar atmosphere ?

(3) To explain the other characteristics of these lines noted by Lyot (1939) and in the eclipse expeditions, namely, the great breadth of these lines towards their base, sometimes amounting to 1 A., which gradually diminishes outwards, the intensity variations of these lines, etc., along with phases of solar activity.

These may be called "Coronium problems", in contrast to the second set of problems now to be discussed which may be called the "Corona problems". The two sets of problems must be discussed together as they are complementary. The coronium lines are found to occur in the "Inner corona"—which extends from beyond the top of the chromosphere (height, 14,000 km.), sometimes to a distance of about 10′ ($4{\cdot}4 \times 10^5$ km.) from the photosphere. The inner corona shows, besides the coronium lines, a continuous spectrum, which, though nearly a million times fainter, is of the same type as the photospheric spectrum, but with the Fraunhofer lines blurred out. In the outer corona, however, the coronium lines disappear, but the Fraunhofer lines reappear in its continuous spectrum.

The continuous spectrum of the corona has received attention from a number of workers, namely, Minnaert (1930), Grotrian (1933, 1934), and several others. They have proved that it is due to the Rayleigh scattering of photospheric light by an atmosphere of electrons as suggested by Schwarzschild nearly thirty years ago. From the variation of intensity of the coronal light with distance from the photosphere, it is possible to estimate the electron density at different heights, and the figures for a mean corona are reproduced in table 3.

Table 3. Electron density at various heights in the corona*

h (minutes of arc)	*N*	*h* (minutes of arc)	*N*
0·00	$4{\cdot}58 \times 10^8$	22·4	$1{\cdot}79 \times 10^6$
0·48	3·11	25·6	1·35
0·96	2·29	28·8	1·10
1·6	1·56	32·0	$9{\cdot}13 \times 10^5$
3·2	$7{\cdot}04 \times 10^7$	40·0	6·32
4·8	3·84	48·0	5·12
6·4	2·38	64·0	3·81
9·6	1·11	80·0	2·49
12·8	$6{\cdot}13 \times 10^6$	112·0	1·63
16·0	3·73	144·0	1·10
19·2	2·50		

* Taken from Unsöld's *Sternatmosphäre*, 1939, chap. 17.

The great difficulty has been to find the source of the electrons constituting the corona. They cannot arise from thermal or photoelectric ionization of solar atoms, as we have then to postulate in coronal heights the existence of a comparable concentration of atoms and ions, which is impossible on dynamical grounds. The best hypothesis appears to be that of Minnaert (1930), and may be given in his own words : "Anderson (1926) has shown that the corona cannot be in equilibrium if the ordinary physical laws are valid. Instead of assuming, as he does, that very hypothetical laws must be applied, we may attempt to account for the corona by assuming that it really is not in equilibrium, and that its particles are continuously being projected towards space."

According to Grotrian (1934), the continuous spectrum of the scattered rediation from the *inner corona* shows depressions in regions corresponding to chief Fraunhofer absorption lines, but amounting in width to about 100 A., but the lines reappear in the outer corona. He sought to explain the first observation by the hypothesis that the electrons in the inner corona are moving outwards with velocities of the order of 4000 km./sec. According to Moore (1934), the velocity of the coronal streamers (electrons) amounts to 20 to 30 km./sec. These figures probably refer to the outer corona.

Many investigators, including Edlén himself, have sought to explain the occurrence of coronium lines on a temperature basis. The arguments are two-fold :

(1) The coronal lines are, according to measurements of Lyot, quite broad, of the order of 1 A., and if the width be due to Maxwellian motion of the emitting particles, the temperature ought to be $2{\cdot}34 \times 10^6$ °C. This temperature is sufficient to produce the required amount of ionization of the Fe and other atoms.

It is, however, difficult to think of any physical mechanism by which such high temperatures can be produced all over the outer layers of the sun. "Temperature" always means some equilibrium condition, and possibly a small black-body, placed at the coronal heights, would not show a higher temperature than 3000 to 4000° C. We may, however, have high local temperatures over limited regions, as in the case of a rocket burst in our own atmosphere, where we may have a small region around the rocket in which very high temperatures prevail for a short period of time. Several workers have hinted that the production of highly stripped iron, nickel and calcium ions responsible for the emission of coronium lines may be due to the bombardment of the solar atmosphere by meteoric matter in the way imagined by Lindemann and Dobson for explaining meteoric flashes in the earth's atmosphere. But the essence of the Lindemann-Dobson theory is that the meteor, striking the earth's atmosphere with a velocity ranging between 7 and 26 km., drives before it the whole column of air in its path, which is heated by adiabatic compression to a temperature sufficient to bring meteoric matter to luminescence. Lindemann and Dobson found that the gas pressure at the heights where the meteor strikes should be far larger than could be concluded from meteorological considerations. In the sun, the meteoric matter would fall with a velocity of 622 km./sec., but would probably get vaporized long before it reached the chromosphere, and even if some fragments escaped vaporization, the amount of matter in its path would be far too small for production of high temperatures according to the Lindemann-Dobson process. For the meteoric matter which vaporized, the atoms would be rushing with velocities of the order of 622 km./sec. into the solar atmosphere. The effect on these atoms may be obtained by supposing them to remain at rest, and allowing the solar atoms to rush past them with velocities of the order of 622 km./sec. As far as free and bound electrons are concerned, this is equivalent to bombarding the atoms with electrons having an energy of $\simeq 10$ volts, which is not sufficient even to tear the outermost electrons from the meteoric atom. As far as the nuclei of solar atoms are concerned, we need take only H nuclei. Their energy is of the order of 5000 volts, and such particles can tear out only one or two outer electrons at each encounter. The meteoric atoms can be deprived of 10 to 14 electrons only when they plunge very deep into the sun, but not at coronal heights. Further, Waldmeier (1938) has shown that the contour of the width curve of the coronal lines as found by Lyot can also be explained on the supposition that the emitters of coronal lines are streaming outwards or inwards with a velocity of 60 km./sec. Lyot (1934) has further found that the width is largest when the emitters are nearest the sun's limb, and becomes narrower as the height increases. This, combined with Waldmeier's suggestion, shows that the emitters of coronal lines are streaming out of the sun with velocities which go on diminishing as greater heights are reached. The meteoric flash theory is not therefore sufficient to explain either the high ionization or the increasing width of coronal lines towards the solar limb, as actually found by Lyot and Waldmeier (1944).

The writer (Saha, 1942) has ventured to suggest that the Fe and other ions responsible for the emission of the coronium lines are due to some nuclear process identical with or akin to that of nuclear fission, discovered by Hahn and Strassemann in 1939. The story of this discovery may be read in several excellent reports on the subject (Livingston, 1941; Walke, 1941), but the facts necessary for astrophysical purpose may be briefly described. It was found by Hahn and Strassemann that when heavy nuclei like ^{238}U, ^{235}U, ^{232}Th, ^{229}Pa are bombarded by neutrons, fast or slow, they break up according to the scheme (for ^{235}U) (figure 2):

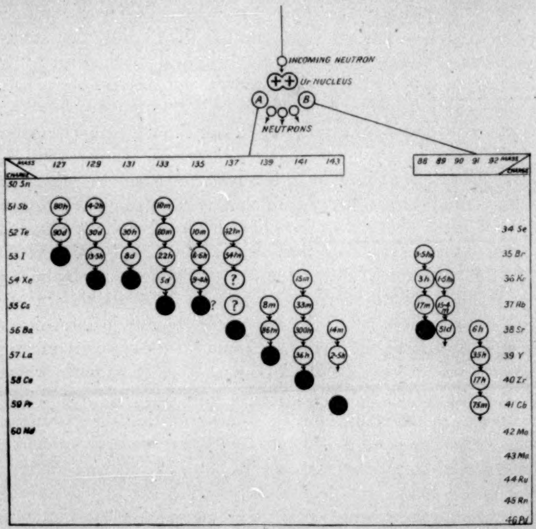
INCOMING NEUTRON
Ur NUCLEUS
A
B
NEUTRONS
MASS
CHARGE
127
129
131
133
135
137
139
141
143
88
89
90
91
92
50 Sn
51 Sb
52 Te
53 I
54 Xe
55 Cs
56 Ba
57 La
58 Ce
59 Pr
60 Nd
34 Se
35 Br
36 Kr
37 Rb
38 Sr
39 Y
40 Zr
41 Cb
42 Mo
43 Ma
44 Ru
45 Rh
46 Pd
80h
90d
4·2h
30d
13·5h
30h
8d
10m
60m
22h
5d
10m
6·6h
9·4h
?
12m
54m
?
?
8m
86m
15m
33m
300h
36h
14m
2·5h
3·5h
3h
17m
1·5h
15·4m
51d
6h
3·5h
17h
75m

Figure 2.

$$^{235}_{92}\mathrm{U} + {}^{1}_{0}\mathrm{n} = {}^{M_1}_{x}\mathrm{A} + {}^{M_2}_{y}\mathrm{B} + Z\,.\,{}^{1}_{0}\mathrm{n} + Q.$$

${}^{M_1}_{x}$A and ${}^{M_2}_{y}$B are nuclei having respectively the charge numbers x and y, and mass-numbers M_1, M_2 ; Z is the number of neutrons, generally 3 or 4, which evaporate in the process (Szilard and Zinn, 1942) ; Q is the energy evolved in the process.

$$x + y = 92, \quad M_1 + M_2 = 236 - Z.$$

The A products have been found to have x varying from 46 to 60, the B products have y varying from 35 to 46. The reaction is exothermic, as can be seen from mass relationships, and Q is $\simeq 200$ mev. for binary fission, and it is distributed, according to the law of conservation of energy and momentum, between A and B, A receiving $QM_2/(M_1+M_2)=Q_A$ and B receiving $QM_1/(M_1+M_2)=Q_B$, respectively.

Neither the A nor the B products are stable on account of the high proportion of neutrons, but each has to emit 3 or 4 β-rays successively, till they are reduced to stable forms, as might be illustrated in the chain processes

A	Xe→	β Cs→	β Ba→	β La→	β Ce (stable)
$M=141$	54	55	56	57	58
		15^m	33^m	300^h	36^h
B	Sr→	β Y→	β Zr→	β Nb→	β Mo (stable)
$M=91$	38	39	40	41	42
		8^h	38^m	17^h	75^m

The fission process is beautifully illustrated in the Wilson-chamber photographs taken by Corson and Thornton (1939), Böggild *et al.* (1941) in Prof. Bohr's laboratory before Denmark was invaded.

What is important for our purpose is the high energy with which the fission fragments are thrown out in the reaction. To take an example : If $x=54$, $M_1=141$, $y=38$, $M_2=91$, $Z=4$, we have $Q_A \simeq 80$ mev. and $Q_B \simeq 120$ mev. The velocities corresponding to these energies are $V_A \simeq 4{\cdot}7\,c\alpha$, $V_B \simeq 7{\cdot}1\,c\alpha$. These velocities are much larger than the orbital velocity not only of the outer electrons of the stable products, but also of many of their inner electrons. Bohr (1941), Knipps and Teller (1941) and Lamb (1941) have pointed out that as soon as the fission fragments are produced in any medium, they lose most of their outer electrons and can retain only those of their inner electrons whose orbital velocities are larger than, or comparable to, their own velocity. The fission particles therefore start as heavily ionized ones bereft of a large number of their outer electrons, and Bohr and Wheeler (1939) quote a Russian worker, Perlov (?), as having experimentally proved that the charge may be as high as 20.

The presence of Fe or Ni amongst the fission fragments has not yet been reported with definiteness, but considerations of energy and probability do not rule them out. Nishina and his co-workers (1939) have shown that the probability of a symmetric fission in which one fragment is much larger than the other increases with the energy of the bombarding neutrons. Further, ternary and quarternary fission are allowed by considerations of energy and probability, and Q in some cases may be as high as 250 mev., which is larger than the 200 mev. maximum energy evolved in the binary fission process. It may be supposed that as a result of either of such processes taking place in the sun, smaller fragments are produced which, after a number of β-emissions, ultimately stabilize as nuclei of elements from Ca to Ni and are emitted with energies of the order of 60 mev. It is gratifying to note that after the writer had postulated such a process for the origin of coronal emitters, ternary and quarternary fissions were reported by Lark-Horowitz (1941) and theoretically treated by Present (1941).

It can be shown that if one of the heavy fission-elements undergoes a ternary or a quaternary fission, the fragments, after a number of β-emissions, will be elements from Ca to Ni (the limit on both sides is rather elastic), and they will be emitted with an energy of approximately 60 mev., i.e., in the case of Fe atoms with a velocity of 6·4 $c\alpha$. Let us now turn to table 4, which shows the velocity of the outermost electrons of iron, and its ions. We find that the 2 p-electron of Fe XVII has a velocity of 9·6 $c\alpha$. This will therefore be retained, but if we take Fe XVI, the 3s-electron is found to have a velocity of 6 $c\alpha$. We can therefore conclude that in a fission process of the type envisaged here, occurring in the reversing layer, the iron atoms which normally have the electron composition $1s^2\ 2s^2\ 2p^6\ 3s^2\ 3p^6\ 3d^6\ 4s^2$ will have lost the outer 15 electrons, namely, $3s\ 3p^6\ 3d^6\ 4s^2$, and will start as Fe XVI with the electron composition $1s^2\ 2s^2\ 2p^6\ 3s$. It will now be interesting to follow the physical processes to which such a highly charged ion produced anywhere in the sun can give rise, as it passes through the solar atmosphere. These are :

Table 4.* Stripped iron ions and their electron structure, etc.

Ion	Electron structure	Fundamental state	Value of the lowest terms in volts	$\sqrt{\frac{\text{I.P.}}{13 \cdot 54}} = \frac{z_i}{n}$	Remarks.
$_{26}$Fe I	$..3d^6 4s^2$	$^5D_4$	7·83	0·76	
Fe II	$..3d^6 4s$	$^6D_{9/2}$	16·5	1·10	Forbidden lines found in η Carinæ. Bowen (1936).
Fe III	$..3d^6$	^5D	30·48	1·50	
Fe IV	$..3d^5$	^6S	56·8	2·05	
Fe V	$..3d^4$	$^5D_0$	..	(2·37)†	Bowen (1940) gives metastable lines found in nebulae. D. Kundu thinks that some of these lines may occur in the corona.
Fe VI	$..3d^3$	$^4F_{3/2}$	..	(2·69)	,, ,,
Fe VII	$..3d^2$	^3F	..	(3·01)	,, ,,
Fe VIII	$..3d$	^2D	150·4	3·33	$^2D_{3/2}$–$^2D_{5/2}$ = 1875 cm.$^{-1}$ No metastable line available.
Fe IX	$..3p^6$	$^1S_0$	233·5	4·15	No metastable state.
Fe X	$..3p^5$	^2P	261	4·39	λ 6374·75 $^2P_{3/2} \leftarrow {}^2P_{1/2}$.
Fe XI	$..3p^4$	^3P	288·9	4·62	λ 7892.
Fe XII	$..3p^3$	^4S	320	(4·91)	Has no metastable line in the available range.
Fe XIII	$..3p^2$	$^3P_{012}$	346	(5·06)	10746·80. 10797·95.
Fe XIV	$..3p$	^2P	373	5·25	λ 5303 $^2P_{1/2}$–$^2P_{3/2}$.
Fe XV	$..3s^2$	$^1S_0$	454	5·79	No metastable state.
Fe XVI	$..3s$	$^2S_{1/2}$	487	5·99	,, ,,
Fe XVII	$..2p^6$	$^1S_0$	1259·7	9·65	,, ,,

* Reproduced from the author's paper, "On a physical theory of the solar corona", *Proc. Nat. Inst. Sci.* **8,** 99 (1942).

† Parentheses ( ) denote that the value is extrapolated.

(*a*) ***Ionization by collision.*** The ion goes on knocking electrons and nuclei from the atoms which it encounters in its way, just as an α-particle does when it is projected in a cloud-chamber. In this process, the ion continuously loses energy, and it is possible to calculate its *range* with the aid of the Bohr-Bethe formula (1936), provided we assume that the solar atmosphere consists mainly of H atoms with few C and N atoms (as given by Menzel). The range is found on certain plausible assumptions to be $R_{\mathrm{H}} \simeq 1{\cdot}31 \times 10^{21}$ H atoms/cm^2 for Fe XVI projected with a velocity of $6{\cdot}4\ c\alpha$.

We can draw very important conclusions from this calculation. Nuclear processes giving rise to Fe XVI, or similar highly charged iron or other ions may occur throughout the whole *solar interior*, but most of such particles have no chance of ever passing out of the solar atmosphere. Most of them will stop dead earlier. If the number of H-particles in the reversing layer is taken to be $1{\cdot}8 \times 10^{22}$/cm^2 (Unsöld, 1939), R_{H} is far less than this number, and it is obvious that only those fission particles which are produced rather high up in the "reversing layer" have a chance of escaping through the chromosphere and emerging into the inner corona.

(*b*) ***Possibility of the further loss of an electron by the ion.*** The Fe ion may itself lose a further electron by collision with atoms, but the probability of this event vanishes when the velocity of the ion reaches a certain limiting value. For the solar atmosphere, the limiting velocity, under certain plausible assumptions, is $V_e \simeq c\alpha . z$, where z is the net charge on the ion. The Fe XVI ion cannot therefore lose any further electron.

(*c*) ***Capture of electrons by the ion.*** The Fe XVI may capture an electron from any one of the atoms in its path, or even a free electron, and become Fe XV: $1s^2\,2s^2\,2p^6\,3s^2$ (normal) or $3s\,nx$, where nx is a higher orbit. The probability of the capture at first increases as the velocity of the ion diminishes. When the capture is in an excited orbit, the iron is expected to execute one or more quantum transpositions, emitting X rays, and ultimately we shall have normal Fe XV. This has no metastable levels, so no visible radiation can be emitted by Fe XV.

The Fe XV ion will now pass through the same career as Fe XVI, but the electron composition of the next ion formed is $1s^2\,2s^2\,2p^6\,3s^2\,3p$, and hence we have two metastable levels, ${}^2P_{1/2}$ and ${}^2P_{3/2}$. The strong coronal line λ5303 is due to the forbidden transition ${}^2P_{3/2} \rightarrow {}^2P_{1/2}$. The emission of λ5303 necessarily indicates that some amount of X radiation due to the allowed transition $3s^2\,nx \rightarrow 3s^2\,3p$, $\lambda \simeq 80$A., is also being emitted. The capture can take place at all velocities of Fe XV, from $s = 6$ down to $s = 0$, but the formula of Brinkmann and Kramers has been worked out only for capture in S-orbits and for high velocities of the ion. It has still to be worked out for small s and for capture in p-orbits; hence at this stage it is not possible to give any quantitative estimate. The next ions from Fe XIII to Fe X are all formed by successive capture of electrons from the solar atoms or of free electrons in the solar atmosphere, and thus the $3p^x$-shell is formed ($x = 1$ to 5), which gives us the coronal radiation given in table 2.

The possibility of any one of the Fe XIV to Fe X ions emerging out of the chromosphere to the coronal heights therefore depends upon : (i) the probability of a fission of the type mentioned above taking place in the sun, (ii) the region where the fission takes place. Bohr and Wheeler (1940) have shown that only heavy nuclei like ^{238}U, ^{235}U, ^{232}Th, ^{229}Pa are capable of fission. These can occur in the solar interior as well as in the reversing layer, but ions formed in the interior are stopped dead earlier, and only such as originate in the reversing layer can escape to coronal heights. The origin of the coronium emitters is therefore to be found in the upper part of the reversing layer.

At this stage some of the probable doubts and objections in the mind of the reader may be anticipated :

(1) Have we in the sun's atmosphere or interior sufficient U or Th atoms, which alone have been shown by Bohr and Wheeler (1939) to be capable of fission by neutron-bombardment ?

U has not yet been traced in the sun, probably owing to the extreme complexity of its spectrum. But the presence of lines of singly-ionized Th has recently been definitely established by Moore and Babcock (1943).

(2) Why should we get only Fe, Ni and Ca in the corona, and not any of the contiguous elements, say Co, Mn, or Cu, A or K?

An investigation carried out by D. Kundu (1942) at Calcutta shows that Fe, Ni and Ca are spectroscopically better suited for identification than any other elements in this group excepting Co. But Co is probably respresented by a faint line in the corona, λ4359, which Kundu attributes to Co XV. Subsequently, through the courtesy of the Astronomer Royal of England, the writer has been able to have access to a copy of Edlén's paper (1942) in which the same opinion has been expressed.

But even if Co, Mn and other elements of the group are subsequently found to be represented by some of the fainter coronal lines not yet identified, it is clear that these elements are represented far less strongly than Fe, Ni and Co. Edlen has tried to connect the phenomenon with the so-called cosmic frequency of elements. But probably the real reason is that in a nuclear process there is a greater probability of the occurrence of even-numbered atomic elements than of odd-numbered ones. Each one of the former is represented by four or more isotopes, but the latter generally (for example, Sc, V, Mn and Co) by a single isotope. There is, therefore, a greater chance of fission products ultimately transforming themselves after β-emissions to Fe, Ni and Ca than to Co, Mn and Sc.

(3) Why do we not observe the forbidden lines of Fe ions from Fe IX to Fe II, and of the corresponding ions of Ni, amongst the coronium-lines ?

Fe IX has no metastable state and Fe VIII has the composition $1s^2\ 2s^2\ 2p^6\ 3s^2\ 3p^6\ 3d$. The ($3d\ ^2D_{3/2}$–$^2D_{5/2}$) separation is too small to give a line in the visible range. Some of the forbidden lines of Fe VII to Fe III having the composition of $3d^x$ have been traced by Bowen in the nebulae, and of Fe II in η Carinæ, and by Merrill (1943) in BF Cygni and other stars; Kundu thinks, too, that some forbidden lines of Fe V can be identified with fainter, doubtful lines in the solar corona. But these doubtful lines require further investigation, both as regards wave-length measurements and identification.

It is clear that even if subsequent investigations prove that the forbidden lines of the $3d^x$-complex (Fe VIII to Fe II) occur in the corona, they would prove to be extremely faint compared to the forbidden lines of the $3p^x$ combination. This may be due partly to the fact that the probability of capture of an electron in a *d*-orbit is far smaller than that in a *p*-orbit. Exact calculations are difficult and are being carried out, but the finding is questionable.

The complete establishment of these ideas will require a colossal amount of experimental and theoretical investigations, the nature of which is clearly indicated in the text. But the value of the hypothesis can also be assessed from a discussion of its bearing on the associated problems of the solar corona mentioned earlier.

If the considerations presented here regarding the origin of emitters of coronium lines prove to be correct, it is obvious that the electrons constituting the inner and outer corona are simply the δ-rays liberated by the coronium-emitters (Fe XIV and others) from H and other atoms in the upper reversing layer, and the chromosphere in the process of ionization by collision as these highly charged emitters of coronium lines pass through the solar atmosphere. The velocity of these electrons is given by the relation $V_e = 2V_i \cos\phi$, where V is the velocity of the ion and ϕ the angle between the direction of emission of the δ-electron with the original direction of motion of the ion. It is clear that $V_e \simeq 2V_i \simeq 2c\alpha s$, and may have as high values as $2c\alpha$. The swifter electrons are mostly emitted inside the reversing layer and inside the chromosphere, and will be able to escape with velocities of the order $2c\alpha$; they probably constitute the electron atmosphere which we know as the corona. The theory has evidently to be further worked out to yield more details about the corona.

The coronal problems are almost unique in astrophysics, because if we leave out the sun, the coronal lines are not observed in the very wide range of astrophysical phenonomena ; neither in spectra of normal or peculiar stars, nor in those of novae or supernovae, except in the solitary case of recurrent novae (RS Ophiuchi), as was discovered by Adams and Joy (1933), and confirmed by Swings and Struve (1943). But it is inconceivable to think that the sun should be a solitary exception. Probably the same physical processes which give rise to coronal lines are occurring everywhere, but the scale, compared with those of ordinary stellar emission, is far too low for the lines to be observable. We are able to observe them on the sun merely on account of our proximity to this star, and that only on special occasions (time of total eclipse) or by special devices (Lyot).

Is it possible to give more definiteness to the question of the *scale* of coronal emission compared to those of ordinary photospheric or chromospheric emissions? The photosphere emits 1500 cal./sec. per cm.^{2} of its area, the chromospheric emissions in Hα come to about $\frac{1}{50}$ of the corresponding photospheric emission in Hα, and according to estimates of Lyot, the coronal emission in the green line is of the order of 10^{-6} A. of the corresponding photospheric emission.

The ideas presented in this lecture may be compared with those of Rosseland (1934):—

"Considering, for instance, the most familiar case, that of the sun, it is surprising how few theories are of such an obvious character as to deserve unreserved applause. It will probably be admitted generally that the interpretation of the origin of Fraunhofer lines is now so far advanced that a revision of fundamental principles may be unnecessary in this field. Proceeding a little further to the interpretation of spectroheliograms, the ground is already getting considerably more insecure. And when we proceed still further, we meet the enigmas of the sunspots, the prominences, the chromosphere, and the corona, none of which can at present be said to be understood, even in the most liberal interpretation of the term.

"The enigmatic character of these phenomena is not so much concerned with the generally admitted fact that we do not understand their common cause, which underlies solar activity as a whole. It is more that we do not know how to interpret the individual manifestations in an intelligible manner. We know of no simple mechanism at present according to which magnetic fields of the magnitude observed in sunspots could be generated. The motion of prominences is recognized as quite different from any motion which could be produced by the combined action of gravitation and electromagnetic forces on a mass of gas in a vacuum, and the agglomeration of matter in the corona surpasses by billions the amount to be expected on any simple hydrostatic theory. These various facts have stimulated speculation to the breaking point, it being even suggested that here we witness our recognized physical laws set at naught by nature herself. Although these speculations are not likely to be taken very seriously by the experienced physicist, they bring out forcibly the unsatisfactory state of solar theory today."

Rosseland's view in 1934 was : "Chromosphere, corona and prominences would in that case form a complex of dynamic phenomena, the theory of which must be based on considerations of the expansive motion of matter moving away from the sun in a more or less radial direction. It does not follow, of course, that all matter in a streamer is moving with the same velocity."

Rosseland concludes : "Though we definitely do not know the nature of these primary particles, the existence of which is indicated by general arguments, there are reasons to believe that they are electrically charged."

Rosseland has considered the equilibrium(?) of the electrified atmosphere, but the physical factors introduced (for example, resistance to the motion of positively and negatively charged particles) are of a vague character. Probably the ideas introduced here will impart definiteness to these factors.

The idea of temperature-equilibrium can be applied to the photosphere and the reversing layer, and that, too, very approximately. The general chromospheric phenomena and other associated ones like prominences are probably partly due to temperature, partly to radiation pressure, and probably nuclear reactions giving rise to α-particles and protons play some part. The coronal phenomena are of a different type—arising from a process akin to or identical with fission, and they are just like rocket-bursts in our atmosphere. The three types of phenomena intermix and produce a complicated picture.

The author had the privilege of discussing the theory of the corona given here with Professor Dirac during a short visit to Cambridge. Dirac made the most interesting suggestion that the β-rays emitted by the fission products may turn out to be the high-energy electrons which are wanted for explaining auroral phenomena. For it is well known that Störmer's theory of the aurora has not been able to explain why the zone of maximum frequency of the aurora is at a distance of 22° from the magnetic poles (see Hewson, 1937). This proves that the corpuscular rays responsible for the auroral phenomena cannot be photo-electrons, or even β-rays of moderate energy. They can be either β-rays of energy of the order of 5 to 10 mev., or α-particles, but the last possibility is generally ruled out on other grounds. The β-rays expected to be given out by fission products have the requisite energy, but there are other factors, and the problem may be left at this stage.

This article was prepared in course of the author's tour through England and U.S.A., in 1944–1945 on a Government of India Mission, and he had the pleasure of discussing its contents with many friends, to whom his grateful acknowledgments are due. He is particularly indebted to Dr. J. A. Fleming, director of the Geophysical Institute, Washington, D.C., and Mr. Allan Shapley for unstinted help in the final preparation of the manuscript.

REFERENCES

ADAMS and JOY, 1933. "Spectrum of RS Ophiuchi." *Pub. Astr. Soc. Pacific*, **45**, 301.

BABCOCK, 1934. "He lines in the Sun." *Pub. Astr. Soc. Pacific*, **46**, 132.

BETHE, 1939. "Energy-production in stars." *Phys. Rev.* **33**, 434.

BÖGGILD *et al.*, 1941. "Range and straggling of fission-particles." *Phys. Rev.* **59**, 275.

BOHR, 1940. "Scattering and stopping of fission fragments." *Phys. Rev.* **58**, 659.

BOHR and WHEELER, 1939. "Mechanism of nuclear fission." *Phys. Rev.* **56**, 426.

BRINKMAN and KRAMERS, 1930. "Capture of electrons by a-particles." *Proc. K. Akad. wet. Amst.* **33**, 973.

CORSON and THORNTON, 1939. "Disintegration of uranium." *Phys. Rev.* **55**, 509.

EDLÉN, 1942. "On the identification of coronal lines." *Z. Astrophys.* **22**, 30.

GROTRIAN, 1933. "Variation of intensity of coronal lines." *Z. Astrophys.* **7**, 26.

HEWSON, 1937. "A survey of the facts and the theories of the aurora." *Rev. Mod. Phys.* **9**, 403.

JACOBSEN, 1935. "Capture of electrons by swift a-particles." *Phil. Mag.* **10**, 401.

KNIPPS and TELLER, 1941. "Energy loss of heavy ions." *Phys. Rev.* **59**, 659.

LAMB, 1941. "Passage of uranium fragments through matter." *Phys. Rev.* **58**, 596.

LARK-HOROVITZ and SCHREIBER, 1941. "U fission with Li-D neutrons." *Phys. Rev.* **60**, 156.

LIVINGSTONE and BETHE, 1937. "Report on nuclear physics." *Rev. Mod. Phys.* **9**,

LYOT, 1939. "Study of the solar corona and prominences." *Mon. Not. Roy. Astr. Soc.* **99**, 580.

MERRILL, 1943. "The spectrum of F-Cygni." *Astrophys. J.* **98**, 473.

MERRILL, 1944. "Spectroscopic observations of A*x* Persei, etc." *Astrophys. J.* **99**, 481.

MINNAERT, 1930. "Continuous spectrum of the corona." *Z. Astrophys.* **1**, 209.

MOORE and BABCOCK, 1943. "Thorium in the Sun." *Pub. Astr. Soc. Pacific*, **55**, 22.

NISHINA *et al.*, 1939. "Fission of thorium by neutrons." *Nature, Lond.*, **144**, 547.

OPPENHEIMER, 1928. "Quantum theory of capture of electrons." *Phys. Rev.* **31**, 349.

PANNEKOEK and MINNAERT, 1928. "Observations of solar lines, etc." *Proc. K. Akad. wet. Amst.* **13**, .

PEREPELKIN and MELNIKOV, 1935. *Publications of the Pulkowa Observatory*, no. 122, 14.

PRESENT, 1941. "Possibility of ternary fission." *Phys. Rev.* **59**, 467,

ROSSELAND, 1933. "On the theory of the chromosphere and the corona." *Proc. Oslo Akad.*

RUSSELL, 1941. "A puzzle solved." *Scientific American*, **165**, 70.

RUTHERFORD, 1924. "Capture and loss of electrons by a-particles." *Phil. Mag.* **47**, 277.

SAHA, 1921. "On a physical theory of stellar spectra." *Proc. Roy. Soc.* A, **99**, 135.

SAHA, 1942. "On a physical theory of the solar corona." *Proc. Nat. Inst. Sci. India*, **8**, 99.

SWINGS, 1943. " Edlén's identification of the coronal lines, etc." *Astrophys. J.* **98**, 116.
SWINGS and STRUVE, 1943. *Astrophys. J.* **97**, 204.
TURNER, 1940. " Nuclear fission." *Rev. Mod. Phys.* **12**, 1.
UNSÖLD, 1939. *Sternatmosphäre.*
WALDMEIER, 1937. " On the significance of contours of corona-lines." *Z. Astrophys.* **15**, 44.
WALDMEIER, 1944. " Observations of corona before and after total sola reclipse, etc." *Z. Astrophys.* **20**, 250.
WALKE, 1940. *Rep. Progr. Phys.* **6**, 16.

ON TRACING RAYS THROUGH AN OPTICAL SYSTEM

(Fifth paper)

BY T. SMITH, F.R.S.
(Communication from the National Physical Laboratory)

MS. received 23 *February* 1945

ABSTRACT. An iterative method of tracing rays through an optical system which is suitable for operation by a fully automatic recording machine is described. The rays may be axial or skew, and the surfaces of any rotationally symmetrical form suitable for optical working. The relation of this method to earlier schemes and the advantages to be gained by successive approximations are considered.

FROM time to time experiments have been made at the National Physical Laboratory on methods of tracing single rays and pencils of rays through a series of lenses. It has been assumed that a calculating machine would be employed instead of tables of logarithms, and for this and other reasons the methods have differed from those described in Conrady's *Applied Optics*, which, it is believed, are still used to a considerable extent in the optical industry. An examination of the four earlier papers bearing the same title as the present note (Smith, 1915, 1918, 1920, 1921) will show that much of the original structure has been retained (though the notation has changed), but that some modifications have tended consistently in a definite direction. For example, the first paper gives formulae for paraxial rays, general skew rays, and the foci of sagittal pencils, which exemplify applications of the matrix formula

$$\begin{pmatrix} B & D \\ A & C \end{pmatrix} = \begin{pmatrix} 1 & D_0 \\ . & 1 \end{pmatrix} \begin{pmatrix} 1 & . \\ A_1 & 1 \end{pmatrix} \begin{pmatrix} 1 & D_1 \\ . & 1 \end{pmatrix} \begin{pmatrix} 1 & . \\ A_2 & 1 \end{pmatrix} \cdots \begin{pmatrix} 1 & . \\ A_n & 1 \end{pmatrix} \begin{pmatrix} 1 & D_n \\ . & 1 \end{pmatrix} \quad \ldots\ldots(1)$$

to a system of n retracting surfaces. In this equation A_p represents a power associated with surface p and $-D_p$ the equivalent distance between surfaces p and $p+1$, i.e. the distance measured along the ray between these surfaces divided by the refractive index of the corresponding medium. The A, B, C, D on the left are well-known functions which determine the properties of the complete optical train. In the second paper the foci of tangential pencils are obtained by a slight generalization of the factors representing single refractions. The factor $\begin{pmatrix} 1 & . \\ A_p & 1 \end{pmatrix}$ is replaced by $\begin{pmatrix} B_p & . \\ A_p & C_p \end{pmatrix}$, where $B_pC_p = 1$. It will be seen that in all cases the identity

$$BC - AD = 1$$

is satisfied. These formulae are still employed, and it is difficult to see how they can be simplified. They may be varied (Smith, 1930) to an almost unlimited extent without losing their main properties, and they lend themselves admirably to the rapid solution of problems which must be frequently encountered in industrial practice.

In some applications the values to be inserted in the elementary matrix factors are not known initially; they will be known when a preliminary calculation, which is usually considered the ray-tracing proper, has been made.

It is in this preliminary stage that a definite line of evolution is apparent. In the original scheme the variables* defining the position of a ray were the angle ψ it made with the axis of symmetry of the instrument and the length h of the perpendicular to the ray from the centre of curvature of the refracting surface, which was assumed to be spherical. If μ is the refractive index and ϕ the angle between the ray and the normal, the equations used were

$$\begin{aligned} \mu h &= \mu' h', \\ \sin\phi &= hR, \\ \sin\phi' &= h'R, \\ \psi' &= \psi - \phi + \phi', \end{aligned}$$

where accents are applied to symbols relating to the refracted ray and R is the curvature of the surface. At the following surface the first perpendicular is $h' + a \sin\psi'$, where a is the distance along the axis between the two centres of curvature. As systems are usually specified by radii of curvature (r) and axial distances (t) between successive surfaces, a is calculated from

$$a = t - r + r'.$$

This computing scheme is not without merits. It is simple to understand and to operate. Some common superfluous operations, such as finding the point of intersection of a ray with the axis after each refraction, are avoided. But experience suggested that improvements could be made in two respects. To obtain the greatest accuracy in calculations when only a small number of significant figures is retained, and particularly to obtain reliable differences between a number of calculations of the same type on the same system, the quantities involved should not be of very diverse magnitudes. In general this condition will not be satisfied if the centres of curvature are taken as reference points. This objection applies generally to all schemes which make use of the centres of curvature. The first change was therefore to drop the perpendiculars from the pole of the surface instead of from the centre of curvature. This ensured that the lengths used to define the position of a ray were roughly of the same magnitude at all surfaces. To retain this advantage throughout it was necessary to avoid using a radius of curvature as a multiplying factor. Each surface was therefore specified by its curvature instead of its radius; from the optical viewpoint this is clearly the scientific choice.

---

* The curvature of a surface which is convex towards the incident light is positive ; distances along the axis in the direction in which light travels are also positive. Perpendiculars to rays are positive if the foot of the perpendicular is above the axis. The angle ψ is positive if an anti-clockwise rotation from the positive direction along the axis is needed to bring a vector into coincidence with the onward direction of the ray ; ϕ is positive if an anti-clockwise rotation from the direction of the normal would bring a vector into coincidence with the ray.

The second improvement was to eliminate all angular measures. The equation already given for ψ' is in appearance very simple, but the appearance is misleading when the numerical operations implied are taken into account. Three references to trigonometrical tables are required at each refraction, and subsidiary calculations for interpolation are usually involved. The whole process is therefore rather slow, notwithstanding its simplicity. In appearance the improved scheme looks more complicated. It will be best appreciated if refraction is first considered at a surface where there is no aberration. In that case $\mathfrak{h}$, the length of the perpendicular to the ray from the pole of the surface, is unaltered by refraction, and the equations are

$$\begin{aligned} \sin\phi &= \sin\psi + \mathfrak{h}R, \\ \mu'\sin\phi' &= \mu\sin\phi, \\ \sin\psi' &= \sin\psi - \sin\phi + \sin\phi'. \end{aligned}$$

Owing to the occurrence of aberration, $\mathfrak{h}$ and $\mathfrak{h}'$ are not equal, and the last equation is not true. But the difference between $\mathfrak{h}$ and $\mathfrak{h}'$ is of aberrational magnitude, and the value of $\sin\psi'$ just suggested is subject to a small correction. The correct formulae then consist of the first two equations together with

$$\begin{aligned} \mathfrak{h}' - \mathfrak{h} &= \frac{\mathfrak{h}\,(\sin\phi - \sin\phi')\,(\sin\phi' + \sin\psi)}{\tfrac{1}{4}\sigma^2 + \kappa}, \\ \sin\psi' &= \sigma - (\mathfrak{h}' - \mathfrak{h})R, \end{aligned}$$

where

$$\sigma = \sin\psi - \sin\phi + \sin\phi'$$

and

$$\kappa = \tfrac{1}{4}\{(\cos\psi + \cos\phi + \cos\phi')^2 - 1\}.$$

The $\mathfrak{h}$ for the next surface is equal to $\mathfrak{h}' + t\sin\psi'$.

Since $\mathfrak{h}' - \mathfrak{h}$ is of aberrational magnitude, the denominator $\tfrac{1}{4}\sigma^2 + \kappa$ need only be known to a small number of significant figures. It represents twice the ratio of the first order to the total aberration, and at the National Physical Laboratory critical tables are now * used to evaluate it. One gives cosines when the sines are known, and two others, $\tfrac{1}{4}\sigma^2$ and κ, from the known values of σ and the sum of the three cosines.

This way of calculating rays is strongly preferred to all others that have been tried by those members of the Laboratory staff who have done much work of this kind. Differences of path and some other useful quantities are obtained from the values of $\mathfrak{h}' - \mathfrak{h}$ with almost trivial additions to the work, so that much information is obtained from the trace of a single ray.

A few years ago it was realized that the process of elimination and simplification could be carried further. A self-checking scheme for computing both axial and skew rays automatically, through surfaces of any shape, was under consideration. It was supposed that by means of punched cards a machine might be given the initial coordinates of a ray and a specification of the system through which it was to be traced. The machine would then carry out a cycle of operations and print all useful results. The cycle would be repeated, either for

* The original tables are not critical.

the instrument as a whole or alternatively surface by surface, until all the quantities repeated themselves exactly, when the work would be completed and the machine would in the one case stop and in the other proceed to the next surface.

To those who have only used the traditional methods of ray tracing the most surprising feature of the new scheme may well be the disappearance of Snell's law of refraction. The angles ϕ and ϕ' made by the incident and emergent rays with the normal at the point of refraction do not appear either explicitly or in disguise. These are the unessential quantities which have now been eliminated.

The most important quantities are the coordinate, measured parallel to the axis, of the point of refraction, and the product of the refractive index and the cosine of the angle the ray makes with the axis. If the point of refraction is x, y, z and the modified direction cosines of the ray are ξ, η, ζ, the main quantities when the axis of z coincides with the axis of the instrument are z and ζ. The equation of each surface will normally be referred to its pole as origin, and the standard form adopted is

$$s=f(z),$$

where s is the subnormal. A_p and D_p are then given by

$$\left.\begin{aligned} A_p &= \frac{\zeta_p-\zeta_{p-1}}{s_p}, \\ -D_p &= \frac{t_p-z_p+z_{p+1}}{\zeta_p}. \end{aligned}\right\} \qquad \ldots\ldots(2)$$

If correct values are inserted for all the z's and ζ's, the analytical form of the law of refraction,

$$\frac{\xi_p-\xi_{p-1}}{x_p}=\frac{\eta_p-\eta_{p-1}}{y_p}=-\frac{\zeta_p-\zeta_{p-1}}{s_p},$$

shows that, if $A_{0,p}$, $B_{0,p}$, $C_{0,p}$, $D_{0,p}$ are the values of A, B, C, D obtained by terminating equation (1) immediately after refraction at the pth surface,

$$\begin{pmatrix} \xi_p & -x_p \\ \eta_p & -y_p \end{pmatrix}=\begin{pmatrix} \xi_0 & -x_0 \\ \eta_0 & -y_0 \end{pmatrix}\begin{pmatrix} B_{0,p} & D_{0,p} \\ A_{0,p} & C_{0,p} \end{pmatrix}. \qquad \ldots\ldots(3)$$

The accuracy of the values taken for ζ and z is judged by verifying that the conditions

$$\mu^2=\xi^2+\eta^2+\zeta^2$$

and

$$x^2+y^2=2\int_0^z s\,dz$$

are satisfied. Assuming that they are not satisfied within the required limits of accuracy, a recalculation is made, using better values of ζ and z. In terms of the old values, the new values ζ' and z' are

$$\left.\begin{aligned} \zeta' &= \tfrac{1}{2}\left(\zeta+\frac{\mu^2-\xi^2-\eta^2}{\zeta}\right) \\ \text{and}\qquad z' &= \frac{x^2+y^2+2\int z\,ds}{2s}. \end{aligned}\right\} \qquad \ldots\ldots(4)$$

As an illustration of the latter, if the surface is a sphere of radius r, the equation is $s+z=r$, and the improved value of z is

$$\frac{x^2+y^2-z^2}{2s} \quad \text{or} \quad \frac{x^2+y^2-z^2}{2(r-z)}.$$

If the surface is a conicoid of revolution of eccentricity e, so that the equation is $s+\epsilon z=r$, where $\epsilon=1-e^2$, the improved value of z is

$$\frac{x^2+y^2-\epsilon z^2}{2s}$$

It will be seen that the new process is a method of successive approximation, and its success depends on its known rapid convergence. The length of the work depends on the closeness of the initially assumed values of z and ζ to the final values. In completely automatic cyclic operations rapidity in reaching the final result is not necessarily a very important or even a desirable requirement. For example, if the initial values are $z=0$, $\zeta=\mu$, i.e. the paraxial values, and each cycle includes the complete instrument, the first round gives the paraxial properties, the second the first-order aberrations, and thereafter groups of aberrations of increasing size are taken into account until higher-order aberrations produce no measurable change. The calculation of a single ray by the new method then gives information that would only be secured on present practice by tracing several rays. On the other hand there are occasions on which only the final result is needed, as when the effect of a change of glass constants or other minor modification of a known system is to be found. In such cases the known values for the previous construction provide suitable initial values for z and ζ, and the modified values may well repeat after a single cycle has been performed. In some circumstances a graphical trace, such as Dowell's (Dowell, 1926), may be a convenient means of deriving approximate initial values for accurate calculations, and with experienced designers "guessing" may be very effective. Several variations of the process may be arranged to suit a variety of conditions.

Like other iterative methods of calculation, this scheme has the property that mistakes are not important, provided they are not incorrect values of fundamental quantities like μ^2 or r. Errors are automatically eliminated—at the worst they lengthen the time taken to reach the final result. The scheme is therefore valuable as a means of checking results reached by other ways of tracing rays. From its very nature it is not less accurate than any other way of tracing rays in which the same number of figures is retained. If, for example, it were required to check a calculation made by the normal N.P.L. method for rays in an axial plane, or to increase the number of significant figures, A would be taken as $(\mu' \cos\phi' - \mu\cos\phi)R$ and z as

$$\frac{2\mathfrak{h}\,(\sin\phi-\sin\psi)}{(\cos\phi+\cos\psi)^2+(\sin\phi-\sin\psi)^2}.$$

(Checking could be made after a single cycle, since

$$\frac{2\mathfrak{h}\,(\cos\phi+\cos\psi)}{(\cos\phi+\cos\psi)^2+(\sin\phi-\sin\psi)^2}$$

is the value of the transverse coordinate of the point of refraction.)

It is worth noting that the one calculation gives the sagittal foci as well as the exact position of the ray. If the sagittal conditions are well satisfied over the field there is no need to consider the tangential conditions, which are merely differentials of the sagittal expressions. If desired, the independent tangential calculation may be made after evaluating $s\zeta - x\xi - y\eta$.

Equations (1), (2), (3) and (4) are well suited for the development of formulae for aberrations of different orders.

When this method of tracing rays was first evolved it was intended to apply it to several systems of many types before publishing any description. Owing to war requirements there have not been suitable opportunities for such extensive trials, and the experience so far gained has been limited. In view, however, of the interest now being taken in possible uses of non-spherical refracting and reflecting surfaces, and the importance of developing fully-automatic means of tracing rays, it is thought appropriate to publish this note without further delay.

ACKNOWLEDGMENT

The work described above has been carried out as part of the research programme of the National Physical Laboratory, and this paper is published by permission of the Director of the Laboratory.

APPENDIX

To illustrate the rapidity of convergence of a calculation by this method a marginal ray has been traced with a paraxial ray as the starting point. The example has been taken from Conrady's *Applied Optics* (p. 50) as it is likely to be familiar to many readers. The specification of the system and the successive stages from the paraxial ray to the final marginal values are given in table 1. The values of the longitudinal aberration and the change in the focal length from the paraxial value derived at each stage are also given. The values for the former indicate under-corrected aberration at first, changing finally to slight over-correction. The focal-length changes show that the system is not closely corrected for coma.

Table 1

$r_1 = 3{\cdot}55 = -r_2,\quad r_3 = -60,\quad t_1 = 0{\cdot}3,\quad t_2 = 0{\cdot}2,\quad \mu_1 = 1{\cdot}5166,\quad \mu_2 = 1{\cdot}6256$

Successive stages in tracing ray $\zeta_0 = \eta_0 = 0,\ \zeta_0 = 1,\ x_1 = 1,\ y_1 = 0$

Z_1	Z_2	Z_3	ζ_1	ζ_2	ζ_3
0	0	0	1·516600	1·625600	1·000000
0·140845	−0·132853	−0·007632	1·509618	1·621483	0·992102
0·143754	−0·142977	−0·007906	1·509215	1·621396	0·991896
0·143756	−0·143370	−0·007916	1·509214	1·621412	0·991923
—	−0·143382	—	—	1·621413	0·991925

Longitudinal aberration	Focal length change
−0·016819	−0·086012
−0·000926	−0·072701
+0·000004	−0·072058
+0·000039	−0·072036
+0·000040	−0·072035

Table 2. Outstanding errors with different methods of calculation

Method	Longitudinal aberration error	Focal length error
5-figure logarithms	−0·000523 (−0·000223)	+0·000047
6-figure polar perpendiculars	+0·000083	+0·000066
8-figure central perpendiculars, no interpolation	+0·000878	+0·000479
8-figure central perpendiculars, full interpolation	+0·000008	+0·000001
7-figure radian tables	+0·000009	+0·000003
6-figure present scheme	0·000000	0·000000

The accuracy attained in calculations according to this scheme is compared with those of other methods in table 2. Unfortunately it was not possible to use Conrady's results to illustrate the accuracy of the normal logarithmic calculation, as his paraxial result has an error of three units in the fourth decimal place. The marginal ray (but not the paraxial ray) was therefore calculated afresh, using Bremmiker's 5-figure tables. Owing to the long last radius the normal formula does not give a very accurate result, and a value derived by using a formula intended to avoid this uncertainty has been added in brackets. The error in the focal length given by this calculation is not typical of that to be expected with 5-figure logarithms: the particular figures of this example happen —quite accidentally—to give a much better result than could be expected.

On the second line are the values obtained with the method normally used at the National Physical Laboratory. The two following lines are those obtained by the original N.P.L. method, using Gifford's sine tables. In the former each angle was read to the nearest second only. The errors involved in this procedure should be about twice those to be expected from the use of 5-figure logarithms, and the abnormally small error in the focal length found in the logarithmic calculation is clearly shown. When interpolation is used, the increased accuracy due to the additional figures is apparent, though it is to some extent diminished through the use of centres of curvature as reference points instead of the surface poles. The radian tables mentioned are some prepared recently at the N.P.L. for use with the B.S.I.R.A. computing scheme. The last line refers to the method described in this paper. All the errors have been determined by comparison with calculations of ten-figure accuracy.

It has been noted earlier that, after the paraxial trace, the changes made in the first cycle represent approximately the first-order aberrations, the second cycle the second and third orders, and so on. The extent to which this holds may be seen from table 3 and the analytical expressions which follow. For this purpose

Table 3. Successive approximations to A, C, ζ_3, Z_3

A	C	ζ_3	Z_3
0·12567 88492	0·95697 95005	0·99210 24134	−0·00763 17480
0·12705 22669	0·97396 20198	0·99189 60450	−0·00790 55370
0·12683 77581	0·97458 72430	0·99192 34768	−0·00791 56913
0·12682 74221	0·97460 11302	0·99192 47981	−0·00791 59169
0·12682 70639	0·97460 15419	0·99192 48439	−0·00791 59236

values have been calculated to ten decimal places and have been carried far enough to give totals accurate to at least the first six places.

Analytical expressions

$$A=0{\cdot}12567\ 88492+0{\cdot}00135\ 95694\,x^2-0{\cdot}00016\ 67749\,x^4-0{\cdot}00003\ 74970\,x^6$$
$$-0{\cdot}00000\ 60264\,x^8-0{\cdot}00000\ 09097\,x^{10}-0{\cdot}00000\ 01357\,x^{12}$$

$$C=0{\cdot}95697\ 95005+0{\cdot}01628\ 90110\,x^2+0{\cdot}00119\ 72985\,x^4+0{\cdot}00011\ 90666\,x^6$$
$$+0{\cdot}00001\ 44030\,x^8+0{\cdot}00000\ 19475\,x^{10}+0{\cdot}00000\ 02790\,x^{12}$$

$$\zeta_3=1{\cdot}00000\ 00000-0{\cdot}00789\ 75866\,x^2-0{\cdot}00020\ 20551\,x^4+0{\cdot}00001\ 84401\,x^6$$
$$+0{\cdot}00000\ 50645\,x^8+0{\cdot}00000\ 08382\,x^{10}+0{\cdot}00000\ 01237\,x^{12}$$

$$Z_3=0{\cdot}00000\ 00000-0{\cdot}00763\ 17480\,x^2-0{\cdot}00026\ 02895\,x^4-0{\cdot}00002\ 13407\,x^6$$
$$-0{\cdot}00000\ 22274\,x^8-0{\cdot}00000\ 02744\,x^{10}-0{\cdot}00000\ 00374\,x^{12}$$

Height of intersection with paraxial image plane :—

$$-0{\cdot}00258\ 03856\,x^3+0{\cdot}00208\ 17289\,x^5+0{\cdot}00042\ 36428\,x^7$$
$$+0{\cdot}00006\ 80900\,x^9+0{\cdot}00001\ 02632\,x^{11}+0{\cdot}00000\ 15177\,x^{13}$$

Path length difference to intersection of ray with paraxial image plane :—

$$0{\cdot}00024\ 32249\,x^4-0{\cdot}00021\ 62703\,x^6-0{\cdot}00003\ 88728\,x^8$$
$$-0{\cdot}00000\ 79604\,x^{10}-0{\cdot}00000\ 11819\,x^{12}$$

Correction for path differences to paraxial principal focus :—

$$-0{\cdot}00032\ 42999\,x^2+0{\cdot}00025\ 81211\,x^4+0{\cdot}00005\ 65035\,x^6$$
$$+0{\cdot}00000\ 88830\,x^8+0{\cdot}00000\ 12493\,x^{10}+0{\cdot}00000\ 01673\,x^{12}$$

This example is of interest for another reason. In discussing results obtained by tracing several rays through this lens, Conrady, speaking of analytical methods of calculating higher-order aberrations, makes use of the phrases " . . . . if we went through the tremendous labour of calculating the true secondary aberration by a direct analytical equation . . . ." and " . . . . the very sensible tertiary aberration (which would utterly defy analytical determination) . . . .". These views are held by other optical workers. For instance Prof. von Rohr told me that I should only waste my time if I attempted such calculations, because the subject was far too complex for treatment in this way. Such opinions obviously lack scientific justification, and that they are wrong is indicated by the results just given. Admittedly the calculations are tedious, but it is certainly possible to calculate any aberrational coefficients that may be required.

It should be realized that the tables of this appendix are intended solely to indicate the comparative accuracy of the particular mathematical processes. No account has been taken of the accuracy that is necessary or sufficient in these optical computations.

REFERENCES

DOWELL, J. H., 1926. " Graphical methods applied to the design of optical systems ", *Proc. Opt. Conv.* p. 965.

SMITH, T., 1915. " On tracing rays through an optical system ", *Proc. Phys. Soc.* **27,** 502 ; 1918. *Ibid.* **30,** 221 ; 1920. *Ibid.* **32,** 252 ; 1921. *Ibid.* **33,** 174 ; 1930. " The general form of the Smith-Helmholtz equation ", *Trans. Opt. Soc.* **31,** 241.

DIRECTIONAL LOCI IN A MAGNETIC FIELD, AND THE LOCATING OF NEUTRAL POINTS

BY DAVID OWEN,
London

MS. received 26 *February* 1945

ABSTRACT. A method of exploration of a magnetic field by means of directional loci is described. The points of intersection of any two loci are neutral points. The method is exemplified in the simpler cases of the combination of the earth's field with the field of a bar magnet and with the field of a circular current.

§ 1. INTRODUCTION

MAGNETIC fields are usually studied by plotting the lines of force in a horizontal plane by means of a compass needle. The procedure for locating a neutral point is usually to track it down by enclosing it within a gradually reduced region bounded by lines of force. The method is ineffective because it becomes impossible to plot the lines accurately close to a neutral point. There is a sort of principle of indeterminacy at play—the nearer the approach to the neutral point, the less accurate the plotting.*

The method here described is to obtain the neutral points as the points of intersection of two continuous curves or loci. The kind of locus considered is that containing all points at which the direction of the field is the same. Any two directions of field may be chosen, but obviously it is advisable to choose directions at right angles to one another; and in cases where the earth's field is involved, these directions should obviously be respectively parallel to and perpendicular to the earth's field. Loci so drawn will be described as the north-south (N–S) locus and the east-west (E–W) locus. Such directional loci are unique. The experimental errors of plotting are non-cumulative, so that the loci can be determined quite definitely. As a point of intersection is approached, the component of field in the chosen direction diminishes to zero and, beyond it, changes sign. The points of intersection are thus points of zero field, or neutral points.

The number of neutral points in any field is even. When the field of a simple bar magnet is superposed on the earth's field, the number of neutral points is two. When the superposed field is that of a circular current, the number of neutral points is either zero or four, according as the strength of the current is below or above a certain critical value. With more complicated fields the number may obviously be greater.

The apparatus required to plot a directional locus consists of a sheet of squared paper on a drawing board and an ordinary small compass needle. Suppose the field to be explored is that of a bar magnet in the earth's field. The squared paper is adjusted on the board so that one set of lines runs magnetically north and south, and the other set therefore east and west. The magnet is now brought up and placed near the centre of the paper with its axis in any desired direction. On moving the compass needle over the paper, some point is soon found where the needle points parallel to the N–S lines. The sharpened point of a pencil is held firmly just above the centre of the needle, the needle is removed, the pencil point moved straight down on to the paper and a dot made. A second point on the locus is chosen about a centimetre away, and so on. Continuing thus, the complete N–S locus is plotted and a continuous graph can be drawn. Similarly the E–W locus can be found. The complete loci will usually extend into all four quadrants round the centre of the magnet. If the experiment is to be restricted to a quick determination of one neutral point, of course only a limited portion of each locus in the neighbourhood of the neutral point is needed. To check the accuracy of setting of the needle at any point of a locus it should be remembered that a small displacement of the needle to one side of the locus will cause an appreciable deviation of direction of one sign, whilst a similar displacement on the opposite side will cause a deviation of opposite sign. If practised at each setting this procedure will ensure correct plotting. With a little experience the loci can be rapidly obtained. The neutral points are thus located with pin-point accuracy with a magnet of reasonable moment, and their distances from the centre of the magnet can be measured within a half per cent.

---

* See, however, *Note added in proof* (p. 301).

To illustrate the use of directional loci a few special cases will be considered: first when the field is that of a bar magnet, and then when the field is that of a circular electric current.

§ 2. BAR MAGNET IN THE EARTH'S FIELD

Since the forms of the loci are easily calculable in the ideal case of a magnetic doublet set with its axis either along or perpendicular to the earth's field, figures showing the forms of these loci will first be given. They will be accompanied by figures showing the loci experimentally plotted in the case of an actual bar magnet. Points on a N–S locus are indicated by a cross (×), and points on an E–W locus by a centred circle (⊙). The neutral points are at N_1 and N_2.

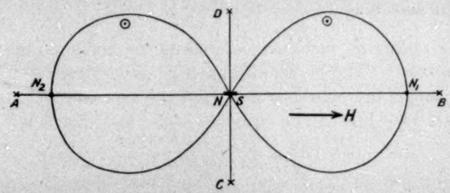

Figure 1. N–S (marked × ×) and E–W (marked ⊙⊙) loci of magnetic doublet along the earth's horizontal field, S pole to the north, neutral points at N_1 and N_2.

Case 1. *Axis along the meridian, S pole towards the north.*—The loci for a doublet are shown in figure 1. The N–S locus consists of a pair of straight lines AB and CD along and perpendicular to the axis of the doublet. The E–W locus is a figure of eight. Denoting the magnetic moment by M and the earth's horizontal field by H, the condition that the field at any point P (r, θ) shall be in the E–W direction is

$$H - \frac{2M}{r^3}\cos^2\theta + \frac{M}{r^3}\sin^2\theta = 0, \quad \text{or} \quad r^3 = M(3\cos^2\theta - 1)/H,$$

which is, therefore, the equation of the locus. Putting $\theta = 0°$ or $180°$ the distance from the doublet to either neutral point is $\sqrt[3]{2M/H}$. At the origin the loops make angles $\cos^{-1}\left(\pm\frac{1}{\sqrt{3}}\right)$ with the axis.

When an actual magnet is used, the N–S locus remains a pair of mutually perpendicular straight lines, along and perpendicular to the axis. Figure 1 *a* shows also (to half-scale) the two separated branches of the E–W locus. A cylindrical cobalt-steel magnet 1 in. long and $\frac{1}{4}$ in. in diameter was used. The measured distances from the centre of the magnet to N_1 and N_2 are 4·42 in. or 11·22 cm. and 4·40 in. or 11·18 cm., mean = 11·2 cm. (± ·5 mm.). Assuming $M = Hr^3/2$, and $H = 0{\cdot}18$, $M = 126{\cdot}4$ c.g.s. Assuming $M = \frac{Hr^3}{2}\left(1 - \frac{2l^2}{r^2}\right)$, and taking $l = 0{\cdot}8 \times$ half-length of magnet, $M = 124{\cdot}4$ c.g.s.

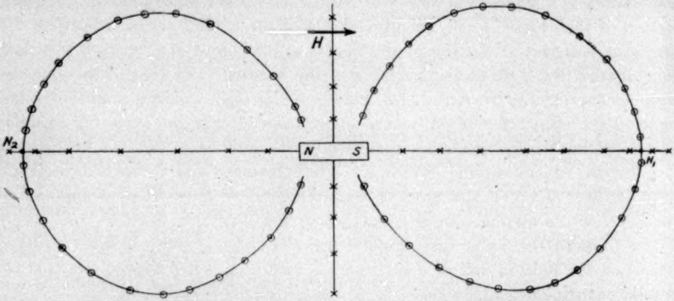

Figure 1 *a*. N–S and E–W loci, and neutral points N_1, N_2 of 1-in. cobalt-steel magnet along earth's horizontal field, S pole towards the north.

Case 2. *Axis along the meridian, N, pole to the north.*—Figure 2 represents the case of a doublet. The N–S locus remains as in Case 1. The E–W locus consists of two loops, the long axis now running east and west, so that N_1 and N_2 lie on the east–west line. The equation of the E–W locus is

$$\frac{M}{r^3}(1 - 3\cos^2\theta) = H.$$

The lengths ON_1 and ON_2 to the centre of the magnet are equal to $\sqrt[3]{\frac{M}{H}}$. At the origin the loops cross the axis at angles $\cos^{-1}\left(\pm\frac{1}{\sqrt{3}}\right)$.

Using the same cobalt-steel magnet as before, the observed plot is shown (to half-scale) in figure 2 *a*. From this $ON_1 = 3{\cdot}48$ in. $= 8{\cdot}84$ cm., $ON_2 = 3{\cdot}46$ in. $= 8{\cdot}79$ cm.,

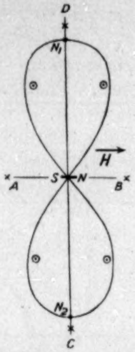

Figure 2. N–S (straight lines AB and CD) and E–W (figure of eight) loci of magnetic doublet along earth's horizontal field, N pole to the north. Neutral points at N_1 and N_2.

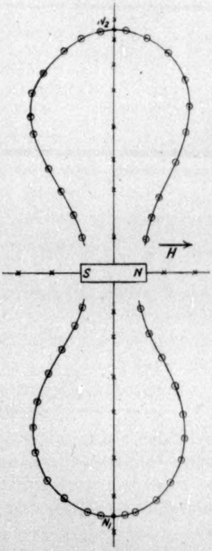

Figure 2 *a*. N–S and E–W loci of 1-in. cobalt-steel magnet, N pole to the north, neutral points at N_1, N_2.

mean value = 8·81 cm. Assuming the formula $M = Hr^3$, the value of M is 123·0 c.g.s., and assuming $M = Hr^3\left(1+\frac{3}{2}\frac{l^2}{r^2}\right)$ the value of M is 125·3 c.g.s.

Case 3. *Axis perpendicular to the meridian.*—The case for the doublet, with N pole to the east, is shown in figure 3. The N–S locus is the pair of straight lines AB and CD making angles $\tan^{-1}\sqrt{2}$ (nearly 55°) with the axis. The equation of the E–W locus is

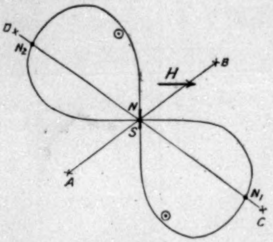

Figure 3. N–S locus (straight lines AB and CD) and E–W locus (figure of eight) of magnetic doublet with axis ⊥ to earth's field, N pole to the west, neutral points at N_1 and N_2.

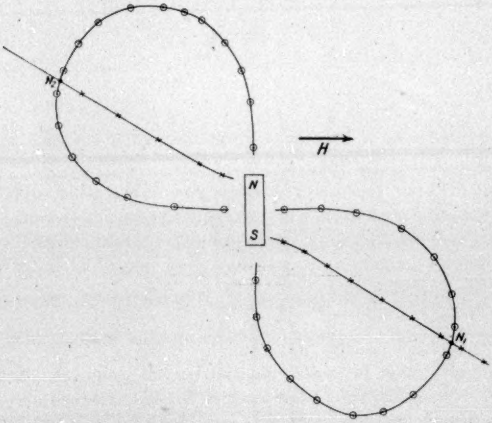

Figure 3 *a*. N–S and E–W loci and neutral points N_1 and N_2 of 1-in. cobalt-steel magnet, axis ⊥ to H, N pole to the west.

$$r^3 = \frac{3}{2}\frac{M}{H}\sin 2\theta.$$

It is a figure of eight whose axis makes an angle of 45° with the magnetic axis, and it touches the axis of the doublet and the equatorial line.

The experimental graphs for the same 1-in. cobalt-steel magnet are shown in figure 3 *a*. Near the magnet the N–S locus deviates appreciably from the straight line pertaining to the doublet.

§ 3. FIELD OF AN ELECTRIC CURRENT

The ideal case of an infinitely long straight conductor of circular section, placed vertically in the earth's field, and carrying a steady current, allows of a simple and suggestive treatment. In figure 4 the smaller circle of radius OA $= a$ represents a section of the conductor. No neutral points exist unless the current I exceeds a limiting value $\frac{1}{2}Ha$. With any current exceeding this value, the current being downwards, an external neutral point N_1 occurs on the east side, such that $2I/ON_1 = H$. A second neutral point exists at N_2 within the conductor, such that $\frac{2I.ON_2}{a^2} = H$. Thus $ON_1 . ON_2 = a^2$. The N–S locus is the straight line running east and west through the centre O of the conductor. For points outside the conductor the E–W locus is the portion of the circle on ON_1 as diameter lying outside the conductor. For points inside the conductor, the E–W locus is the straight line $J_1 J_2$ joining the points where the circle on ON_1 cuts the conductor. At the limiting value of the current the neutral points coincide at A on the surface of the conductor.

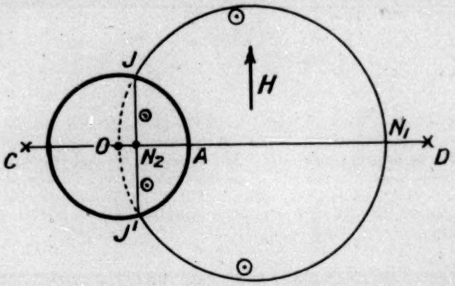

Figure 4. Vertical circular conductor, of radius OA, carrying a downward electric current (exceeding the critical value) in the earth's field. The N–S locus is the straight line COD. The E–W locus is the portion of the larger circle on ON_1 as diameter which is external to the conductor, together with the straight line JJ′ inside the conductor. There is an external neutral point at N_1 and an internal neutral point at N_2.

The case of a circular coil, or rather a short helical coil with horizontal axis, will next be considered. The determination of either directional locus does not in general lend itself to easy theoretical treatment. There is again obviously a limiting value of current below which no neutral points exist. For currents exceeding this value there are four neutral points, two within the conductor and two external to it.

Case 1. *Axis of the coil parallel to H, field due to the current in the same direction as H at the centre of the coil.*—In this case the N–S locus consists of a pair of straight lines, namely, the axis of the coil and the transverse median line.

The E–W loci obtained experimentally are shown to half-scale in figure 5, for currents of 1, 2 and 3 amp., only the branches on one side of the coil being drawn. The corresponding external neutral points are at N′, N″ and N‴. The mean radius of the coil is 3·76 in. and its axial width 0·5 in.

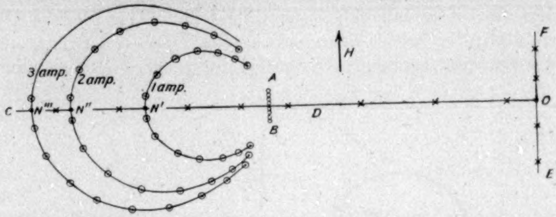

Figure 5. Electric currents through circular coil with axis along the earth's horizontal field, fields on axis in *same* direction as *H*. AB = section of the coil of 8 turns, centre at O. The N–S locus consists of the pair of straight lines CD and the axis of the coil. The branches of E–W loci are shown for currents of 1, 2 and 3 amp., the neutral points being respectively at N′, N″ and N‴. (Complete figure is symmetrical about O. Right-hand half omitted.)

Case 2. *Axis of the coil parallel to H, field due to the current opposed to H at centre of coil.*—The experimental graphs for this case are seen, to half-scale, in figure 6 for six values of the current as indicated on the curves. The complete curves would be symmetrical about the median line of the coil, but only the halves on one side of that line are drawn. For currents of 0·35 amp. and upwards two neutral points lie on the axis of the coil, one on either side of the centre. They coincide at the centre for a current of 0·345 amp. For currents below this

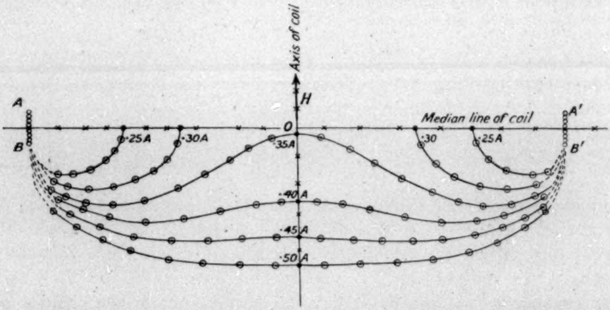

Figure 6. Circular coil of 8 turns, axis along earth's field. Current in direction producing field at centre opposed to earth's field *H*. N–S loci along axis of coil and its median line. The E–W loci are the curves marked ⊙. Neutral points marked • are on axis of coil for currents 0·35 A., 0·40 A., 0·45 A., 0·50 A., and on median line for currents 0·30 A. and 0·25 A. (Neutral points coincide at centre O of coil for calculated current 0·345 A.) Radius of coil 3·76″. (Upper half of complete figure, which is symmetrical about median line, is omitted.)

last value the two neutral points lie on the median line, on either side of the centre. There are two additional neutral points within the conductor.

Case 3. *Axis of the coil perpendicular to H.*—This case is given as an example of a less symmetrical setting of the coil with respect to the earth's field. Figure 7 shows (to half-scale) one branch only of each of the loci, thus determining one of the two external neutral points. The value of the current was 1 amp., and the coil was that used for the previous cases.

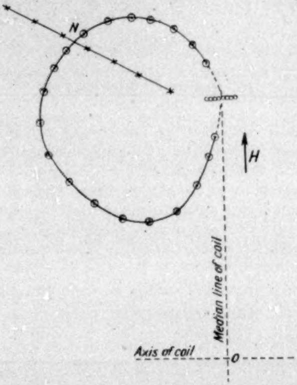

Figure 7. Circular coil of 8 turns, axis perpendicular to earth's field H. Current of 1·0 amp., producing field from west to east along axis. Only one branch of N–S locus (marked ×) and of E–W locus (marked ⊙) shown. Neutral point at N (the second neutral point should be on line joining N to centre O of coil, at equal distance on other side of centre.)

Note added in proof

Since this paper was presented, it has been noticed that there are two special lines of force which provide exceptions to the general rule enunciated in § 1. This pair of lines pass through the neutral point itself. They will be the subject of a brief paper to follow.

A DIFFERENTIAL METHOD OF ADJUSTING THE ABERRATION OF A LENS SYSTEM

By A. L. M'AULAY and F. D. CRUICKSHANK,
Tasmania

MS. received 25 *January* 1944

ABSTRACT. A method is described for computing a highly corrected camera lens system when the general type is given, and a rough design has been made.

The method separates into two parts. First, changes in the rays incident at any surface are expressed as functions of alterations of the surface constants ; secondly, the ray changes are transferred to the final image space and expressed as changes in the aberrations of the system. In this way a table is obtained by the use of which desired modifications of the aberrations can be achieved by suitable surface alterations.

§ 1. INTRODUCTION

The need for the manufacture of camera lenses of a wide range of characteristics became urgent in Australia in 1942. It was necessary to use the stocks of optical glass available in the country. Local requirements and facilities precluded the possibility of producing anything approaching a direct copy of overseas lenses, so that the general problem of design had to be faced. Preliminary work showed that an attempt to obtain the final design of a highly corrected lens system by successive ray tracings was unsystematic and slow. Such methods could not be tolerated in an emergency, and hence a new approach had to be found. It is believed that a considerable advance towards a faster and more systematic method of completing a rough design has been made, and a general outline of it is presented in this paper.

The method described has made possible the design and construction of highly corrected camera lenses from rough data which gave the type only. The work has been developed rapidly by a group with no previous experience in lens design. It is this technical success that gives the method merit. The method is a logical addition to the standard trigonometrical ray-trace, and serves to raise the whole status of the trigonometrical method to that of a powerful and systematic tool for use in the final stages of an optical design. It has been said that the trigonometrical method is empirical and uninstructive, but it will be shown that a most instructive analysis of any optical system can be made on the basis of a ray trace, and that, in particular, a complete and exact description of all the general tendencies of the system is readily available at the price of some computations which can be undertaken by computors without a knowledge of technical optics.

§ 2. THE BASIC PRINCIPLES OF THE METHOD

The primary object of a ray trace is to obtain an analysis of the aberrations of the system. The aberration measures are defined in terms of certain intersection points associated with selected traced rays in the final image space, as described, for example, by Conrady (1929). If the aberrations revealed by the trace of a rough design are too large, the designer's problem is to diminish them by appropriate changes in curvature, thickness, and refractive index within the system.

The ray trace provides a complete specification of the paths followed by the selected rays through the system. Suppose now that a change is made at surface i of the system. As a result, each of the selected rays will be refracted at this surface slightly differently, and their paths through the remainder of the system will differ from the original traced paths. Each ray will finally leave the last surface of the system at a point displaced a small distance from the emergence point of the corresponding traced ray, and in a direction inclined at a small angle to that of the traced ray. The intersection points associated with the emergent rays, and hence the aberrations of the system, will now be changed. The essence of the present method is the development of an analysis which will permit the computation of the aberration changes due to a small change made at any surface of the system. In doing this, the detailed information from the trace is used, and the traced path of each ray is used as a convenient reference frame relative to which is described the new path of the ray resulting from the particular change. For this purpose, certain auxiliary variables are chosen, and by means of changes in these, the new path of the ray can be described relative to the original path. For the variables of the trace generally we use the notation of Conrady (1929). Several sets of variables may be selected from among the quantities L, L', U, U', I, I', ... of the trace, and the relative merits of each set could be debated. The writers have found after some experience in the use of the method that the differentials dU, dU', dp, dp', as defined in the next section, are simple to use and lead to expressions which have certain advantages in computation.

§ 3. SPECIFICATION OF THE CHANGED RAY PATH AT A SINGLE SPHERICAL REFRACTING SURFACE

Suppose that the path of a selected incident ray is traced trigonometrically through a single spherical refracting surface. The ray path is specified by the quantities (L, U) and (L', U') and is represented by B P B′ in the figure.

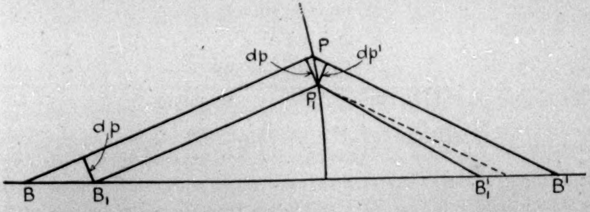

BPB′ is the traced ray path. Line through new incidence point parallel to traced refracted ray shown broken. Sin U and dp are negative, as shown.

Change in incidence point. Suppose that the incidence point of the ray is changed from P to P_1, the direction of the ray remaining unchanged. The path of the ray through the surface would now be represented by $B_1P_1B_1'$. We propose to specify the change in incidence point by the perpendicular distance, *dp*, between the two rays, the quantity being positive when the new parallel ray lies above the original. The new ray will have an intersection length $L+dL$, compared with L for the original path, and

$$dp = \sin U \,.\, dL. \qquad \ldots\ldots(1)$$

Notice that *dp* is not the total differential of the familiar quantity $L \sin U$. We are never particularly interested in the integral quantity p, except possibly in a formal way, but it is important to stress that relative to a given ray path, (L, U), which intersects the refracting surface, the quantity $dp = \sin U . dL$ uniquely defines a neighbouring incidence point.

On the other side of the surface it is natural to specify the same incidence-point displacement by another quantity, dp', which is the perpendicular distance between the original refracted ray and a line parallel to this drawn through the new incidence point. The relation between dp and dp' for small displacements of the incidence point is

$$dp' = (\cos I'/\cos I) \,.\, dp$$

or

$$\frac{\partial p'}{\partial p} = \frac{\cos I'}{\cos I}. \qquad \ldots\ldots(2)$$

Change of direction. A change in the direction of the ray incident at P is specified by dU, and the resulting change in the direction of the refracted ray by dU'. It will now be seen that any new path differing by small amounts in direction and in location of incidence point from the original ray-path can be specified relative to the original path by the quantities dp, dU, on the incidence side of the surface, and by the corresponding quantities dp', dU', after refraction at the surface.

§4. THE EFFECT OF SMALL CHANGES MADE AT A SINGLE SPHERICAL REFRACTING SURFACE

We consider now the effect on the direction of the refracted ray of various changes which can be made at a single surface at which an incident ray is refracted. Writing down the standard ray-tracing equations in the form

$$(L-r)\sin U = r \sin I, \qquad \ldots\ldots(3)$$

$$N' \sin I' = N \sin I, \qquad \ldots\ldots(4)$$

$$U + I = U' + I', \qquad \ldots\ldots(5)$$

we differentiate (4) and (5), putting $N/N' = n$, and obtain

$$dU' = dU - \left(n\frac{\cos I}{\cos I'} - 1\right) dI - \frac{\sin I}{\cos I'} dn. \qquad \ldots\ldots(6)$$

If the direction of the incident ray changes from U to $U+dU$, the change in the angle of incidence, I, is $dI = -dU$, and hence, from (6),

$$dU' = \frac{\partial U'}{\partial U} dU = dU - \left(n\frac{\cos I}{\cos I'} - 1\right)(-dU),$$

whence

$$\frac{\partial U'}{\partial U} = n\frac{\cos I}{\cos I'}. \qquad \ldots\ldots(7)$$

If the position of the incidence point is changed by an amount dp, the change in I, obtained by differentiating (3) with U and r constant, is

$$dI = \frac{\sin U . dL}{r \cos I} = \frac{dp}{r \cos I},$$

which, on combination with (6), gives

$$\frac{\partial U'}{\partial p} = \left(1 - \frac{\partial U'}{\partial U}\right) \Big/ (r \cos I). \qquad \text{......(8)}$$

For a small variation in the relative refractive index, n, equation (6) gives at once

$$\frac{\partial U'}{\partial n} = -\frac{\sin I}{\cos I'}. \qquad \text{......(9)}$$

If a small change is made in the curvature, c, of the surface, the change in I, obtained by differentiating (3) with U constant, is

$$dI = \frac{L \sin U}{\cos I} . dc,$$

which, on combination with (6), gives

$$\frac{\partial U'}{\partial c} = \left(1 - \frac{\partial U'}{\partial U}\right) \frac{L \sin U}{\cos I}. \qquad \text{......(10)}$$

§ 5. THE TRANSFER COEFFICIENTS

We consider next the problem of the effect on the complete ray-path of a small change made at one surface of a system of k spherical refracting surfaces. Suppose that the path of a selected incident ray has been traced through the system. After refraction at any surface i of the system, the ray-path is specified by the quantities L_i', U_i', in the usual way. A small change is now made at this surface such that the ray, after refraction at the same incidence point on the surface, takes a new direction specified by $U_i' + dU_i'$. The path of the ray through the remainder of the system will be different from the original traced path, and finally the ray will emerge from the last surface at a point displaced by some amount, dp_k', from the emergence point of the traced ray, and in a direction inclined at an angle, dU_k', to that of the traced ray. We may express dU_k' and dp_k' in terms of dU_i' by writing

$$dU_k' = \frac{\partial U_k'}{\partial U_i'} . dU_i', \qquad \text{......(11)}$$

$$dp_k' = \frac{\partial p_k'}{\partial U_i'} . dU_i'. \qquad \text{......(12)}$$

In a similar manner, if a small change is made at surface i resulting only in an incidence-point change, dp_i, the inclination angle, U_i, of the ray remaining unchanged, the ray will emerge from the last surface at a point and in a direction specified by some other values dp_k', dU_k', relative to the emergent traced ray. In this case we may write

$$dU_k' = \frac{\partial U_k'}{\partial p_i} . dp_i, \qquad \text{......(13)}$$

$$dp_k' = \frac{\partial p_k'}{\partial p_i} . dp_i. \qquad \text{......(14)}$$

The equations (11) to (14) define the *transfer coefficients* $\partial U_k'/\partial U_i'$, $\partial p_k'/\partial U_i'$, $\partial U_k'/\partial p_i$, $\partial p_k'/\partial p_i$, which can be calculated for a traced ray at each surface of the system. They determine the effect of a dU'-change or a dp-change made at any surface on the path of the ray as it leaves the last surface of the system. The transfer coefficients for dU'-changes and for dp-changes are the fundamental transfer quantities from which all others may be conveniently derived. It may be thought confusing to use the pair of differentials dU' and dp for the description of small changes in the system, one of these relating to a quantity before refraction and the other to a quantity after refraction of the ray at the surface, but in practice any change which is made in a system can be described in terms of either a single dU'-change or a single dp-change, so that the transfer coefficients selected are not only sufficient for the present problem, but also require less computation than any other set. It is to be stressed that what is in view is to fashion a powerful designing tool, considerations of mathematical elegance being sacrificed to this end.

It will be shown in a subsequent paper that certain relations connect the transfer coefficients at two successive surfaces of the system, such that if the values of the coefficients are known for surface $(i+1)$ the coefficients for surface i may be calculated from them. At the last surface of the system it is obvious that the transfer coefficients have simple values, for

$$\partial U_k'/\partial U_k' = 1; \quad \partial p_k'/\partial U_k' = 0,$$

while $\partial p_k'/\partial p_k$ and $\partial U_k'/\partial p_k$ are calculated from equations (2) and (8) respectively. The computation of the transfer coefficients can thus commence from the last surface and continue backwards, surface by surface, through the system until the first surface is reached.

§6. THE TRANSFER COEFFICIENTS FOR THE INTERSECTION POINTS

The next step in the development of the method is to determine the changes in the positions of the intersection points in the final image-space associated with the traced rays due to the differential changes made within the system. In a normal trace it is usual to select three rays of the axial pencil, the marginal, zonal and paraxial rays. Associated with these rays are the intersection points M(L_m', 0), Z(L_z', 0), Px(l', 0) of each of these rays with the principal axis, their positions being specified by rectangular coordinates relative to the pole of the last surface. Omitting the detail, given in a subsequent paper, it can be shown that

$$\frac{\partial L_m'}{\partial U_i'} = \left(\frac{\partial p_k'}{\partial U_i'} - S_k' \cdot \frac{\partial U_k'}{\partial U_i'}\right)_m \operatorname{cosec} U'_{mk} = (C_{U_i'})_m \operatorname{cosec} U'_{mk}, \quad \ldots\ldots(15)$$

$$\frac{\partial L_m'}{\partial p_i} = \left(\frac{\partial p_k'}{\partial p_i} - S_k' \cdot \frac{\partial U_k'}{\partial p_i}\right)_m \operatorname{cosec} U'_{mk} = (C_{p_i})_m \operatorname{cosec} U'_{mk}, \quad \ldots\ldots(16)$$

in which S_k' is the distance measured along the ray from the last surface to the intersection point, and the C-quantities are introduced as convenient abbreviations for the bracketed functions of the transfer coefficients in the first expressions. Corresponding expressions hold for the intersection points Z and Px.

For an oblique pencil it is usual to trace a set of three rays denoted by the symbols *a*, *pr*, and *b* in the Conrady notation. Associated with these rays are the points Ab(L'_{ab}, H'_{ab}), the intersection of the rays *a* and *b*; Pr(L'_{ab}, H'_{pr}), the point at which the principal ray cuts the plane through Ab at right angles to the axis; Prf(l', H'_{prf}), the point at which the principal ray strikes the plane through the paraxial focus at right angles to the axis. Finally, though not related to a traced ray, there is the ideal image point, Id(l', H_{id}). This point shows where the principal ray would strike the paraxial image plane if the paraxial value of the magnification held throughout the field.

For the point Ab it can be shown that

$$\frac{\partial L'_{ab}}{\partial U'_{ai}} = (C_{U_i'})_a \operatorname{cosec}(U_a' - U_b')_k \cos U'_{bk}, \qquad \ldots\ldots(17)$$

$$\frac{\partial H'_{ab}}{\partial U'_{ai}} = -(C_{U_i'})_a \operatorname{cosec}(U_a' - U_b')_k \sin U'_{bk}, \qquad \ldots\ldots(18)$$

with corresponding expressions for changes in the *b* ray.

For the points Pr, Prf, it follows similarly that

$$\frac{\partial H'_{pr}}{\partial U_i} = (C_{U_i'})_{pr} \sec U'_{prk}, \qquad \ldots\ldots(19)$$

$$\frac{\partial H^p{}_{rf}}{\partial U_i'} = (C_{U_i'})_{prf} \sec U'_{prk}. \qquad \ldots\ldots(20)$$

Exactly similar relations hold for the transfer coefficients for small *dp*-changes.

§7. THE TRANSFER COEFFICIENTS FOR ACTUAL SURFACE CHANGES

In an actual design, the variables at the disposal of the designer are surface curvature, refractive index, and the axial separation between successive surfaces. For our purposes the axial separation is best specified by the symbol *d*. In order to change the separation, d_i, between the surfaces $(i-1)$ and i by an amount ∂d_i, the surface i and all succeeding surfaces are moved through ∂d_i. From the equations of the preceding section it follows at once that for the axial points, M, Z, and Px,

$$\frac{\partial L'}{\partial c_i} = C_{ci} \operatorname{cosec} U_k'; \qquad \ldots\ldots(21)$$

for the point Ab,

$$\frac{\partial L'_{ab}}{\partial c_i} = [(C_{ci})_a \cos U'_{bk} - (C_{ci})_b \cos U'_{ak}] \operatorname{cosec}(U_a' - U_b')_k, \qquad \ldots\ldots(22)$$

$$\frac{\partial H'_{ab}}{\partial c_i} = -[(C_{ci})_a \sin U'_{bk} - (C_{ci})_b \sin U'_{ak}] \operatorname{cosec}(U_a' - U_b')_k; \qquad \ldots\ldots(23)$$

while for the points Pr, Prf,

$$\frac{\partial H_{pr}}{\partial_{ci}} = (C_{ci})_{pr} \sec U'_{prk} - \frac{\partial L'_{ab}}{\partial c_i} \tan U'_{prk}, \qquad \ldots\ldots(24)$$

$$\frac{\partial H'_{prf}}{\partial c_i} = (C_{ci})_{prf} \sec U'_{prk} - \frac{\partial l'}{\partial c_i} \tan U'_{prk}. \qquad \ldots\ldots(25)$$

Corresponding expressions for the transfer coefficients with respect to *n* and *d* are obtained by replacing *c* throughout by *n* or *d*. The *C*-quantities entering into these expressions are defined by

$$C_{ci} = C_{U_i'}(\partial U_i'/\partial c_i), \qquad \ldots\ldots(26)$$

$$C_{ni} = C_{U_i'}(\partial U_i'/\partial n_i), \qquad \ldots\ldots(27)$$

$$C_{di} = C_{p_i}(\partial p_i/\partial d_i). \qquad \ldots\ldots(28)$$

Direct differentiation of the expression for the ideal image-point yields the required expressions for the transfer coefficients for this point. Thus for an infinitely distant object

$$H'_{id} = -f' \tan U_{pr},$$

whence

$$\frac{\partial H'_{id}}{\partial c_i} = \frac{y}{u_k'^2} \tan U_{pr} \frac{\partial u_k'}{\partial u_i'} \frac{\partial u_i'}{\partial c_i}, \qquad \ldots\ldots(29)$$

U_{pr} being the inclination angle of the principal ray at the first surface. The differential coefficients involved are those normally computed for the paraxial ray. Similar expressions hold for the transfer coefficients with respect to n and d.

§ 8. THE TRANSFER COEFFICIENTS FOR THE ABERRATIONS

The last stage of the development can now be made by writing down expressions for the rate of change of each aberration with respect to the curvature, refractive index, and axial separation. Thus for the spherical aberration

$$\frac{\partial LA'}{\partial c_i} = \frac{\partial l'}{\partial c_i} - \frac{\partial L'}{\partial c_i}, \qquad \ldots\ldots(30)$$

for the curvature of the tangential field

$$\frac{\partial X_T'}{\partial c_i} = \frac{\partial L'_{ab}}{\partial c_i} - \frac{\partial L'}{\partial c_i}, \qquad \ldots\ldots(31)$$

for the tangential coma

$$\frac{\partial\, coma_T'}{\partial c_i} = \frac{\partial H'_{pr}}{\partial c_i} - \frac{\partial H'_{ab}}{\partial c_i}, \qquad \ldots\ldots(32)$$

and for the distortion

$$\frac{\partial\, dist'}{\partial c_i} = \frac{\partial H'_{id}}{\partial c_i} - \frac{\partial H'_{prf}}{\partial c_i}. \qquad \ldots\ldots(33)$$

If additional zonal and principal rays for the colours r and v, for which the system is achromatized, are traced, the chromatic aberrations can be brought into the general scheme, giving

$$\frac{\partial Lch'}{\partial c_i} = \frac{\partial L'_{zr}}{\partial c_i} - \frac{\partial L'_{zv}}{\partial c_i}, \qquad \ldots\ldots(34)$$

$$\frac{\partial Tch'}{\partial c_i} = \frac{\partial H'_{prr}}{\partial c_i} - \frac{\partial H'_{prv}}{\partial c_i}. \qquad \ldots\ldots(35)$$

Corresponding expressions hold for transfer coefficients with respect to n and d. A computation of these coefficients, which measure the aberration change per unit change in curvature, axial separation, and refractive index at any surface of the system, provides the designer with complete information for the final balancing of the aberrations of the system. It provides a very complete analysis of the tendencies of the system. The expressions given above cover the general aberrations deducible from the tracing of tangential rays. The method is capable of extension in various directions to include aberrations which are of special importance in particular cases.

The transfer coefficients developed for changes of refractive index refer to changes at one surface. In practice, any change of glass involves two surfaces. By compounding the effects of simultaneous changes at two surfaces we obtain a series of transfer coefficients giving the changes in the aberrations, other than the chromatic aberrations, for a refractive index change for any *component* of the system. The colour aberrations being particularly related to the dispersions of the glasses, we develop transfer coefficients for these aberrations with respect to dispersion changes. The transfer coefficients for glass changes form a most valuable part of the general machinery of the method.

A degree of freedom not so far discussed is the position of the diaphragm. The effect of a differential displacement of the diaphragm is easily described in terms of the transfer coefficients for *d*-changes at the first surface of the system. As an additional piece of information, the transfer coefficients for a *dp*-change of the principal ray at the first surface give the *t*-focus of the system.

§ 9. THE METHOD IN PRACTICE

As an example of the use of the foregoing method, a detailed account of one particular stage in the correction of a certain photographic lens is given. The example is chosen at random, but gives a fair idea of the order of accuracy of the method when a number of changes are made simultaneously, some of these being not of differential size. The trace of the rough design at the particular stage of development gave the aberrations in the first line of table 1, an axial pencil and two oblique pencils having been traced at 22° and 32° respectively.

Table 1

LA_m'	LA_z'	X'_{T22}	coma'_{T22}	dist'_{22}	X'_{T32}	coma'_{T32}	dist'_{32}
−1·256	−0·0600	−1·185	−0·0014	0·0085	−3·520	−0·1280	0·0150
−0·624	0·210	0·407	−0·0047	−0·0130	0·010	−0·0530	0·0840

The step undertaken at this stage was to attempt to reduce the heavy negative curvature of field at 22° and 32°, to improve the over-corrected spherical aberration, and to hold, if possible, the well-corrected coma and distortion at 22°. A study of the transfer coefficients of the system showed that there were surfaces providing opportunity for a general move in this direction. The surfaces selected had the coefficients given in table 2.

Table 2

Surface	LA_z'	X'_{T22}	coma'_{T22}	dist'_{22}	X'_{T32}	coma'_{T32}	dist'_{32}
1. $\partial/\partial c$	1879·3	1003·1	−19·19	82·68	1299·3	−6·24	284·64
4. $\partial/\partial c$	510·0	−707·9	−110·5	44·30	−1673·5	−181·3	166·96
5. $\partial/\partial d$	−0·0135	0·3417	−0·0035	−0·1013	0·2294	−0·0039	−0·3981
6. $\partial/\partial d$	−0·0075	0·7681	−0·0093	−0·0094	1·808	0·0034	−0·0479
7. $\partial/\partial d$	0·0025	−0·2663	0·0091	0·0772	−0·9908	0·0384	−0·2839

After a careful study of these coefficients, the following changes were made:

$$\delta c_1 = 0{\cdot}0001653, \quad \delta d_5 = -0{\cdot}613, \quad \delta d_7 = -0{\cdot}817;$$

$$\delta c_4 = -0{\cdot}0001987, \quad \delta d_6 = 1{\cdot}263.$$

The second line of table 1 gives the residual aberrations found by a trace of the system after alteration. The large amounts of curvature have been removed, rather overshooting the mark at 22°, the coma and distortion at 22° are still inappreciable, while the coma at 32° and the spherical aberration have moved appreciably in the right direction.

Although the coefficients are exact to first order for single changes of differential magnitude only, they give a very good approximation to the effects of a number of larger changes made simultaneously in the system. Naturally, it is to be expected that as the aperture of the system becomes greater the approximation to the aberration changes becomes less reliable, but a series of steps enables the correction to be carried out successfully.

REFERENCE

Conrady, 1929. *Applied Optics and Optical Design* (Oxford).

IMPERFECTIONS OF CRYSTAL LATTICES AS INVESTIGATED BY THE STUDY OF X-RAY DIFFUSE SCATTERING

By A. J. GUINIER,
Laboratoire d'essais du Conservatoire National des Arts et Métiers, Paris

MS. received 7 *April* 1945

ABSTRACT. A perfect crystal diffracts **x** rays only in discrete directions, given by the Bragg-Laue laws. All scattering observed in directions other than these, except Compton scattering, is due to imperfections of the crystal. The experimental method of obtaining useful scattering patterns and the principles of the calculation of actual structure from the distribution of anomalous scattering are described. Examples of application of this method to the study of thermal atomic movements, lattice deformations under mechanical stresses, defects of periodicity in diamond and in fibrous crystals, space-arrangement of atoms in solid solutions (order-disorder transformation, age-hardening) and scattering by small particles are briefly outlined.

§1. INTRODUCTORY

The theory of the diffraction of x rays by a small crystal is based upon the hypothesis that this crystal is strictly periodic, that is to say, any given atom and all its homologues are situated just at the nodes of a perfect geometric lattice. Then calculation shows that each system of the network of planes can reflect the incident rays according to the optical laws, but only for fixed incidence angles given by the well known Bragg law. In other directions, interferences annul the diffracted radiation. Thus a perfect lattice does not give rise to any scattering out of the selective reflexion directions, except for the continuous Compton scattering, which is very weak for the relatively long wavelengths we are considering. We may therefore enunciate the principle that *all diffuse scattering proceeds from some imperfections of the crystal lattice.*

Our purpose here is to show how this scattering is theoretically related to displacements of the atom, how it can be experimentally detected, and also to give a general survey of the various studies carried on in our Laboratory on this subject.

In the following theoretical treatment of the subject, we shall rely largely on a recent paper by Ewald (1940).

Let us consider a diffracting body (figure 1); let $\rho(\vec{x})$ be the electronic density at the extremity M of the vector $\vec{x}$; let $\vec{S}_0$ and $\vec{S}$ be the unit vectors along the incident and diffracted rays, and let us call $\vec{b}$ the vector $\frac{\vec{S}-\vec{S}_0}{\lambda}$. If A_e is the amplitude of the wavelet diffracted by one electron, according to the Thomson formula, the amplitude of the wave diffracted by the whole body is

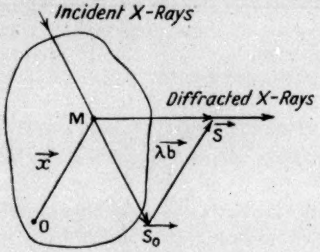

Figure 1. Diffraction of x rays.

$$F(\vec{b}) = A_e \iiint_{(v)} \rho(\vec{x}) e^{-2\pi i \vec{b}.\vec{x}} dv_x. \qquad \ldots\ldots(1)$$

This equation states that $\frac{F(\vec{b})}{A_e}$ is the Fourier transform of $\rho(\vec{x})$, being defined for all vectors $\vec{b}$ of a space, called the *reciprocal space*. The formula (1) permits the calculation of the diffraction pattern for any given distribution of matter in the diffracting body.

If $\rho(\vec{x})$ is a periodic function, i.e. if the crystal lattice is perfect, $F(\vec{b})$ is zero at every point of the reciprocal space, except at a set of points which are the nodes of the reciprocal lattice, each one corresponding to the selective reflection upon one set of reticular planes. This is another and more general form of Bragg's law. If on the other hand the crystal is perturbed, $\rho(\vec{x})$ is no longer periodic, and $F(\vec{b})$ has a finite value for any vector $\vec{b}$. In fact, the lattice imperfections we consider are small perturbations of the perfect lattice. Then, as for a perfect crystal, the function $F(\vec{b})$ remains considerable at the nodes of the reciprocal lattice, but now is not zero between these points. This corresponds to the scattering observed in addition to the Bragg-Laue spots, due to the normal selective reflexions.

The experimental problem consists in finding $\rho(\vec{x})$ from measurements of the scattering. Let us direct a monochromatic beam upon the sample studied, *fixed* during the exposure. The photometry of the pattern gives the values of the scattered intensity in all directions $\vec{S}$, the direction of the incident beam being $\vec{S_0}$. The results of the experiment can be easily interpreted by means of the Ewald construction (figure 2). The intensity scattered in any direction $\vec{S}$ gives the absolute value of $F(\vec{b})$ at the corresponding point of the reflexion sphere; each experiment gives a section of the reciprocal space. By varying the orientation of specimens in repeated experiments, it is possible to find the modulus of $F(\vec{b})$ at every point of a large part of the reciprocal space.

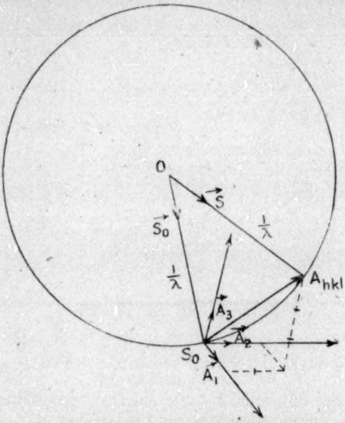

Figure 2. Ewald's construction.

These are the experimental data. How can one determine $\rho(x)$ from these data? Mathematically, $\rho(\vec{x})$ is found by the inversion of the Fourier integral (1),

$$\rho(\vec{x}) = \frac{F(\vec{b})}{A_e} \iiint e^{+2\pi i \vec{b}.\vec{x}} dv_b, \qquad \ldots\ldots(2)$$

the integral being extended over the whole reciprocal space. Therefore, theoretically, if $F(\vec{b})$ is known, $\rho(\vec{x})$ is known too. But the experiments give only the absolute value $|F(\vec{b})|$. One finds here a difficulty which is typical of the study of crystal structures by means of x-ray diffraction; in fact, there is no general method of working out the data of the scattering patterns. The calculations must be adapted to each case.

The existence of some diffuse scattering in addition to the selective reflexion is a proof of some lattice imperfections, but an accurate determination of these imperfections is not easy. We cannot deal here with the mathematical calculations involved. We will only show what results can be obtained. But, as an example, we shall give the application to a particular case of a general method of calculation, similar to Patterson's method used in the study of structures.

§ 2. THE EXPERIMENTAL PROCEDURE

What are the conditions necessary for obtaining useful scattering patterns ? First of all, the anomalous scattering is generally very weak when compared to the selective reflexion. Moreover, the scattering areas may be very extensive and possess complicated forms. It follows that:

1. The method must be such that crystals with perfect lattice do not give any scattering, except the Compton scattering; secondary fluorescence radiation, and scattering originating outside the specimen, must be eliminated. Above all, the incident radiation must be strictly monochromatic, for, if the principal radiation were accompanied by a continuous spectrum, the diffraction effects of the latter would be much greater than the scattering to be studied.

2. In spite of the monochromatization, the incident beam must be very intense, for the phenomena we are looking for are very weak.

3. In most cases the sample must be a single crystal held in a fixed position during the exposure. With polycrystalline samples, the scattering observed in each direction is an average value and the pattern becomes generally very difficult to interpret. To sum up, for a scattering pattern, one must use a *monochromatic beam* and an *immovable crystal.* The conditions are then quite different from those of ordinary diffraction patterns, where either the crystal is immovable but the beam polychromatic, or the crystal is rotated and the beam monochromatic. To obtain a beam which is both monochromatic and intense, we use an apparatu (figure 3) which we shall now describe very briefly (Guinier, 1939 a). The

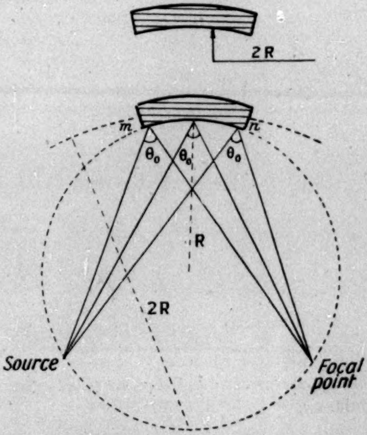

Figure 3. Reflexion by a cut and bent crystal.

monochromator is a bent quartz crystal which gives a reflected beam, monochromatic and convergent, with an aperture angle of 2 or 3°. We use a lamella, cut and bent, as described by Johansson (1933), so that the focusing of the reflected beam is theoretically accurate. The X-ray source is the very sharp focus of a tube, with a target parallel to the monochromator crystal.

The diffraction camera is designed in order to use the whole energy of the convergent beam with the greatest efficiency. For instance, to make a Debye-Scherrer pattern, the photographic film and the sample are on the same cylinder as in Seeman-Bohlin's device (figure 4 *a*). Thus the lines are very sharp, whatever the aperture of the incident beam through the sample. Figure 5 gives some examples of such patterns: the time of exposure is the same as with an ordinary Debye-Scherrer camera.

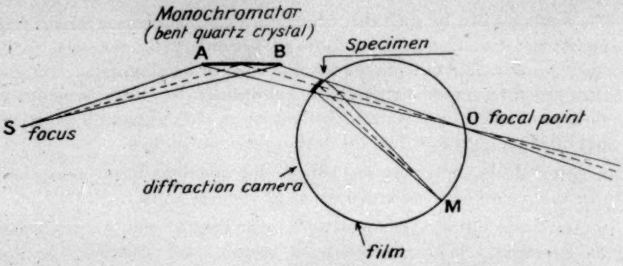

Figure 4 *a*. Device for powder patterns with monochromator.

For single crystal patterns it is not sufficient to record the scattered rays only in the equatorial plane: the sample is on the axis of a cylindrical camera placed in such a way that the monochromatic beam converges on a point of the cylindrical film (figure 4 *b*). Focusing is not obtained with mathematical accuracy, but in the central part of the pattern the spots are at least as well defined as in a usual pattern. The whole apparatus can be placed in an evacuated box, in order to avoid scattering by the air.

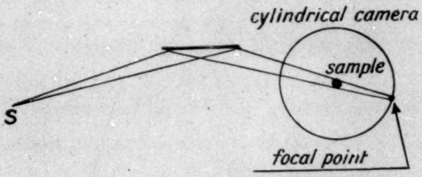

Figure 4 *b*. Device for rotating-crystal patterns.

§3. SOME APPLICATIONS OF THE STUDY OF X-RAY SCATTERING

We may now review some examples of lattice imperfections which produce anomalous scattering. They are of various kinds, but not every lattice imperfection produces observable scattering. One can only study by this method perturbations which extend over a large part of the crystal. For instance, it is

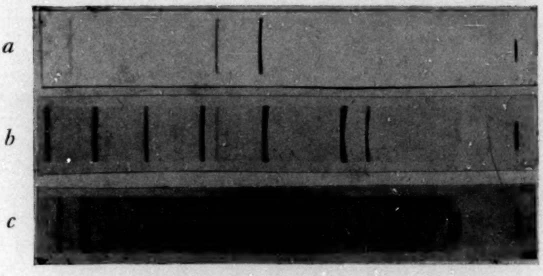

Figure 5. Powder patterns with monochromatic CuKα radiation.

(*a*) Nickel foil (exposure, 5 min.).
(*b*) NaCl.
(*c*) Aluminium alloy with a small amount of Al_2Cu.

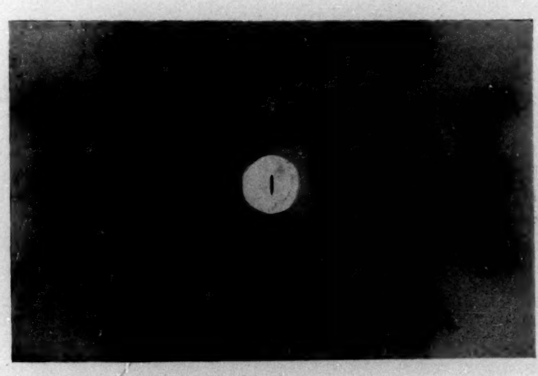

Figure 6. Thermal scattering pattern: lamella of KCl parallel to (100) plane, normal to the incident x ray (exposure, 6 hours).

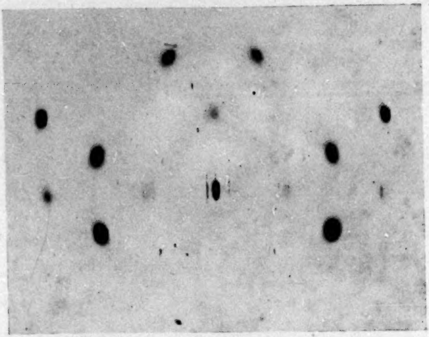

Figure 7. Scattering pattern by an aluminium crystal after a 30% extension.

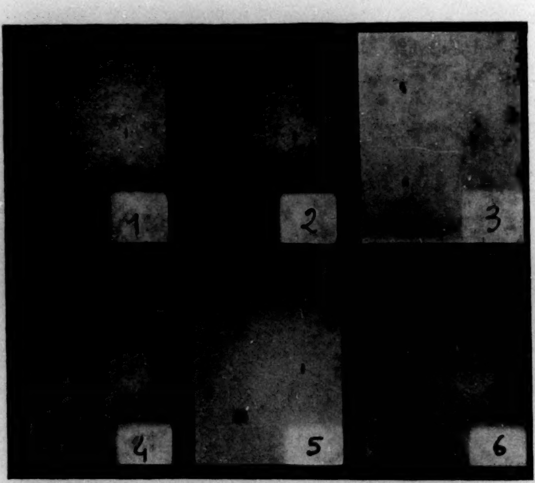

Figure 10. Anomalous scattering by diamond (with MoKα radiation). The Bragg spots 111 and $11\bar{1}$ appear in photograph no. 3. From this position the crystal is rotated around the 001 axis.

(111) Nodes inside the reflexion sphere {no. 1 rotation, 4°·5).
no. 2 rotation, 1°·5).

(111) Nodes outside the reflexion sphere {no. 4 rotation, 1°·0).
no. 5 rotation, 3°·5).
no. 6 rotation, 5°·5).

not possible to distinguish a perfect crystal from a mosaic crystal, because the latter is formed by a collection of small blocks joined together with slight disorientations, each block having a perfect lattice, so that the disturbed regions represent too small a volume of the whole crystal.

Thermal motions of atoms

A first type of lattice imperfection, very important on account of its general occurrence, is the thermal agitation of atoms. Every crystal lattice, at every temperature, presents this kind of imperfection. Thus, on all scattering patterns, the "thermal" scattering is visible to a greater or less extent. This scattering, though observed many years ago by a great number of authors, has only recently been carefully studied. Now there is a considerable amount of literature on this subject.* It is the most important, and the most generally known, of lattice imperfections investigated by x-ray scattering. One of the aims of this paper is to show that there are other various kinds of imperfections revealed by the same method. It is not possible, here, to enlarge upon this very extensive and somewhat difficult subject; we will only reproduce some photographs (figure 6) obtained with the apparatus above described. The interesting feature is that they are obtained with quite short exposures. For the photograph of NaCl, the time of exposure is 6 hours, whilst a similar pattern obtained by Gregg and Gringrich (1941) with a plane crystal monochromator required 100 hours.† The results of the study of thermal scattering are, mainly, the determination of the elastic constants of crystals and the comparison of the propagation velocities of the elastic waves in different directions, these two factors determining the atomic movements in the crystal. Thus, x-ray scattering now becomes an important method for the study of the elastic properties of solids.

Lattice deformations under mechanical stresses

A monocrystalline aluminium wire is progressively extended by traction. Gliding occurs upon one or many sets of (111) planes. It is well known that during this process the crystal undergoes rotations and, in addition, asterisms appear on Laue patterns, because the differences of the orientations of the mosaic blocks grow larger. We attempted to discover some perturbations inside the individual blocks by studying the scattering patterns. The pattern of figure 7 corresponds to a 30% extension of the wire: *it is identical with the pattern obtained before distortion*: the only new feature is the appearance of faint Debye-Scherrer spots in addition to the diffuse spots due to the thermal agitation. This result, though negative, is interesting. One might have imagined that, whilst gliding, the successive glide-planes would be displaced parallel to themselves with some irregularities. If this hypothesis had been true, we should have seen the diffraction pattern of the two-dimensional lattices of aluminium planes (111). This pattern is formed by anomalous spots corresponding to the intersection of the reflexion sphere with the (111) axes of the reciprocal lattice. We have never succeeded in observing any such spots. We think therefore that, whilst gliding, blocks comprising a considerable number of (111) planes move together and remain without internal defects. Gliding takes place upon a few planes far apart: thus the perturbed domains have too small a relative volume to scatter more than a negligible amount of energy. In regions where the atomic disorder is too great, the metal recrystallizes; the newly formed microcrystals give rise to the Bragg spots, visible on the photograph. Thus, during the deformation of the wire, the monocrystal is broken into several crystals, but no lattice deformations of these new crystals can be revealed by the x-ray scattering.

---

* See, for example, *Proc. Roy. Soc.* A, August 1941.

† Private communication.

Defects of periodicity in crystals

One-dimensional defects. An example is given by the anomalous scattering of diamonds (Lonsdale, 1941; Raman, 1941; Guinier, 1942 a).

Let us consider a lattice as a set of identical planes parallel and regularly spaced. Each of these planes gives, for all incident rays, a diffraction pattern. On account of the perfectly regular spacing of successive planes, these patterns vanish completely by interference, except for the special directions which correspond to the selective reflections. But, if the interplanar spacings were distributed at random, the diffraction pattern of the whole would be that of a unique plane. What is it? Let us construct the reciprocal lattice of the two-dimensional lattice: the scattering zones in the reciprocal space are the rows normal to the plane, passing through the nodes of the plane reciprocal lattice.

In fact, however, in actual disturbed lattices, the subplanar spaces do not take all possible values but vary over a range which remains near the value of the perfect lattice; furthermore, sets of normally spaced planes can persist. Consequently, the reciprocal space contains, firstly, the nodes of the reciprocal space of the ideal lattice, corresponding to a strong diffracted intensity, and secondly, zones of low intensity, corresponding to the patterns of the plane lattice, along the rows defined above. The scattered intensity varies along the row in accordance with the distribution of the interplanar spacings. As an example of the interpretation of a scattering pattern, we shall show how a statistical scheme of the irregularities of the perturbed planes may be deduced from the variations of the scattered intensity.

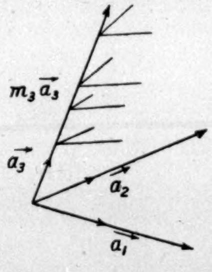

Figure 8. Succession of (001) planes slightly displaced.

Consider a lattice built upon the three axes $\vec{a}_1$, $\vec{a}_2$, $\vec{a}_3$. We suppose the successive (001) planes to be displaced along the direction $\vec{a}_3$ (figure 8). The coordinates of any atom (structure factor f) are $m_1 \vec{a}_1$, $m_2 \vec{a}_2$, $m_3 \vec{a}_3$, *but only* m_1 *and* m_2 *must be integers.* Let M_1, M_2, M_3 be the number of unit cells along the three axes, in the diffracting body. The scattered intensity is:

$$I = f^2 \left[\sum_0^{M_1} \sum_0^{M_2} \sum_0^{M_3} e^{-2\pi i(\vec{b}\,.\,m_1\vec{a}_1 + \vec{b}\,.\,m_2\vec{a}_2 + \vec{b}\,.\,m_3\vec{a}_3)} \right]^2. \qquad \ldots\ldots(3)$$

We put x_1, x_2, x_3 for the coordinates of $\vec{b} = \dfrac{\vec{S} - \vec{S}_0}{\lambda}$ in the reciprocal space, referred to the axes of the reciprocal lattice $\vec{A}_1$, $\vec{A}_2$, $\vec{A}_3$. Thus,

$$\vec{b} = x_1 \vec{A}_1 + x_2 \vec{A}_2 + x_3 \vec{A}_3.$$

Substituting in equation (3),

$$I = f^2 \left| \sum_0^{M_1} e^{-2\pi i x_1 m_1} \right|^2 . \left| \sum_0^{M_2} e^{-2\pi i x_2 m_2} \right|^2 . \left| \sum_0^{M_3} e^{-2\pi i x_3 m_3} \right|^2 .$$

In the first two factors, m_1 and m_2 are integers: thus they are only different from zero if x_1 *and* x_2 *are integers.* This means, as we have stated above, that the vector $\vec{b}$ must terminate on one of the reciprocal lattice rows parallel to $\vec{A}_3$. If this condition is fulfilled, the intensity is

$$I = f^2 M_1^2 M_2^2 \left| \sum_0^{M_3} e^{-2\pi i x_3 m} \right|^2,$$

or

$$I = f^2 M_1^2 M_2^2 \; \Sigma_{m_3} \Sigma_{m_3'} \, e^{-2\pi i x_3 (m_3 - m_3')}$$

$$= 2f^2 M_1^2 M_2^2 \, \Sigma\Sigma \cos 2\pi x_3 \,.\, \Delta m_3 m_3'. \qquad \ldots\ldots(4)$$

$\Delta m_3 m_3'$ represents the absolute value of the difference in ordinate between the two reticular planes m_3 and m_3', the unit of length being $|\vec{a}_3|$. On an axis OZ, we plot from the origin O a segment equal to $\Delta m_3 m_3'$ for each pair of reticular planes of the actual crystal. The total number of points is M_3^2. Let $f(z)$ be the linear density at abscissa z, i.e. $f(z)dz$ is the number of points lying between z and $z + dz$.

The sum (4) can be replaced by the integral

$$I = 2f^2 M_1^2 M_2^2 \int_0^\infty f(z) \cos 2\pi x_3 z \, dz. \qquad \ldots\ldots(5)$$

This formula determines the scattered intensity I along a row of the reciprocal lattice, when the spacing of the planes, or $f(z)$, is known. Conversely, after inversion, this Fourier integral gives $f(z)$ as a function of I, that is to say, as a function of the scattered intensity which is measured in the experiment. In this method *the amplitude of the scattered radiation does not appear*: the difficulty encountered in the general method (formula 2) is avoided. $f(z)$ is proportional to

$$\int_0^\infty I(x_3) \cos 2\pi x_3 z \, dx_3. \qquad \ldots\ldots(6)$$

Thus photometric measurements of scattering patterns lead to an accurate knowledge of the perturbations of reticular planes by means of the function $f(z)$.

As an example, let us assume that the spacing of two neighbouring planes remains close to the theoretical value but that the perturbations are accumulated from cell to cell, so that the difference between the ideal and actual spacings of two planes grows larger with increasing distance between them. What is the form of $f(z)$? At first, M_3 points meet at the origin. If the crystal were perfect, the M_3-1 spacings between consecutive planes would give M_3-1 points at $z=1$: actually, these M_3-1 points are grouped about this value. The curve $f(z)$ shows a narrow maximum about $z=1$. The spacings between every second plane are grouped about $z=2$, but they diverge rather more: the second maximum is wider and lower than the first, etc. When z is big enough, $f(z)$ tends towards a constant value. There is no long-range order. Figure 9 gives a schematic function of this type. The corresponding variation of I, according to the formula (5), is plotted below. The scattered intensity presents maxima for $z=1$, 2, etc., that is to say, about the nodes of the reciprocal lattice of the perfect crystal. The scattering is chiefly observed *around the node of index* 1 and is *weaker for greater indices*. Furthermore, it is symmetrical on each side of the node.

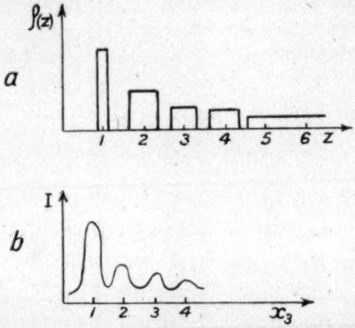

Figure 9. (*a*) Successive interplanar spacings ; (*b*) diffracted intensity plotted against the ordinate along the rows (001).

Scattering of this type has been effectively observed in the case of diamond by several physicists. When the crystal is so directed that a (111) node is near to the reflexion sphere, three faint but distinct spots are visible on the pattern (figure 10) around the point where the (111) diffraction spot would appear. They become fainter and diverge from each other as the distance from the node to the sphere increases. These three spots correspond to the intersection of the sphere with the three rows parallel to the cubic axes passing through the (111) node. From the above considerations we conclude that diamonds contain regions where the planes parallel to the faces of the cubic cell are irregularly displaced ; and since the scattering is localized near the reciprocal lattice nodes, and mainly near the 111 nodes, the deformations must be of the general type described above: this conclusion is the direct and geometrical result of the experiment.

What can be the origin of these structure irregularities ? They seem to be peculiar to the diamond, and especially to one of the two kinds of diamond (type II). Friedel (1924) has shown that there is an allotropic transformation of the diamond at a very high temperature. This second form of unknown structure is not stable at ordinary temperatures. Let us assume that this second form is produced from diamond crystals by moving (100) planes without perturbations of the atoms in these planes. Then the disturbed regions of diamonds revealed by anomalous scattering would appear as regions where the allotropic transformation to the diamond form is stopped at an intermediate stage. In the study of some alloys we encounter such phases with imperfectly periodic structure, intermediate between two well-known crystalline forms. In the case of the diamond, one of the lattices is unknown, so that the explanation is still only hypothetical.

Two-dimensional defects: example of fibrous crystals

Let us consider the crystalline lattice as a set of parallel rows and let us suppose that, without the disposition of atoms along these rows being disturbed, they are slightly displaced by irregular translations.

In this case it is the diffraction pattern of the *one-dimensional lattice* of the fibres which can be observed. These fibres being normal to the monochromatic incident x rays, this pattern is formed by the well-known " layer lines " of the fibrous crystal patterns. In the perfect crystal patterns, these layer lines are only made visible by the succession of discrete diffraction spots; but, for imperfect crystals, the latter lines are formed by continuous streaks. This phenomenon is observed with some fibrous substances, as in the case of *asbestos*. Figure 11 is a pattern of chrysotile, obtained with CuKα radiation. It must be noticed how essential is the use of pure monochromatic radiation, for the continuous spectrum would also produce streaks on the central line. A striking feature is that the intensity of the streak is not constant along the whole lines. Streaks start from some diffraction spots, but not from all spots, and on one side only: they are directed towards large diffraction angles. This proves that the perturbations of the fibre are not distributed at random. Aruja, who has also obtained these patterns with chrysotile, thinks that complete sheets of fibres are displaced in some directions. His hypothesis is verified by the photometric measurements of the streaks, and this work is a good example of the accurate information of real crystal structures obtainable by careful study of diffuse scattering.

§4. ARRANGEMENT OF THE ATOMS IN A SOLID-SOLUTION CRYSTAL

Order-disorder transformation

A crystal of an ideal solid solution is to be imagined as formed by a perfectly regular lattice, at the nodes of which two kinds of atoms are distributed at random. The periodicity is then rigorous for the *positions* of atoms, but not for their diffracting power (or structure factor): this latter lack of periodicity is a cause of scattering. Let a crystal contain N atoms: $p_A N$ of these are of type A and have a structure factor f_A, and $p_B N$ are atoms of type B and have a structure factor f_B.

Von Laue has shown that the solid-solution crystal gives rise, on one hand, to the diffraction pattern of a crystal with the same lattice, all the nodes of which are occupied by a unique fictitious atom of structure factor $p_A f_A + p_B f_B$, and, on the other hand, to a diffuse scattering, the intensity of which is

$$I = N p_A p_B (f_A - f_B)^2.$$

This formula depends only on the scattering angle, but not on the crystal orientation; it shows a maximum in the direction of the incident beam, as in the case of a gas. Laue's calculations have not previously, I believe, been experimentally verified. We have undertaken this verification and have chosen, for this purpose, the equiatomic gold-silver alloy, because of the advantages that the two atoms have very different structure factors but almost equal radii: thus, for any atomic distribution, the lattice deformations remain very small.

The patterns we have obtained are in opposition to Laue's theory. The scattering presents no maximum at the centre of the pattern. The lower curve of figure 12 represents the scattering of a sample formed by two distinct sheets of pure gold and pure silver. It is mainly due to the thermal effect. The upper curve represents the scattering by a sheet of the Au–Ag alloy, and the dotted curve the scattered intensity according to the Laue's formula. If the latter were correct, the observed curve would be nearly the sum of the lower and the dotted one. But it is not true. There appears a faint and wide ring, the maximum of which lies at the place of the 100 line of the crystal. The intensity of this ring is of the same order of magnitude as the maximum intensity given by Laue's formula.

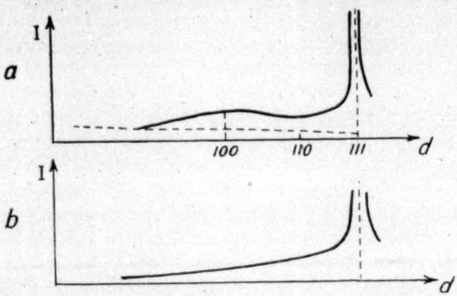

Figure 12. Intensity of scattered radiation from an Au–Ag alloy. (*a*) Au–Ag alloy; (*b*) metals Au+Ag.

Hence Laue's hypothesis is not valid, i.e. the *two kinds of atoms are not distributed at random*. Probably a silver atom, for instance, tends to be surrounded by gold atoms and vice versa. In a face-centred cubic lattice of parameter a, an atom, say an Ag atom, has 12 neighbours at a distance of $a/\sqrt{2}$, then 8 at a, and so on. If the Ag and Au atoms were distributed at random there would be (6 Au and 6 Ag) at $a/\sqrt{2}$, (4 Au and 4 Ag) at a, etc. Actually there must be fewer Ag atoms among the first neighbours and more in the second, that is to say, there is, between two neighbouring Ag atoms, a preferred spacing, as between two molecules in a liquid. The effects upon the scattering pattern will be similar; a ring appears at an angle which corresponds to this preferred distance: in the case considered it is the distance a, that is to say, the (100) spacing, which explains our experimental results.

The scattering pattern seems to show that perfect disorder in a solid solution does not exist: however, no ordered super-lattice has ever been found in Au–Ag

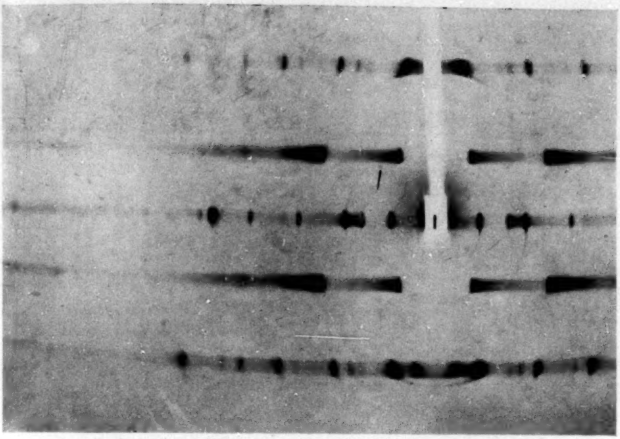

Figure 11. Scattering pattern of chrysotyle (CuKα radiation).

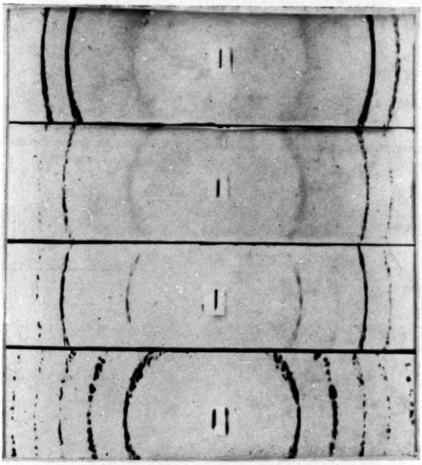

Figure 14. Scattering patterns of Au–Cu_3 alloys.

Scattering patterns of annealed samples.

(1) Annealed, 2 hours at 100° c.
(2) Annealed, 2 hours at 250° c.
(3) Annealed, 2 hours at 300° c.
(4) Annealed, 2 hours at 350° c.

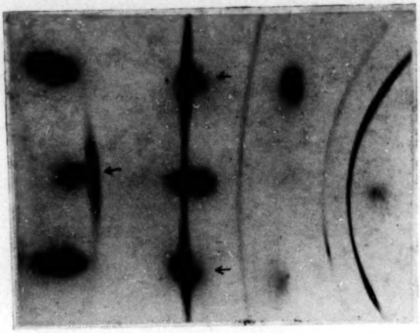

Figure 17. Scattering pattern of AuCu$_3$ crystal (surrounded by microcrystals). The arrows show the scattering zones around normal nodes.

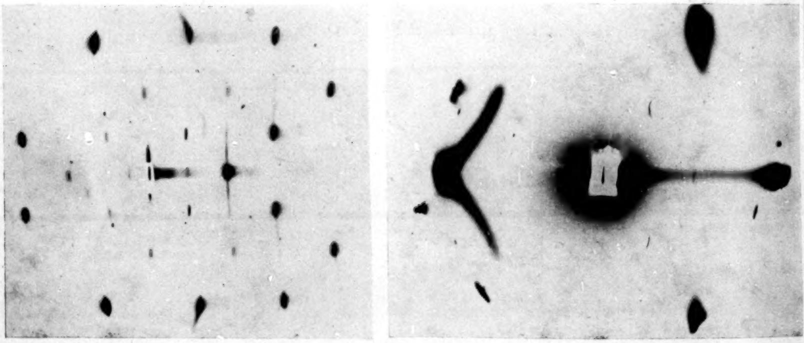

a *b*

Figure 18. Scattering patterns of age-hardened alloys : (*a*) Al-Cu alloy ; (*b*) Cu-Be alloy.

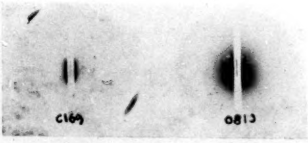

a *b*

Figure 19. Small-angle scattering by charcoal: (*a*) before activation ; (*b*) after activation.

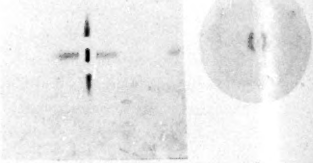

a *b*

Figure 20. Small-angle scattering by age-hardened alloys : (*a*) Al-Cu ; (*b*) Al-Zn.

alloys. But, even in this case, the nature of an atom has some influence on that of its neighbours: there exists what Bethe has called *short-range order*, but to a small extent. We have also investigated an alloy which can take an ordered form, namely $AuCu_3$. In its disordered state (quenched) one finds also on its scattering pattern a broad ring, as in the case of Au–Ag, but notably more intense (figure 13). Even in this case there is no perfectly disordered state at room temperature, and the degree of short-range order is greater than in the case of Ag–Au. Experiments are now being carried out to see whether the same applies above the critical temperature.

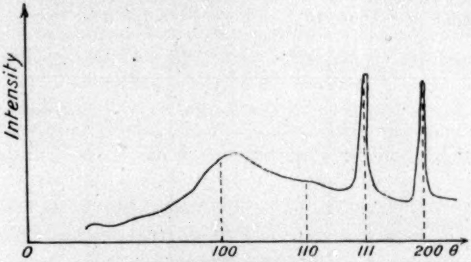

Figure 13.—Scattering patterns of Au–Cu_3 alloys. Scattered intensity from a quenched sample.

Let us consider next the transformation from the disordered to the ordered state: during the annealing of the alloy this change is quite progressive on the pattern (figure 14); the broad ring splits into two distinct lines, the one at the (100) position and the other at the (110). These two rings, at first diffuse, become narrower and more intense; at the same time, rings of higher indices make their appearance. Sykes and Jones (1936), studying these phases of transformation, concluded that the lattice was formed by juxtaposition of small domains which are ordered, but out of phase. Let us give an example in the schematic case of a one-dimensional lattice and an equiatomic mixture of A and B. The lower line of figure 15 shows the ordered state and the upper line a partially ordered state, with several elementary ordered domains; thus, the normal lines are not modified and the superstructure lines are broadened by the well-known effect of small-size crystal. With further ordering, the elementary domains grow larger, and the lines become more distinct. We think that such a representation is far too simplified when applied to the earlier stages of the

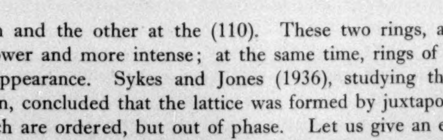

Figure 15. (*a*) Perfect order ; (*b*) partial order with out-of-phase domains.

ordering process. A more accurate theory of the patterns will link the scattering with the parameter measuring the short-range order. Let us consider again the case of a one-dimensional lattice, a row of N equally spaced atoms with a period 1, which comprises $N/2$ atoms A and N/2 atoms B. The short-range order can be defined by the probability, τ, that any atom may have a neighbour of the same nature; τ varies from $\frac{1}{2}$ to 0 when the lattice passes from the perfectly disordered to the perfectly ordered state. The scattering pattern can be calculated throughout as a function of τ (figure 16). For $\tau = \frac{1}{2}$ one finds the lines of a disordered lattice (period 1) and a continuous background given by Laue's formula. As τ tends to 0, the scattering intensity presents maxima, midway between successive diffraction lines. These maxima become higher and narrower as τ decreases. When τ equals 0, the superstructure lines take the place of what were scattering maxima. These considerations conform with the observed phenomena in the case of a three-dimensional lattice. Thus, the scattering patterns are proved to be a new experimental tool for the quantitative study of order in solid solutions.

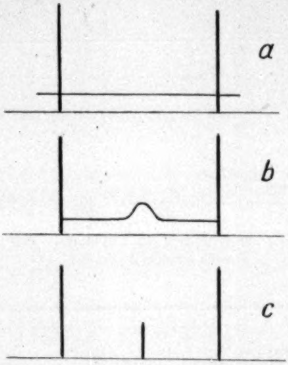

Figure 16. Scheme of scattered and diffracted intensity.
(*a*) Perfect disorder ; (*b*) partial order ; (*c*) perfect order.

Up to the present, we have presumed that the solid-solution lattice, ordered or not, was perfectly regular. But this is probably not generally true. The irregular distribution of atoms of different volumes produces lattice deformation. This is shown by the scattering pattern of a monocrystal of $AuCu_3$ alloy. As has already been mentioned, the scattering zones around the superstructure nodes are due to a partial order: but no distribution of atoms can explain scattering zones about the normal lattice nodes (see figure 17). These are produced by lattice distortion. It is well known that ordering is often accompanied by the transformation of the cubic lattice into a tetragonal one. This transformation is also progressive, and in the intermediate state the lattice is no longer perfectly periodic, leading to the appearance of anomalous scattering.

Thus, in the study of order-disorder transformation, x-ray scattering has revealed two new features: the short-range order in the so-called "disordered state", and the geometrical lattice deformations.

Age-hardening

Another very interesting kind of solid solution is one containing an excess of one kind of atom, and which is capable of age-hardening. The dissolved atoms, in excess, tend to form a precipitate with a distinct crystalline structure. But before the appearance of the precipitate, the properties of the alloy, mechanical, electrical, etc., have been changed, although microscopic examination does not reveal any crystal modification. This is the phenomenon of age-hardening. The scattering patterns give a very detailed view of the process of precipitation. The first results, in that field, were obtained in 1938 for Al-Cu alloys independently by Preston and by Guinier. Since then, other alloys have been studied by different authors: I have worked especially (1942, 3, 4) on Al-Ag, Al-Zn, Cu-Be alloys. The results of these studies, too, are of great theoretical and practical value in this section of metallography. It is, of course, very interesting to know the actual nature of those lattice perturbations which increase the mechanical strength of metals. Figure 18 shows some examples of scattering patterns corresponding to successive stages of the age-hardening process.

§ 5. SCATTERING BY SMALL PARTICLES

We shall consider finally one more kind of lattice imperfection. The directions of the selective reflection are only defined if the crystal is large enough. When it is very small (dimension less than 500 A.), each node of the reciprocal lattice is replaced by a small region surrounding it: accordingly, the lines of a Debye-Scherrer pattern are broadened. This effect has been extensively studied, and it is possible to determine the size of the particle from the width of the Debye-Scherrer lines. These studies can be carried out with an ordinary camera and polychromatic radiation.

The origin of the reciprocal lattice is also a node: it is, then, also surrounded by a small scattering zone, when the crystal is very small. That is to say, a sample formed by small crystals produces some *scattering at very low angles*. The study of this central scattering is more difficult than that of the broadening of the Debye-Scherrer lines: the use of a monochromatic radiation is advantageous, and the bent crystal monochromator is particularly convenient (Guinier, 1939 b, 1943 b). But, on the other hand, the central scattering gives more useful information: it is independent of the internal structure of the particle—it depends only on the size and the shape of the particle. It follows that the method can be used also for *amorphous substances*. The central scattering is characteristic of the divided state of matter. For instance, figure 19 shows two photographs relating to similar samples of charcoal, but the second is activated charcoal. The central spot is broad (3 or 4°), which proves that, after the activation treatment, the matter is in a very finely divided state.

In the age-hardening alloys, the atoms of the solute, before precipitation, gather into small clusters dispersed in the crystal of solid solution. These clusters produce central scattering, and then the size and shape of these submicroscopical clusters can be determined. Figure 20 gives two examples, the first concerning Al-Cu (Guinier, 1942 a) and the second Al-Zn (Guinier, 1943 a).

§ 6. CONCLUSION

The Bragg-Laue theory and the X-ray diffraction patterns relate only to the ideal geometric lattice. In our knowledge of the structure of the solid state they form a first approximation. Next, physicists try to build a model of the actual crystal and are more and more concerned with lattice imperfections. The disturbed lattice is very often encountered, especially in the case of alloys. The study of the diffuse scattering, produced by some kinds of lattice imperfections, is in many cases a very useful experimental method. In this brief review we have attempted above all to show how varied are the fields of application of the scattering patterns.

REFERENCES

EWALD, P. P., 1940. *Proc. Phys. Soc.* **52,** 167.

FRIEDEL, 1914. *Bull. Soc. franç. Mine.* **47,** 60.

GREGG, R. Q., and GRINGRICH, N. S., 1941. *Phys. Rev.* **59,** 619.

GUINIER, A., 1938. *C.R. Acad. Sci., Paris,* **206,** 1972 ; 1939 a. *Ann. Chim.* (*Phys.*) **12,** 161 ; 1939 b. *Ibid.* **12,** 161 ; 1942 a. *C.R. Acad. Sci., Paris,* **215,** 114 ; 1942 b. *J. Phys. Radium,* **8,** 124 ; 1943 a. *Metaux et Corrosion,* **18,** 209 ; 1943 b. *J. Chim. Phys.*, **40,** 133 ; 1944. *Rev. Metall.* p. 1.

JOHANSSON, T., 1933. *Z. Phys.* **82,** 507.

LONSDALE, K. and SMITH, 1941. *Phys. Rev.* **61,** 617.

PRESTON, G. D., 1938. *Proc. Roy. Soc.* A, **167,** 526.

RAMAN, C. V. and NILAKANTAN, P., 1941. *Phys. Rev.* **60,** 63.

SYKES, C. and JONES, F. W., 1936. *Proc. Roy. Soc.* A, **157,** 213.

PERMEATION AND SORPTION OF WATER VAPOUR IN VARNISH FILMS*

BY A. MORRIS THOMAS AND W. L. GENT,
Perivale, Middlesex

MS. received 22 *February* 1945

ABSTRACT. An experimental investigation on the moisture permeability and sorption of detached varnish and polystyrene films is described. Details for preparation of samples and methods of test, under various conditions of vapour pressure and temperature, are given. Both the permeability and sorption of the films have been determined at constant moisture concentrations, that is, by using streams of moist air, the amounts permeating and the amounts sorbed being directly weighed. In addition to moisture permeability, some measurements of that of hydrogen and carbon dioxide are reported.

Consideration of the experimental results shows that they can be interpreted by assuming that the diffusion process is analogous to that of substances in solution. There is insufficient evidence to show the effect of vapour pressure and temperature on the moisture permeability, but the results for carbon dioxide and hydrogen indicate that the diffusion process is dependent on the microphysical properties of the film. The effect of structure on diffusion is discussed, and the relations of the results to the problems of electrical insulation are considered.

§1. INTRODUCTION

EXPOSURE of insulating materials to water or its vapour is almost always detrimental to their electrical properties. Cellulosic materials, extensively used owing to their mechanical properties, are badly affected, and so are customarily protected by impregnation with hydrophobic filling waxes, compounds or varnishes. These various organic materials, however, exhibit widely different sorptive and permeability characteristics which it is important to investigate with a view both to practical applications and to elucidating the fundamental factors involved.

---

* Based on Report A/T92 of the British Electrical and Allied Industries Research Association.

These considerations apply equally to any form of electrical insulating material, and the practical aims of research in this field are then, first, to provide data for estimation of the amounts of moisture likely to enter insulated electrical equipment under any condition of humidity and temperature, and secondly, by relation of these properties to the structure of the insulating materials, which determines their electrical and mechanical properties, to provide information which will lead to improvement of the materials.

The experimental problem is threefold: it is necessary to find the rate at which moisture penetrates into the insulating material, that is, the rate of sorption; to determine the amount of moisture sorbed when the rate of sorption is zero, that is, when equilibrium is reached; and to measure the rate at which moisture passes through the material when sorption equilibrium is attained. Two series of experiments are, therefore, covered by this report, namely, those concerned with sorption of moisture in the material before equilibrium is reached, and those in which the movement of moisture at equilibrium is studied. These are the sorption and permeability tests respectively. In all cases constant humidity and temperature are assumed.

Before the beginning of the research no experimental methods of sufficient accuracy were available; these have been developed. Certain tests for moisture permeability had been devised and widely used, especially in America, but although giving self-consistent results they were of little use where the aim was to provide data applicable under all conditions. They are, however, simple methods of comparing permeabilities under the same conditions.

The permeability to hydrogen and carbon dioxide has been measured for certain materials to ascertain how the penetration of gases, such as these, differ from that of a polar vapour such as water. Although not of any immediate practical importance, the results give some insight into the mechanism of permeation and allow definite conclusions as to its nature to be made. It might be supposed that the mechanism is one of simple infiltration of the permeating substance through minute channels in the material, but the evidence suggests that it is a molecular process and closely connected with sorption. The same molecular properties which determine the electrical and mechanical behaviour of these substances also determine the permeability and sorptive capacities. The theoretical considerations are concerned with the elaboration of this view.

So far, the materials used have been confined to representative types of baking varnishes and polystyrene, both as free films; but although the numerical results apply only to these substances, the general arguments advanced are valid for any organic insulating material of the type considered.

§2. DEFINITIONS AND FORMAL THEORY

Fick (1855) suggested that the diffusion of substances in solution could be represented by the two equations

$$\bar{P} = -D\frac{\partial c}{\partial x} \qquad \ldots\ldots(1)$$

and

$$\frac{\partial c}{\partial t} = D\frac{\partial^2 c}{\partial x^2}. \qquad \ldots\ldots(2)$$

The first applies to the equilibrium, or stationary, state, where the concentration gradient $\partial c/\partial x$ at any given point is constant. Equation (2) describes the non-stationary state before equilibrium is reached, the concentration gradient being a function of the x-coordinate, which is in the direction of movement of the diffusing substance. $\overline{P}$, the constant rate of transfer across the concentration difference, is termed the permeability, and D is the diffusion constant.

Wroblewski (1879) suggested that these equations could be applied to the movement of water as vapour in solid materials, and this is borne out by experimental results. It will be shown that a hydrodynamic interpretation of the motion of the permeating substance, that is, permeation through fine channels or micro-pores, is inadmissible for substances such as were used in the present investigation.

On the assumption that D is not a function of c or t, equation (1) may be integrated

$$\overline{P}=D\frac{(C_1-C_2)}{d}, \qquad \ldots\ldots(3)$$

where the C_1 and C_2 are the boundary concentrations inside a slab whose thickness is d. The permeability is a constant for the particular conditions, and, to make it refer to the material, a *permeability constant* is defined as the rate of transfer of mass across unit area and through unit thickness under the influence of unit pressure, or concentration, difference

$$P=\frac{m}{At}\frac{d}{(p_1-p_2)}. \qquad \ldots\ldots(4)$$

$$P'=\frac{m}{At}\frac{d}{(c_1-c_2)}. \qquad \ldots\ldots(5)$$

Whereas for the solution system there is a continuous phase, so that $C_1=c_1$, $C_2=c_2$, the system vapour-solid is discontinuous at the surfaces and $C\neq c$. The relation that these quantities bear to one another depends on the sorptive properties of the material under consideration,* and if it is assumed that Henry's law may be applied, that there is a linear relation between the external concentration or vapour pressure and the internal equilibrium concentration, then

$$C=Sp \qquad \ldots\ldots(6)$$

or

$$C=S'c, \qquad \ldots\ldots(7)$$

where S and S' are the sorption constants for the material. On writing equation (3) in the form of equation (4),

$$\overline{D}=\frac{m}{At}\frac{d}{(C_1-C_2)}, \qquad \ldots\ldots(8)$$

it is seen that the relation between the sorption, diffusion and permeability constants for the material is

$$P=SD. \qquad \ldots\ldots(9)$$

---

* Because of the attraction of the solid for water molecules, the concentration inside the material is greater than that in the vapour phase. It follows that the concentration difference within the material is also greater. Consequently, the constants derived from Fick's equation will be different by a factor which is the ratio of the concentrations in the solid and vapour phases. The coefficient calculated from the concentrations in the vapour phase is the permeability constant ; that derived from the internal concentration is the diffusion constant, and is analogous to the coefficient for diffusion in solution.

By inspection of equation (2) it is clear that its solution will yield a kinetic relation between C and t involving D, and a solution of particular interest is for the sorption at both faces of a detached film in an atmosphere containing water vapour at a particular partial pressure. In such a case the boundary conditions are

$$C_1 \text{ (at } x=0) = C_2 \text{ (at } x=d) \text{ for all values of } t,$$
$$C_0 = 0 \text{ at } t=0,$$

C_1 being defined by equation (6), where p is the ambient vapour pressure, and C_0 the initial concentration in the film. Equation (2) then gives the solution,

$$C_t = C_1\left\{1 - \frac{4}{\pi}\sum_{n=0}^{n=\infty}\frac{1}{2n+1}\sin\frac{(2n+1)\pi x}{d}\exp-\left[\frac{D(2n+1)^2\pi^2 t}{d^2}\right]\right\},$$

where n is an integer. The total amount sorbed by the film is

$$m = \int_0^d C_1(x,t)\,dx,$$

which on substitution becomes

$$m = m_s\left\{1 - \frac{8}{\pi^2}\sum_{n=0}^{n=\infty}\frac{1}{(2n+1)^2}\exp\left[-\frac{D(2n+1)^2\pi^2 t}{d^2}\right]\right\}. \qquad \ldots\ldots(10)$$

The series converges rapidly and, when m/m_s is greater than 0·4, equation (10) may be written as

$$\frac{D\pi^2 t}{d^2} = \ln\frac{m_s}{(m_s - m)} + \ln\frac{8}{\pi^2}. \qquad \ldots\ldots(11)$$

where m is the mass of water sorbed in time t and m_s is the value at equilibrium. From equation (11), D may be calculated if the rate of sorption be determined, and since in the same experiment S will be found from the equilibrium value of m, a comparison of the value of P from equation (9) and by direct experiment is possible.

The assumptions implicit in the derivation of the three constants and their relationships are given below.

1. The movement of water vapour in non-porous solids is similar, formally, to that of substances in solution.

2. The amount of water vapour sorbed is directly proportional to the ambient vapour pressure.

3. The diffusion constant is not a function of the amount of water sorbed.

4. The time required for the surface to come into equilibrium with the ambient vapour is vanishingly small.

For real substances these assumptions are not necessarily valid, and experimental results should indicate how far they may be used, and (by consideration of the deviations) the real nature of the processes.

§ 3. MATERIALS

The compositions of the varnishes used in the investigation are given in table 1. The films were prepared without alteration of the viscosity of the varnish, as received from the maker.

Four polystyrene films were investigated, details of which are given in table 2, three of the films being of different manufacture.

§4. EXPERIMENTAL METHODS

Although the investigation was primarily concerned with varnishes, which are normally used as thin films or as impregnants, other materials may be studied advantageously in this manner. For films up to 0·015 cm. in thickness, equilibrium is established within a few hours for both permeation and sorption.

Preparation of varnish films

In many researches, e.g. Gettens (1932), Gettens and Bigelow (1933), Payne and Gardner (1937), Payne (1939), the varnish has been supported on paper or on glass cloth (Payne, 1939). Although such a method is useful for comparative tests, it is of little use for determination of absolute values of the constants, as the thickness of the varnish film and effect of the base material are always indefinite. When constants referring only to the varnish are required, detached films must be used.

Table 1. Compositions of varnishes *

Varnish No.	Components	Per cent	Solvent	Per cent
1	Tung oil Phenolic resin (100%)	40·6 12·0	Mixed petroleum distillate and terpene	47·4
2	Gilsonite Boiled linseed oil	33·6 13·2	White spirit	53·2
3	Spirit soluble phenolic resin (100%)	38·4	Methylated spirit Acetone	53·9 7·7
510	Tung oil Phenolic resin (100%) Drier	41·2 11·6 1·2	Mixed petroleum distillate and terpene	46·0
602	1 part of No. 510 and 1 part of :		Congo Copal ester .. 53% Boiled linseed oil .. 17% Solvent .. .. 25·8% Drier .. .. .. 4·2%	

* Varnish 1 also contained drier of unspecified amount. The suppliers of the varnish state that Nos. 1 and 510 were identical in composition.

The baking times were 2 hours per coat for varnishes Nos. 1, 2, 510 and 602, and 3 hours per coat for varnish No. 3. The baking temperature was 105° c. in all cases.

Table 2. Details of polystyrene films

Film No.	Thickness (cm.)	Description
1358	0·0025	Unplasticized
1358A	0·0075	Unplasticized
1359	0·0125	Unplasticized
1360	0·0025	—

The first necessity for precise measurements is that the films be uniform in thickness, and it is, therefore, not possible to prepare them by brushing or spraying. In general, two methods have been used: first, spinning on a horizontal plate (Lishmund and Siddle, 1941), or secondly, spreading by means of a doctor blade moving at a fixed height above the base on which the film is to be formed. The second method has been employed in this investigation.

The second necessity is that the film when formed should be easily removed from the base material. Most investigators have used tinned-iron plates from which the film may be stripped, but it has been found more advantageous to use 3-mil tin-foil which is dissolved off by mercury.

The apparatus used in this investigation is shown in figure 1. The doctor blade is attached to two differential screws, with large knurled heads, which are supported in an iron angle at the ends of which are steel runners sliding in steel grooves clamped to the brass base plate. It is on this plate that the tin-foil is stretched by application of a slight tension to the clamps at each end. The gap beneath the blade edge is made parallel by adjustment of the differential screws and then set to about 0·005 cm. A small quantity of the varnish is poured on the foil and the blade carrier moved slowly along the guides so that the excess of varnish is pushed in front. Just before the edge of the base plate is reached, the carrier is reversed and the movement repeated in the opposite direction. The to-and-fro motion is carried out three times, and the excess of varnish pushed over the sloping edge of the base plate and removed. The foil is released and baked for the appropriate time. Further coats of varnish are added by replacing the foil and repeating the process. To avoid dust, which gives rise to pinholes and irregularities, the whole apparatus is covered by an enclosure with curtain-sides and roof of cellophane. During baking, the film is covered with a shield of the same material. The films are substantially uniform over an area of 10 cm. × 15 cm. Most of the films used were manipulated with ease, but those of varnishes 2 and 3 presented special difficulty.

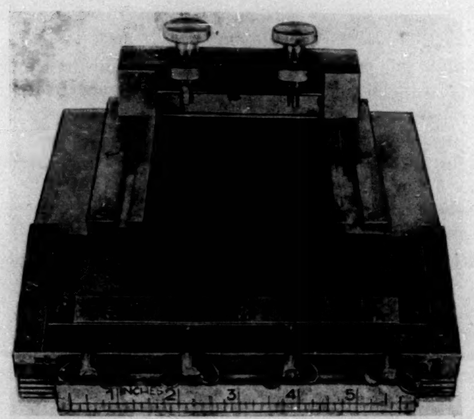

Figure 1. Apparatus used for the preparation of varnish film samples.

Films of varnish No. 2 are fragile, due to the shortness of the mixture, and further, at temperatures above 40° c. the viscosity decreases so much that the film becomes semi-liquid. For this reason no values of permeability constant were obtained at 50° c., and those at 40° c. were subject to some uncertainty. The tendency to fluidity is due to lack of polymerization, the film being produced by desolvation. This mode of formation also gave rise to difficulty in the sealing of rings into the permeability apparatus. Rubber rings were used normally, but with this varnish it was found that after three days the rubber had sorbed all of the oil and left only a powder of gilsonite, the centre of the film becoming separated. The effect was overcome by using cellophane masking rings over the area of contact with the rubber.

Fragility of films of varnish No. 3 is due to their brittle nature. The unevenness of pressure obtained with rubber sealing rings caused the films to shatter like glass. To avoid this, rings of waxed filter paper were used, the whole permeability cell being warmed to 60° c. to ensure complete sealing. It is not certain that the films of varnish No. 3 were homogeneous, for polymerization is complete after baking of each coat, so that interdiffusion with the added liquid varnish does not occur.

In all cases the thickness of a film was measured by a dial micrometer reading to 0·0001 cm. A number of readings were taken over the area under test. The softer films presented some difficulty as the impact of the micrometer foot caused compression, giving a lower value than the true thickness. For this reason a circular plate of 1 cm^2 area was preferred to a spherical point.

The apparent thicknesses of polystyrene films when measured with the micrometer led to values of density <1, and it was necessary to determine the density directly. It seems probable that the surface is corrugated, and that the crests alone contribute to the dimension.

Production of standard humidities

It is of the first importance both in the permeability and sorption experiments to maintain a constant, standard humidity. To accomplish this, two methods are available for flowing gas streams; the first is the use of saturated salt-solutions which give a known vapour pressure, and the second is to mix such volumes of saturated and dry gas that the resulting mixture has the requisite humidity. The first and simpler method has been used.

Gravimetric checks were made on the humidity of the gas streams, but, in general, the values from *International Critical Tables* were assumed to be correct. The salts which have been used are listed in table 3.

Table 3. Humidities of saturated solutions

Salt	Relative humidity (%)	Variation with temperature
Potassium sulphate	96	None
Potassium tartrate	70	None
Cobalt chloride	67·4, 20° c. 56·7, 40° c.	Linear

Measurement of permeability

A variety of forms of apparatus have been described by several authors and comprehensive reviews of the subject have been written by Lishmund and Siddle (1941) and by Carson (1937). To obtain significant results it is necessary that the vapour pressures at the surfaces of the film under test should be of definite and known values. In the majority of the methods used, where the film is exposed over a solution or dehydrating agent without mixing of the air other than by convection, it is probable that the vapour pressure is by no means equal to its supposed value (see, for example, Abrams and Brabender, 1936). The error may be avoided by passing streams of air at definite humidities over the surfaces at such rates that no vapour-pressure gradients are formed.* This method (Wosnessensky and Dubnikow, 1936) was successfully developed.

The apparatus (figure 2) consists essentially of a humidifying train producing a stream of gas at the required humidity which then passes over the film, contained in the permeability cell. The moisture which permeates through the film is taken up by a dry-gas stream and then removed by drying tubes to determine the amount.

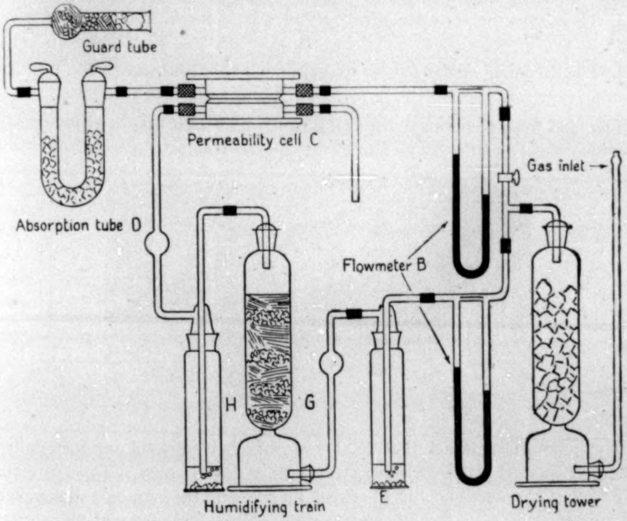

Figure 2. Moisture permeability apparatus.

Gas, from a cylinder, is initially dried with silica gel and split into two streams, the rates of which are measured by the flow-meters B. One stream passes through the cell C to remove the water which has penetrated, and which is estimated gravimetrically by the absorption tubes of phosphorus pentoxide D. The other stream is pre-humidified by the water bubbler E. The vapour pressure is finally corrected by passing the gas through the tower of moist crystals G and the final bubbler H. After flowing over the film, the stream is released into the atmosphere.

---

* The authors are indebted to Dr. G. Barr for advice on this subject.

It was found that a streaming rate of 1 litre per hour was sufficient to prevent the formation of any vapour-pressure gradient over the surfaces of the film, and the flowmeters were constructed accordingly. The pressure difference developed across a capillary was measured, and the meters were calibrated by displacement of water, the necessary corrections being made.

To ensure further that the practical conditions correspond to those required, the permeability cell was constructed with the following necessities in mind:—

1. A definite area of film must be exposed to the humid air or gas.

2. The only leakage from the moist to the dry side of the film must be through the film.

3. There must be no leakage from either side of the film to the outer atmosphere.

4. The thickness of the gas layers adjacent to the surfaces of the film must be small enough to prevent the formation of vapour pressure gradients.

The final form of permeability cell adopted and used for the experiments is shown in figures 3 and 4. The film of varnish was clamped between two shallow brass cylinders of internal diameter 1·5 in., which were held symmetrically in place by two steel plates provided with bolts and wing nuts. To ensure complete sealing, the areas of contact between the film and the cylinders were covered with rubber gaskets. Each compartment of the cell was provided with diametrically opposite openings to serve as inlet and outlet respectively for the gas streams, and a third opening for connection to a small external manometer for checking the pressure and indicating leakages in the system.

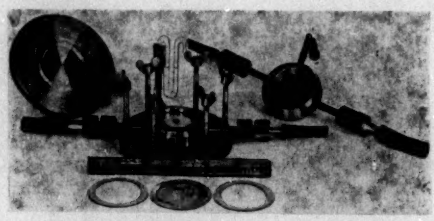

Figure 3. Moisture penetration cell. (General view.)

The amount of moisture permeating through the films used in these experiments was of the order of 1 mg. per hour. To obtain five values of the permeation per hour within three days and with 5% accuracy the minimum weight measured was 3 mg., an analytical balance being used.

The use of phosphorus pentoxide supported on silica gel was found to be superior to that of any other absorbent and it was the most convenient to handle. Other absorbents used were silica gel, phosphorus pentoxide on glass wool and on pumice, and sulphuric acid on pumice.

Before beginning an experiment the apparatus was first tested for leakage by sealing the outlets and allowing the pressure to rise until the manometers showed a positive reading. The stream was cut off and the reading taken after ten minutes. With absence of leaks no change was observed.

One day was allowed for the humidifying train and permeability cell to come into thermal equilibrium, the thermostat being controlled to ± 0°·2 c. A further day was allowed with gas streams running, for the apparatus and film to come into moisture equilibrium.

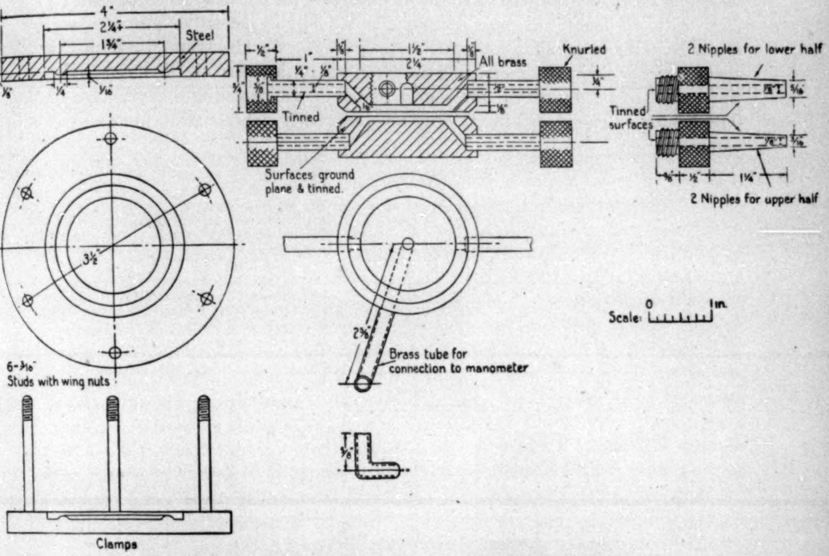
4"
2¼"
1¾"
Steel
¼"
1/16"
6-3/16"
Studs with wing nuts
3½"
Clamps
½"
1"
¼"
⅛"
1½"
2¼"
All brass
Knurled
Tinned
Surfaces ground
plane & tinned.
2⅜"
Brass tube for
connection to manometer
⅝"
2 Nipples for lower half
Tinned
surfaces
½"
1¼"
2 Nipples for upper half
Scale: 0 1in.

Figure 4. Moisture penetration cell. (Working drawing.)

To prevent oxidation of the film during the tests, nitrogen was used as carrier for the water vapour.

A series of tests on the permeation of hydrogen and carbon dioxide through films of varnish 1 and of polystyrene were carried out. For these experiments the gas was substituted for the moist stream, the barometric pressure being substituted for the vapour pressure. For the estimation of hydrogen which had permeated to the nitrogen, the stream was passed over copper oxide at a cherry-red heat, and the hydrogen estimated as water in the manner already described. Carbon dioxide was absorbed in soda-lime.

Measurement of sorption

Determination of small quantities of water vapour sorbed from the gaseous phase may be effected either by direct measurement of the mass taken up from a practically infinite volume of inert gas at the required humidity, or by measurement of the equilibrium vapour pressure in a finite volume initially containing a known quantity of the vapour. The latter method requires elaborate apparatus and technique which to a certain extent are avoided by use of the former.

Measurement of the mass sorbed, although simple in principle, presents some difficulties because of the small quantities involved. The most satisfactory weighing element is a quartz helix, which obtains the greatest sensitivity with a large ratio of length to cross-sectional area. Highly sensitive elements are, however, subject to vibration which impairs accurate observation. With the available instruments for measuring the extension of the helix, the limit sensitivity was found to be 4×10^{-5} g. for a load of 0·1 g., representing a percentage of 0·04 ± 0·02. Beyond this limit, vibration frequently prevented accurate observation.

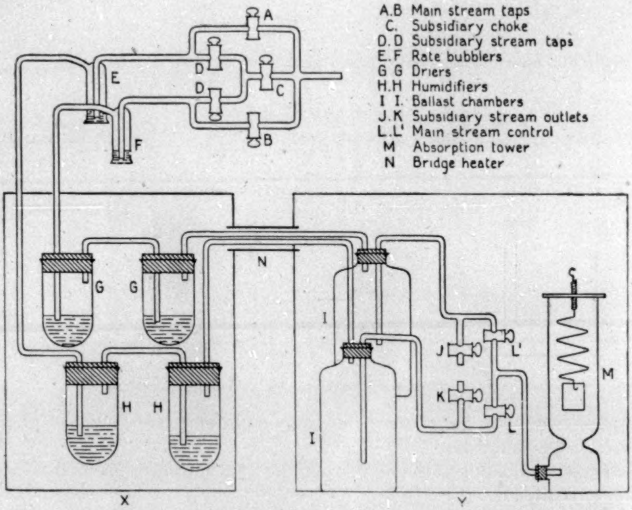
A.B Main stream taps
C. Subsidiary choke
D.D Subsidiary stream taps
E.F Rate bubblers
G G Driers
H.H Humidifiers
I I. Ballast chambers
J.K Subsidiary stream outlets
L.L' Main stream control
M Absorption tower
N Bridge heater
A
D
D
C
B
E
F
N
G
G
I
I
J
K
L'
L
M
H
H
X
Y

Figure 5. Apparatus used for determination of moisture sorption by films.

From the equations (3) and (4) it is evident that measurements of two kinds are required, of equilibrium absorption and of the rate of sorption. It is convenient to combine these in one experiment. Although it is not likely that the amount of sorption will appreciably alter the quantity of water vapour in the carrier gas, it is necessary, in experiments on the rate of sorption, that the humidity should change rapidly from the initial value to that at which the rate is being determined. Preliminary results showed that the sorption of films of the thickness used is practically complete within 30 minutes; consequently the time of change from the initial to the final state must not be greater than $\frac{1}{2}$ min. for reasonable accuracy. Any method which depends on the mixing of static volumes of dry and humid air to give the required vapour pressure is thus uncertain, and a streaming method is preferable.

The final set-up is shown diagrammatically in figure 5, although most of the results were obtained with a simpler apparatus. The later arrangement has independent control of the temperature of the humidifying train, and consequently of the vapour pressure, and also of the film. The incoming air stream is split along three branches: A and B are the dry and humid streams respectively, and C is a subsidiary. The function of the last is to maintain the section of the apparatus not in use, comprising bubblers and ballast chambers, in either dry or humid condition, as the case may be, so that the change from one state to the other can be made in the shortest possible time. C acts as a choke, having a constant setting, and controls the rate of the slow maintaining stream, the direction being determined by the taps D, D. It is released into the atmosphere by either J or K and prevented from entering the sorption tower by the taps L, L′. The humidifiers H, H are filled with saturated salt solution and the driers G, G with strong sulphuric acid.

Dry air was passed at a slow rate through the apparatus for a few hours to remove moisture from internal surfaces and from the film. The position of a mark on the bottom of the helix was read by a cathetometer external to the apparatus, illumination being supplied by a neon lamp behind the sorption tower. It was found that this reduces both aberration and eye-strain. The change to the humid stream was made by opening L and closing K, whereby the whole of the air passes through the humidifiers. The dry side of the apparatus was then isolated by closing the tap L′. Readings of the spring extension were taken initially at 1 min. intervals until the rate of sorption became slow, when the time was increased gradually. When the extension showed no positive change after ½ hour, it was considered that the film was in equilibrium at the particular vapour pressure.

The rate of desorption was found in a similar manner, the operations being reversed.

§ 5. EXPERIMENTAL RESULTS

Permeability constants.

The permeability constants are calculated from equation (4), the unit being g.cm./hour cm^2 mm. Hg. In general the values for permeability constants of varnishes and similar materials are of the order of 10^{-8}. All values given are $P \times 10^8$.

The accuracy of the results for a particular film is of the order of 5% but, as is evident from inspection of the values, films of the same thickness prepared at different times do not show the same result. Where the values of the permeability are small, as in the case of phenol formaldehyde resin, $P \simeq 0 \cdot 5 \times 10^{-8}$, the accuracy is of a lower order because of the minute quantities permeating. All films were used one week after preparation. The results of the tests are given in tables 4 to 7.

Table 4. The moisture permeability constants of films of varnish 1

Temperature of test (°c.)	Thickness (cm.)	Vapour pressure diff. (mm. Hg)	$P\times 10^8$
25	0·0042	20·9	4·9
35		36·1	5·8
25	0·0083	21·9	4·8
30	0·0102	28·5	6·0
35		38·0	6·7
40		50·3	7·1

Table 5. The moisture permeability constants of films of varnish 2

Temperature of test (°c.)	Thickness (cm.)	Vapour pressure diff. (mm. Hg)	$P\times 10^8$
30	0·0053	28·8	2·3
30	0·0054	29·0	2·4
40		51·3	2·5
30	0·0062	28·7	2·6
40		50·7	2·7
30	0·0082	28·6	2·8

Table 6. The moisture permeability constants of films of varnish 3

Temperate of test (°c.)	Thickness (cm.)	Vapour pressure diff. (mm. Hg)	$P\times 10^8$
30	0·0028	29·7	0·42
A 40		52·6	0·35
49·5		85·5	0·34
25	0·0028	21·7	0·55
B 35		38·0	0·46
30	0·0045	29·6	0·59
40		52·5	0·45
49·5		85·2	0·44

Table 7. The moisture permeability constants of films of two baking varnishes at 25° c. and 96% R.H.*

Varnish No.	Thickness (cm.)	Vapour pressure diff. (mm. Hg)	$P \times 10^8$
510	0·0058	21·0	4·3
	0·0150	21·9	5·4
	0·0184	22·2	4·3
602	0·0062	21·7	0·57
	0·0106	21·9	0·42

* In view of the interest shown by varnish manufacturers in the great difference of moisture resistance between varnishes Nos. 510 (Tung oil) and 602 (Tung oil—Congo Copal ester—linseed oil), tests are being carried out on the sorption of the latter to determine whether or not its properties are so modified by the sorbed moisture as to make the permeability constant small. The results will be reported later.

The films A and B, although of the same thickness, were prepared at different times.

The values for all three varnishes were obtained at 96% relative humidity.

The tests on film No. 1360 were carried out at 70% relative humidity, but for the remainder of the films the value was 96%. The results of the tests are given in table 8.

Table 8. The moisture permeability constants of polystyrene films

Film No.	Temperature (°c.)	Thickness (cm.)	Vapour pressure diff. (mm. Hg)	$P \times 10^8$
1360	25	0·0025	13·7	3·7
	30		17·9	3·9
	40		29·1	3·7
	50		51·8	2·9
1358	25	0·0024	21·0	2·3
1358A	25	0·0069	21·3	3·0
1359	25	0·0122	21·6	3·1

Values for the hydrogen and carbon dioxide permeation were found for a film of varnish No. 1 and for polystyrene film No. 1360. The difference of pressure across the film is not corrected for the amount permeated, the quantity being too small. The gas issues at constant pressure, hence the actual pressure of the gas is the atmospheric pressure. The results of the tests are given in tables 9 and 10.

Table 9. The gas permeability constants for a film of varnish 1

Gas	Temperature of test (°c.)	Thickness (cm.)	Pressure diff. (mm. Hg)	$P \times 10^8$
H_2	30	0·0081	754	0·0042
	40		773	0·0051
	50		771	0·0059
CO_2	30	0·0140	754	0·050
	40		773	0·085
	50		771	0·153

Table 10. The gas permeability constants for a film of polystyrene 1360

Gas	Temperature of test (°c.)	Thickness (cm.)	Pressure diff. (mm. Hg)	$P \times 10^8$
H_2	25	0·0025	760	0·0063
	25*		742	0·0064
	30		758	0·0076
	40		753	0·0091
	50		756	0·0104
CO_2	25	0·0025	759	0·066
	25*		742	0·082
	30		758	0·069
	40		753	0·091
	50		758	0·106

* In this test both streams of gas contained water vapour at 70% relative humidity.

Sorption constants

The sorption constant as defined by equation (6) is evidently the concentration in the film for a unit pressure of the gas or vapour sorbed. The unit in which the results are expressed is g./cm.^{3} per mm. of Hg.

These values are given in table 11 with the percentage sorptions by weight

Table 11. Moisture sorption constants for varnishes 1, 2 and 3

Varnish No.	Thickness (cm.)*	Sorption (%)	Sorption constant $\times 10^4$
1	A 0·0029	2·0	9·9
	B 0·0054	2·2	10·3
	C 0·0070	1·2	5·8
2	A 0·0074	1·0	5·1
	B 0·0086	0·9	4·4
3	A 0·0017	2·6	14·2
	B 0·0034	2·6	14·0
	C 0·0049	2·0	10·1

* The letters A, B, C refer to different films.

for varnishes 1, 2, 3. All the values recorded were determined at 25° c. and 96% relative humidity.

The results are not all of equal accuracy. Films 1C, 2B and 3A were the first to be tested, whilst the method was being developed, and may be more in error. The order of accuracy is 7%.

Table 12. Moisture sorption constants for polystyrene films

Film No.	Thickness (cm.)	Vapour pressure (mm. Hg)	Sorption (%)	Sorption constant $\times 10^4$
1358	0·0024	17·9	0·10	0·6
1358A	0·0069	17·9	0·08	0·4
1359	0·0122	17·9	0·07	0·3
		21·4	0·11	0·4

Because of the extremely small values of the sorption of the polystyrene films with consequent uncertainty of the measurements, six determinations were made for each film and the mean taken. The accuracy of the sorption percentages is ±0·02, with a percentage accuracy of *c.* 20.

Rate of sorption

The rates of sorption are not reported numerically, requiring too much space, but specimens of the curves are given in figures 6, 7, and 8 for the three varnishes.

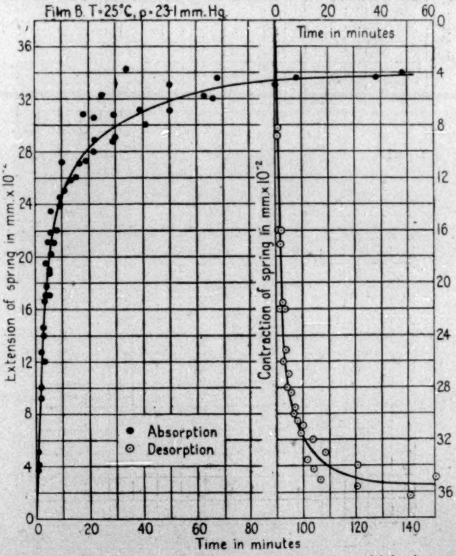

Figure 6. Sorption vs. time for films of tung oil-phenol formaldehyde varnish No. 1.

The points are the results of three rate determinations for both sorption and desorption.

Using the relation developed in equation (11), the values of log $(m_s - m)$ are plotted against t in figures 9, 10 and 11.

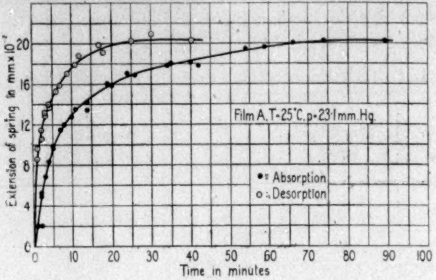

Figure 7. Sorption vs. time for films of linseed oil-gilsonite varnish No. 2.

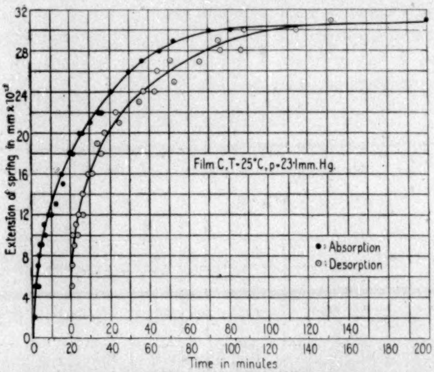

Figure 8. Sorption vs. time for films of phenol formaldehyde resin varnish No. 3.

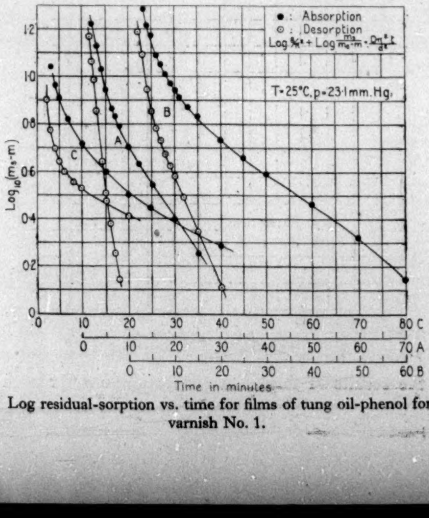

Figure 9. Log residual-sorption vs. time for films of tung oil-phenol formaldehyde varnish No. 1.

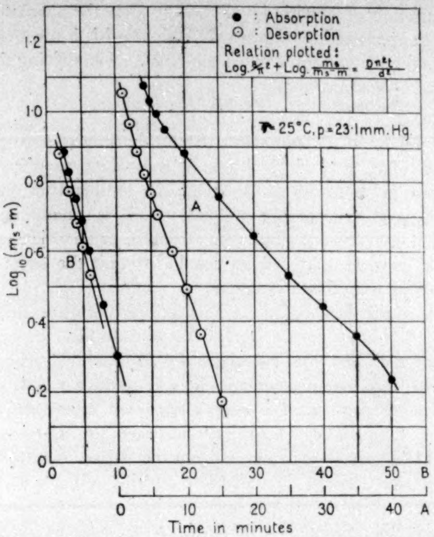

Figure 10. Log residual-sorption vs. time for films of linseed oil-gilsonite varnish No. 2.

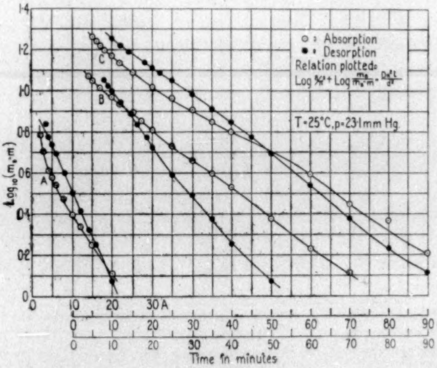

Figure 11. Log residual-sorption vs. time for films of phenol formaldehyde resin varnish No. 3.

§6. DISCUSSION

Nature of the permeation mechanisms

The formal theory already developed (§ 2) assumed that diffusion in solid materials takes place by a process analogous to osmotic diffusion in liquids and not by flow through micro-pores. Such a hydrodynamic flow would be expected to lead to a variation of P with $1/\sqrt{T}$, where T is the absolute temperature. The results of the permeation of gases through varnish 1 and polystyrene show that the temperature coefficient is much too large. Simplifying the relationship to

$$P = k/\sqrt{T}, \qquad \ldots\ldots(12)$$

and using the values of P from table 10 for hydrogen permeation through polystyrene, the values of k, which should be a constant, vary from 10·8 to 18·9 as T varies from 25° C. to 50° C. Further, the temperature coefficient of P, which should be negative according to equation (12), is usually positive.

If, therefore, permeation of gases does not occur as flow through micro-pores in the materials concerned, it can be concluded that the same holds for the permeation of water and other substances.

A crucial test of the theory of an osmotic diffusion of water through varnishes and similar materials is the comparison of the permeability constant determined in the stationary state and that calculated by equation (9) from the diffusion constant obtained from measurements in the non-stationary state using equation (11). In this comparison all the assumptions are involved. Inspection of figures 9, 10 and 11, which show the relation between log $(m_s - m)$ and t, indicates that equation (11) is reasonably valid. From the curves, values of the diffusion constant D have been derived, the unit being cm²/hr. (Table 13.)

Table 13. Diffusion constants for varnishes 1, 2, 3 at 25° C.

Varnish No.	Thickness (cm.)	Mean value of $D \times 10^8$ (cm²/hr.)
1	0·0029 0·0054	12·5 27·0
2	0·0074 0·0086	34·5 82·5
3	0·0017 0·0034 0·0049	2·0 3·2 5·0

These values are the means for the sorption and desorption processes.

From these values, and using the sorption constants of table 11, the permeability constants (table 14) have been calculated from equation (9) and compared with those determined experimentally and given in tables 4, 5 and 6.

The agreement is good in showing the correct order of magnitude. Considering also the approximate constancy of the permeability constant with thickness, there is reason to believe that the mechanism of permeation is one of osmotic diffusion, and that deviations from the formal laws are to be explained in terms of the characteristics of the substance permeating and the material permeated.

Table 14. Experiments and calculated values for the permeability constants at 25° c.

Varnish No.	Thickness (cm.)	Permeability constant $\times 10^8$ (g./hr.cm.mm.Hg)	
		Direct observation	Calculated from D and S
1	0·0029	4·8*	1·2
	0·0054	4·9	2·8
2	0·0074	2·6*	1·8
	0·0086	2·7*	3·6
3	0·0017	0·42*	0·28
	0·0034	0·45*	0·44
	0·0049	0·63*	0·51

* The values are interpolated.

Deviation from ideal behaviour

Examination of tables 4, 5 and 6 shows that permeability constants tend to be larger for thicker films, a result also noted by other authors (Edwards and Wray, 1936; Lishmund and Siddle, 1941; Wray and van Vorst, 1941). The increasing sorption of polystyrene with decreasing thickness (table 12) indicates the presence of a concentration on the surface of the film over and above that existing inside the material. Calculation shows that this surface layer is equivalent to a thickness of 4 molecules. Such a layer may have a lower permeability than the interior, and thus give rise to the variation with thickness mentioned.

The effect of vapour pressure on the permeability constant has not been determined in the present investigation, but investigations on baking varnish (Edwards and Wray, 1936), rubber (Lowry and Kohmann, 1927; Taylor, Hermann and Kemp, 1936), and cellophane (Simril and Smith, 1942) show that, in general, there is a considerable increase of sorption with vapour pressure, especially in the region of 80–100% relative humidity. This super-sorption must be a consequence of the polar nature of the water molecule as opposed to the non-polar character of a gas, e.g. hydrogen, the solubility of which closely follows the linear law. First there may be a liquid condensation on the hydrophilic groups in the material, and secondly, intra-micellar penetration of water molecules, which causes swelling and exposure of more hydrophilic groups. Payne (1939) has shown that the permeability of a material is greatest with respect to a vapour which in its liquid state dissolves or disperses the material. If liquid sorption takes place, it is to be expected that the binding force at a high concentration will be smaller than that exerted when the water molecule is sorbed directly on a hydrophilic group. Thus movement at higher concentrations will be freer, and if there is some disruption there will be more traversable paths.

Variation with temperature

All the considerations so far have dealt with processes at constant temperature. It was stated in § 6 that the variation of the gas permeability with temperature is not only in the wrong direction, but of too great a magnitude to be accounted for by a flow through micro-pores. Barrer (1941) showed that permeation and diffusion of gases through organic materials was by an activated mechanism, similar to that of the movement of atoms and ions in fluid and solid media. It was found that the variation of permeability and diffusion constants with temperature could be represented by the equations

$$P = P_0 \times \exp\left(-E/\boldsymbol{R}T\right), \qquad \ldots\ldots(13)$$

$$D = D_0 \times \exp\left(-E'/\boldsymbol{R}T\right), \qquad \ldots\ldots(14)$$

where the E and E' are activation energies. The activation energy for the permeation process is compounded of that for diffusion and that for sorption, this latter being in fact the heat of solution.

It has been calculated from equation (13) that the activation energy for the permeation of hydrogen and carbon dioxide through polystyrene (table 10) is 3800 calories per gramme molecule in both cases, and for the permeation through varnish 1 (table 9) the energies are 3400 calories per gramme molecule and 11,400 calories per gramme molecule for hydrogen and carbon dioxide respectively. The first two values are lower than those found by Barrer for permeation of hydrogen through rubbers, ebonite, bakelite and cellulose derivatives, the range being 5000 to 10,000 calories per gramme molecule.

Although the permeability constants of the varnishes, given in tables 4 and 5, increase with temperature, the fact that the vapour pressure also increased does not allow a decision to be made. A similar consideration applies to the interpretation of the negative temperature coefficient of P for phenol formaldehyde resin and the constancy of P for polystyrene. Until the variations of permeability constant with temperature and vapour pressure are studied independently, it will not be possible to decide whether or not the process is activated. It is clearly of the greatest importance to determine this since Barrer has shown that the activation energies for gas permeation are closely related to the energies associated with mechanical changes in the case of rubbers.

Comparison of diffusion rates

It has been urged that diffusion of water through varnishes and similar materials is of a fundamentally different nature from that of gases in view of the great differences in the permeability constants for the two substances. These differences are magnified in two ways, first by the fact that the permeability constant is in terms of the mass permeating and not of the numbers of molecules, and secondly, because the sorption of water is much greater than that of gases. The first distortion is easily overcome by dividing the constants by the molecular weight of the gas or vapour permeating; it is then in terms of gramme molecules, and consequently directly proportional to the number of molecules passing. The order of permeability constant is then

$$\text{Water vapour} = 0{\cdot}3 \times 10^8, \quad \text{gas} = 0{\cdot}002 \times 10^8$$

for a film of varnish 1 at 30° C. The different effects of sorption are more difficult to eliminate, the true comparison being between the diffusion constants which give the amounts moving through the material under unit concentration gradient within the material. The diffusion constant is thus independent of the degree of sorption (see Gettens and Bigelow, 1933). Only a few values of D are known, and these have been collected in table 15.

Table 15. Moisture diffusion constants for several materials

Substance	°c.	$D \times 10^6$ (cm.^{2}/sec.)
Varnish 1	25	0·013
Varnish 2	25	0·015
Varnish 3	25	0·0011
Polystyrene	25	0·21
Values quoted by Irany (1941)		
Polyvinyl acetal	20	0·047
	40	0·062
Polyvinyl butyral	25	0·0035
Polyvinyl acetate	40	0·0056
Methyl methacrylate	25	0·027
Phenol formaldehyde	25	0·0022

There are no figures for the diffusion constant for gases permeating through any of the materials of table 15. The order of the value of the diffusion constant may, however, be obtained by assuming the average value for the solubility of hydrogen in organic materials; it is generally in the region of 0·05 ml. at N.T.P./cm.^{3} of solid/atm., from which the sorption constant may be found. From the known values for the permeability constant the diffusion constants may be calculated, and these are given in table 16.

Table 16. Calculated hydrogen diffusion constants at 25° c.

Substance	°c.	$D \times 10^6$ (cm.^{2}/sec.)
Varnish 1	25	1·7
Varnish 3	25	0·017
Polystyrene	25	3·0

In all cases the diffusion constant is greater for the gas than for moisture (see table 15), the variation being greater than any probable deviation of the hydrogen solubility from the value assumed. It is probable the solubility will be smaller, which will increase the diffusion constant. The values for varnish 1 and polystyrene are of the order of those which Barrer found in 1941 for rubbers; the lower value for phenol formaldehyde is in accord with the low value of the moisture diffusion constant (table 15) and probably results from its structure.

Structure and diffusion

The effect of the external factors, vapour pressure and temperature, has been considered on the assumption that the hydrophilic groups are of the greatest importance in determining the sorption and permeation characteristics. Whilst, however, a satisfactory explanation of the deviations and variations of the constants is possible, the factors determining the absolute diffusion rate and sorptive capacity depend on the structure of the material. It is to be expected that both the chemical nature of the ultimate molecular units and the manner in which these are aggregated into the solid will be the determining factors.

Practically all the materials used as organic insulating materials consist of giant molecules whose structure is a repetition of simple units. Such a repetition may be chain-like as in substances such as polystyrene, tung oil, rubber, or it may be three-dimensional, as in vulcanized rubber, and the condensation products of formaldehyde with phenol, urea or melamine. In the chain-polymeric materials, molecular aggregates, termed micelles, are constituted by secondary valence forces, but in the three-dimensional polymers a more rigid structure arises by primary valence forces cross-linking the molecules. However, the energies necessary to break a primary and a secondary valence bond are about 30,000 and 6000 calories per Avogadro number of bonds broken respectively, so that the probability of a secondary valence bond rupturing is

$$[\exp(-6000/\boldsymbol{R}T)/\exp(-30{,}000/\boldsymbol{R}T)] = 10^{20} \text{ times}$$

more than that of a primary bond. The values of table 16 show that the difference of permeation cannot be accounted for by such a difference in mechanism. In fact, no activation energies for permeation of gases through various membranes are much above 10,000 calories per gramme molecule. The conclusion is, therefore, that diffusion takes place along the micelle boundaries and through holes arising from the rupturing of secondary valence bonds, and differs only in degree in chain-like and three-dimensional polymers. A unifying concept is that of a structure consisting of regions of order and disorder, diffusion occurring through the disordered regions at a rate depending on their volume relative to the whole. The activation energy is then a measure of the energy necessary to produce sufficient disorder in the ordered regions for the molecule to pass through, and its magnitude depends on the cohesive forces between the molecules or parts of molecules in the ordered region. On this basis the low diffusion rate through paraffin wax (which has an ordered molecular lattice, providing no inter-crystalline cracking is present) may be explained as well as the decreased permeability of polystyrene film when it is partly oriented by stretching (Badum and Leilich, 1938). Further, the increased order produced by cross-linkages in three-dimensional polymers will lower the rate of diffusion, as is shown by Sager (1934).

§ 7. CONCLUSIONS

The experimental methods which have been developed are capable of giving consistent results to an accuracy of about 5% for the permeability measurements and about 7% for the sorption measurements. The most likely source of error in both cases results from the use of saturated salt solutions for humidification of the gas streams. For the varnishes a further error is introduced in that similar films prepared from the same material show permeability characteristics which may vary by 4%. Such variation is likely to arise from inequality of thickness. At the present stage of the research, which is largely exploratory, these errors are not serious, and the methods, capable of improvement if necessary, provide adequate means of investigation.

The results of this and other investigations show that the moisture permeability constants for varnishes and lacquers have a 10-fold range, which is about in the middle of the 10^4-fold range of constants for all classes of dielectrics. There is, in general, an increase of permeability constant with increase of vapour pressure and temperature, although the extent to which either of these separately is responsible has not yet been determined. The degree of variation of the constant varies widely.

A variation of permeability constant with thickness of film also occurs, but this may be due to a slow surface process.

The relationship between permeability, diffusion and sorption constants approaches that predicted by theory. The deviations arise because the assumptions on which the theory is based take no account of the real nature of sorption phenomena nor of the molecular structure of the material. It is assumed that during the process of permeation no physical interaction, other than simple solution, takes place. Actually this is not so, and to interpret the facts of permeability and sorption the concepts of molecular physics must be employed.

It is not yet possible to give a detailed picture of the mechanism of permeability. Nevertheless, some observations on the effect of structure are permissible:

1. The greater the occurrence of water-attractive groups the higher the permeability of the substances.

2. The greater the degree of order in the structure, that is, the greater the regular molecular orientation, the less is the permeability.

These two factors acting together determine the permeability of any organic insulating material of the types considered. In varnishes the effects are about balanced; more permeable substances, such as cellulose derivatives, have much greater sorptive powers; the less permeable materials, such as highly vulcanized rubbers, and waxes, have more ordered structure. The importance of the structure of the material has been recognized in the manufacture of Styroflex oriented polystyrene, which has only half the moisture permeability of the randomly oriented material.

Further, the two factors are clearly important for the dielectric and mechanical behaviour of insulating materials. Thus it seems possible that relationships between these properties and the moisture permeability may be developed in terms of the physical and chemical properties of the molecules.

ACKNOWLEDGMENTS

The authors are indebted to Mr. N. A. Bennett for advice on the types of varnish on which the research should be carried out, to Messrs. Griffith Bros. (London), Ltd., who supplied the experimental varnishes referred to in table 1, and to the Director of the British Electrical and Allied Industries Research Association for permission to publish this paper.

APPENDIX

References to moisture permeability constants cited in the literature

Moisture permeability constants for a considerable range of materials have been determined by various workers, and collections of these values will be found in the publications of Taylor, Hermann and Kemp (1936), Carson (1937), and

Barrer (1941). The dispersion of these values is shown diagrammatically in figure 12.

Values of the moisture permeability constant are gathered together in table 17 for varnish and lacquer films, paints being omitted since the pigment affects the permeability. Except for the values of Lishmund and Siddle (1941), which were determined by a method somewhat similar to that described in this report, all of the permeability constants were found by the use of a variation of the Muckenfuss pot.

In essentials this apparatus consists of a cup or jar over the mouth of which the varnish film is fixed. The cup may contain a desiccant, in which case the gain in weight is found on exposure to a humid atmosphere, or a humidifying agent may be used in the cup and the loss in weight in a dry enclosure found. The desiccating or humidifying surface in the cup may be some way from the surface of the film, resulting in a gradient of vapour pressure due to the finite time of diffusion of water vapour in air. It has been calculated that if the distance is not greater than 1 cm. no appreciable error is involved for permeability constants of the order of 10^{-8}. For larger values of the constant, as for cellulosic materials, $P = 10^{-6}$, the error is of the order of 70%. With elevated temperatures, difficulty is experienced in sealing the film to the cup: sealing at room temperature results in ballooning of the film on heating, due to expansion of the air. With these limitations the method is useful for industrial purposes.

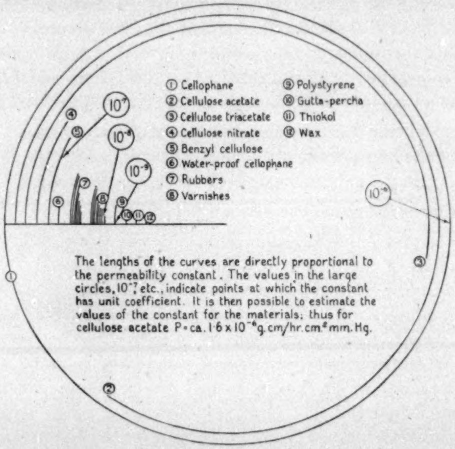

Figure 12. Moisture permeabilities of some non-porous insulating materials.

The values for the permeability constant are given in the units used throughout this report and under the following conditions whenever possible:—

25° c., 96% R.H., 0·005 cm. thickness.

Values at other temperatures, vapour pressure differences or thicknesses are to be found in the references quoted.

Table 17. Moisture permeability constants for varnishes as free films at 25° c., 96% R.H. and a thickness of 0·005 cm.

Material	$P\times10^8$ (g.cm./hr. cm^{2}mm.Hg)	Material	$P\times10^8$ (g.cm./hr. cm^{2}mm.Hg)
Nitrocellulose		*Synthetics*	
+alkyd resin (1)	0·4	Vinyl resin (1)	0·8
	3·0	Glycerol phthalate (4)	1·3
		,, ,, (5)	6·2
		,, ,, (4)	0·3
+alkyd resin+dibutyl phthalate (2)	4·0	Phenol formaldehyde resin (4)	1·2
		,, ,, ,, (6)	0·6
+alkyd resin+dibutyl phthalate+castor oil (2)	4·5	Alkyd resin (7)	7·2
+dammar (2)	2·5		
		Oil varnishes	
+dammar + dibutyl phthalate (2)	3·3	Ester gum (4)	0·9
		Tung oil+phenol resin (7)	2·1
+rosin-maleic acid+dibutyl phthalate (2)	1·1	,, ,, ,, (3)	4·2
		,, ,, ,, (6)	4·9
+ester gum+dibutyl phthalate (3)	1·7		
+diphenyl resin (1)	0·2	Tung oil+linseed oil+phenolic resin (5)	5·1
+vinyl resin (1)	6·0	Linseed oil+alkyd resin (3)	5·0
+phenolic resin (1)	0·9	Linseed oil+bitumen (6)	2·3
+dibutyl phthalate (2)	5·3	Orange shellac (7)	2·5

(1) Wray and Van Vorst, 1936.
(2) Wing, 1936.
(3) Lishmund and Siddle, 1941.
(4) Edwards and Wray, 1936.
(5) Kline, 1937.
(6) This paper, 1945.
(7) Payne, 1939.

REFERENCES

Abrams and Brabender, 1936. *J. Paper Trade,* TS.32, 102.
Badum, E. and Leilich, K., 1938. *Felten u. Guilleaume Rdsch.* **22,** 13.
Barrer, R. M., 1941. *Diffusion in and through Solids* (Cambridge: The University Press).
Carson, F. T., 1937. *Nat. Bur. Stand. Misc. Publication* M127.
Edwards, J. D. and Wray, R. I., 1936. *Ind. Eng. Chem.* **28,** 549.
Gettens, R. J., 1932. *Tech. Studies Field Fine Arts,* **1,** 63.
Gettens, R. J. and Bigelow, E., 1933. *Tech. Studies Field Fine Arts,* **2,** 15.
Irany, P., 1941. *Ind. Eng. Chem.* **33,** 1551.
Kline, G., 1937. *Bur. Stand. J. Res., Wash.,* **18,** 235.
Lishmund, R. E. and Siddle, F. J., 1941. *J. Oil Col. Chem.* **24,** 122.
Lowry, H. and Kohmann, G., 1927. *J. Phys. Chem.* **31,** 23.
Payne, H. F., 1939. *Ind. Eng. Chem.* (*Anal.*), **453,** 11.
Payne, H. F. and Gardner, W. H., 1937. *Ind. Eng. Chem.* **20,** 827.
Sager, T. P., 1934. *Bur. Stand. J. Res., Wash.,* **13,** 879.
Simril and Smith, 1942. *Ind. Eng. Chem.* **34,** 226.
Taylor, R. L., Hermann, D. B. and Kemp, A. R., 1936. *Ind. Eng. Chem.* **28,** 1255.
Wing, H. J., 1936. *Ind. Eng. Chem.* **28,** 788.
Wosnessensky, S. and Dubnikow, L. M., 1936. *Kolloid-Z.* **74,** 183.
Wray, R. I. and Van Vorst, A. R., 1936. *Ind. Eng. Chem.* **28,** 1268.

A SYSTEM OF TRANSFER COEFFICIENTS FOR USE IN THE DESIGN OF LENS SYSTEMS: I. THE GENERAL THEORY OF THE TRANSFER COEFFICIENTS

By F. D. CRUICKSHANK,
University of Tasmania

MS. received 25 *January* 1944 ; *in revised form* 26 *February* 1945

ABSTRACT. A detailed account is given of a series of differential transfer coefficients which specify the changes in the path of a ray in the final image-space resulting from small changes in surface curvature, refractive index and axial separation of successive surfaces, made within the system. Extending the method to the intersection points of the typical rays of a standard trigonometrical trace, transfer coefficients are derived which specify the rate of change of the tangential aberrations with curvature, refractive index and axial separation at each surface of the system. In particular, coefficients are developed which relate the chromatic aberrations in a very simple manner to the dispersions of the glasses of the system.

---

§1. INTRODUCTION

M'AULAY and CRUICKSHANK (1945) have described a simple means of specifying the change in the path of a ray through a lens system resulting from a small alteration made at some surface of the system. Using the original traced path of the ray as a reference frame, the new path is completely defined when the values of the differential quantities dp', dU' are known for the ray at each surface. Particular interest attaches to the values of these quantities at the last surface of the system, for from these the new path of the ray in the final image-space may be deduced. The basic problem is to relate the change in the path of the ray in the final image-space to the alteration within the system which produced it. A solution of this problem is presented in this paper in terms of a system of transfer coefficients, the values of which can be computed for any type of alteration made at any surface of the system. Once a system of transfer coefficients is established, the way is open for the development of designing methods of considerable power. In the paper referred to above, it is shown how the existence of the transfer coefficients leads to a systematic method of making the final correction of the aberrations of a lens system. In subsequent papers it will be shown how an analysis of the surface contributions to the aberrations of finite pencils may be made, and a direct method will be proposed for the estimation of the tolerances to be observed in the production of an optical system. The notation employed follows that of Conrady (1929).

§2. THE TRANSFER COEFFICIENTS FOR dU'-CHANGES AND dp-CHANGES

Suppose that the path of a selected ray has been traced trigonometrically through a system of k spherical refracting surfaces. After refraction at surface i of the system, the path of the ray is described by the quantities L_i', U_i'. Let a small change be made now at surface i such that the ray after refraction at the same incidence point on the surface takes the new direction specified by $U_i' + dU_i'$. The path of the ray through the remainder of the system will be different from the original traced path, and the ray will finally emerge from the last surface at a point displaced by some amount, dp_k', from the emergence point of the traced ray, and in a direction inclined at an angle, dU_k', to that of the traced ray. We may express these differential quantities, dp_k', dU_k', in terms of dU_i' by writing

$$dU_k' = \frac{\partial U_k'}{\partial U_i'} dU_i', \qquad \text{......(1)}$$

$$dp_k' = \frac{\partial p_k'}{\partial U_i'} dU_i'. \qquad \text{......(2)}$$

Similarly, if a small change made at surface i results only in an incidence point displacement, dp_i, the inclination angle, U_i, of the ray remaining unchanged, the ray will emerge from the last surface of the system at a point and in a direction specified by some other values, dp_k', dU_k', relative to the emergent traced ray. For these we may write

$$dp_k' = \frac{\partial p_k'}{\partial p_i} dp_i, \qquad \text{......(3)}$$

$$dU_k' = \frac{\partial U_k'}{\partial p_i} dp_i. \qquad \text{......(4)}$$

Equations (1) to (4) define the four *transfer coefficients*, $\partial p_k'/\partial U_i'$, etc., which can be calculated for a traced ray at each surface of the system. The method of calculation depends upon relations deduced in the next section. The transfer coefficients specify the effect of a dU'-change or a dp-change made at any surface on the path of the ray as it leaves the last surface of the system. These particular quantities are chosen as the fundamental transfer coefficients because any real change made in the course of an actual design can be described in terms of either a single dU'-change or a single dp-change.

§ 3. THE RELATION BETWEEN THE TRANSFER COEFFICIENTS AT SUCCESSIVE SURFACES OF THE SYSTEM

Denoting any two successive surfaces of the system by the subscripts i and j, we follow out the effect on the ray-path of a change dU_i' made at surface i. From

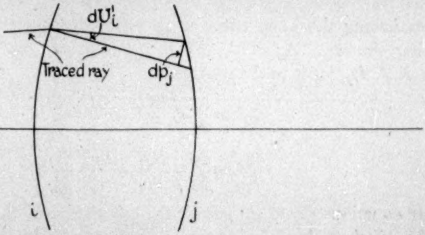

Figure 1.

figure 1 it is seen that, relative to the traced path, the ray will now meet surface j with an incidence-point displacement $dp_j = -D_i' dU_i' = D_j dU_i'$, and with an inclination angle change $dU_j = dU_i'$, where $D_j = -D_i'$ is the distance between the two surfaces measured along the traced ray. Further, the change dU_j alone would produce in turn a change $dU_j' = (\partial U_j'/\partial U_j) dU_i'$ in the direction of the ray after refraction at surface *j*. Hence, the change dU_i' at surface *i* is equivalent in effect to the change $dp_j = D_j\, dU_i'$, together with the change $dU_j' = (\partial U_j'/\partial U_j)\, dU_i'$, at surface *j*. Expressing the resulting dp_k', dU_k' in terms of each of these equivalent changes, we have

$$\frac{\partial U_k'}{\partial U_i'} dU_i' = dU_k' = \frac{\partial U_k'}{\partial U_j'} dU_j' + \frac{\partial U_k'}{\partial p_j} dp_j$$

$$= \frac{\partial U_k'}{\partial U_j'} \frac{\partial U_j'}{\partial U_j} dU_i' + \frac{\partial U_k'}{\partial p_j} D_j\, dU_i',$$

whence

$$\frac{\partial U_k'}{\partial U_i'} = \left(\frac{\partial U_k'}{\partial U_j'} \frac{\partial U_j'}{\partial U_j} + \frac{\partial U_k'}{\partial p_j} D_j\right), \qquad \ldots\ldots(5)$$

and similarly,

$$\frac{\partial p_k'}{\partial U_i'} = \left(\frac{\partial p_k'}{\partial U_j'} \frac{\partial U_j'}{\partial U_j} + \frac{\partial p_k'}{\partial p_j} D_j\right). \qquad \ldots\ldots(6)$$

Next we follow out the effect on the ray path of a small change of incidence point, dp_i, made at surface *i*. It is seen from figure 2 that relative to the traced path the ray will now leave surface *i* after refraction with a change in inclination angle $dU_i' = (\partial U_i'/\partial p_i)\, dp_i$ and with an incidence-point displacement

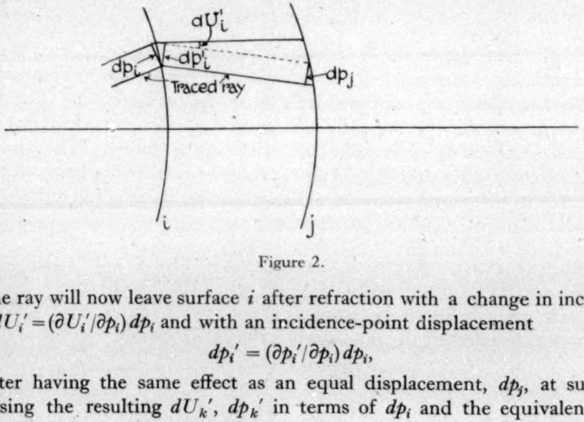

Figure 2.

$$dp_i' = (\partial p_i'/\partial p_i)\, dp_i,$$

the latter having the same effect as an equal displacement, dp_j, at surface *j*. Expressing the resulting dU_k', dp_k' in terms of dp_i and the equivalent set of changes dU_i', dp_j, leads to the relations

$$\frac{\partial U_k'}{\partial p_i} = \frac{\partial U_k'}{\partial U_i'} \frac{\partial U_i'}{\partial p_i} + \frac{\partial U_k'}{\partial p_j} \frac{\partial p_i'}{\partial p_i}, \qquad \ldots\ldots(7)$$

$$\frac{\partial p_k'}{\partial p_i} = \frac{\partial p_k'}{\partial U_i'} \frac{\partial U_i'}{\partial p_i} + \frac{\partial p_k'}{\partial p_j} \frac{\partial p_i'}{\partial p_i}. \qquad \ldots\ldots(8)$$

The four equations (5) to (8) permit the calculation of the transfer coefficients for surface *i* when those for surface *j* are known. At the last surface of the system it is obvious that the transfer coefficients have simple values, for

$$\frac{\partial U_k'}{\partial U_k'} = 1 \quad \text{and} \quad \frac{\partial p_k'}{\partial U_k'} = 0,$$

while $\partial U_k'/\partial p_k$ and $\partial p_k'/\partial p_k$ are calculated in the usual way (see M'Aulay and Cruickshank (1945), equations (2) and (8)). The transfer coefficients for the surface $(k-1)$ may now be obtained by equations (5) to (8), and so the computation may be continued surface by surface through the system until the first surface is reached. At each surface the computation involves four pairs of multiplications, there being a common factor in each pair, and four additions.

§4. THE RAY TRACE AND THE TRANSFER COEFFICIENTS FOR THE INTERSECTION POINTS

To investigate the spherical aberration of a system it is usual to trace three rays from an axial object point, the marginal, zonal and paraxial rays. These rays have intersection points with the principal axis in the final image space denoted respectively by M$(L_m', 0)$, Z$(L_z', 0)$, and Px$(l', 0)$, their positions being specified by rectangular coordinates relative to the pole of the last surface. For each oblique pencil traced for the extra-axial aberrations, three rays are selected, denoted by the symbols *a*, *pr* and *b* in the Conrady notation. Associated with these rays are the points Ab(L_{ab}', H_{ab}'), the intersection of the rays *a* and *b*; Pr(L_{ab}', H_{pr}'), the point at which the principal ray cuts the plane through Ab at right angles to the axis; Prf(l', H_{prf}'), the point at which the principal ray strikes the plane through the paraxial focus at right angles to the axis. In addition, we shall be concerned with the ideal image point, Id(l', H_{id}'), which shows where the principal ray would cut the paraxial image plane if the paraxial value of the magnification held throughout the field. If a change is made in the path of any of these typical rays at any surface of the system, the associated intersection point or points in the image space will be displaced. We now develop transfer coefficients to specify such changes.

The axial intersection points, M, Z and Px. We consider first the effect of the change, dU_i', on the position of the point M. Let us suppose that before the change is made in the ray path at surface *i* the marginal ray leaves the last surface of the system along the path PM, while after the change is made it follows the path P′M′ in figure 3. Relative to the traced ray PM, the displacement of

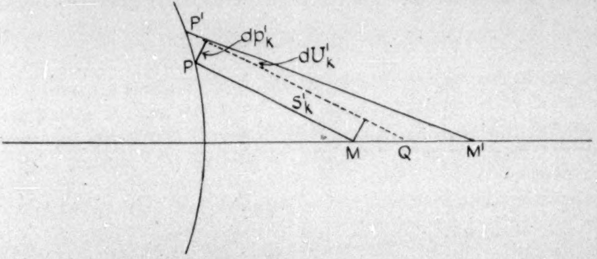

Figure 3.

the emergence point is $dp_k' = (\partial p_k'/\partial U_i')\,dU_i'$, and the change in direction is $dU_k' = (\partial U_k'/\partial U_i')dU_i'$, and each of these contributes to the shift of M. The effect of the displacement dp_k' alone would be to move the intersection point from M to Q, while the direction change dU_k' would, in addition, move it from Q to M′. For differential changes we have, to first order,

$$\mathrm{MQ} = dp_k' \operatorname{cosec} U'_{mk}, \qquad \mathrm{QM}' = -S'_{mk}\, dU_k' \operatorname{cosec} U'_{mk},$$

where S'_{mk} denotes the distance PM. Hence we have,

$$\frac{\partial L_m'}{\partial U_i'} dU_i' = \mathrm{MM}' = \left(\frac{\partial p_k'}{\partial U_i'} dU_i' - S_k' \frac{\partial U_k'}{\partial U_i'} dU_i'\right)_m \operatorname{cosec} U'_{mk},$$

whence

$$\frac{\partial L_m'}{\partial U_i'} = \left(\frac{\partial p_k'}{\partial U_i'} - S_k' \frac{\partial U_k'}{\partial U_i'}\right)_m \operatorname{cosec} U'_{mk}. \qquad \ldots\ldots(9)$$

Similarly, the consideration of the effect of a change, dp_i, leads to

$$\frac{\partial L_m'}{\partial p_i} = \left(\frac{\partial p_k'}{\partial p_i} - S_k' \frac{\partial U_k'}{\partial p_i}\right)_m \operatorname{cosec} U'_{mk}. \qquad \ldots\ldots(10)$$

It is convenient to introduce the symbol C as an abbreviation, its meaning being defined by

$$C(U_i') = \left(\frac{\partial p_k'}{\partial U_i'} - S_k' \frac{\partial U_k'}{\partial U_i'}\right), \qquad \ldots\ldots(11)$$

$$C(p_i) = \left(\frac{\partial p_k'}{\partial p_i} - S_k' \frac{\partial U_k'}{\partial p_i}\right). \qquad \ldots\ldots(12)$$

Quantities of this C-type enter characteristically into all expressions for the transfer coefficients for the intersection points, as we shall see presently. Actually, the C-quantity measures the rate of change of the intersection point with the variable concerned along a direction at right angles to the traced ray. Where it is necessary to distinguish the C-quantities of different rays we do so by writing the appropriate suffix, e.g. $C(p_i)_m$. Rewriting equations (9) and (10),

$$\frac{\partial L_m'}{\partial U_i'} = C(U_i')_m \operatorname{cosec} U'_{mk}, \qquad \ldots\ldots(13)$$

$$\frac{\partial L_m'}{\partial p'} = C(p_i)_m \operatorname{cosec} U'_{mk}. \qquad \ldots\ldots(14)$$

Corresponding expressions follow for the transfer coefficients for the zonal and paraxial intersection points Z and Px.

The intersection point Ab. For this point there are changes in two coordinates

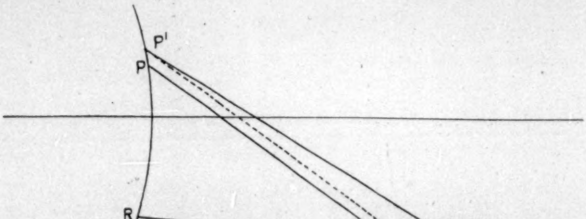

Figure 4.

to be considered. We begin by considering the effect of the change, dU'_{ai}, made in the path of the ray a at surface i. In figure 4, P Ab and R Ab represent the emergent traced paths of the rays a and b before any change is made. As a result of the change, dU'_{ai}, the ray a will now leave the last surface of the system along a new path P′Ab′, the point Ab′ being the new position of the intersection point. Relative to the emergent traced path, the new ray has an incidence-point displacement, $dp_k' = (\partial p_k'/\partial U_i')_a \,.\, dU'_{ai}$, and a direction change, $dU_k' = (\partial U_k'/\partial U_i')_a \,.\, dU'_{ai}$. For small changes we have, to first order,

$$\text{Ab Ab}' = \text{Ab Q} + \text{Q Ab}' = (dp_k' - S'_{ak} dU_k') \operatorname{cosec} (U_a' - U_b')_k.$$

Resolving this displacement along directions parallel to and perpendicular to the principal axis, and differentiating with respect to U'_{ai}, we obtain

$$\begin{aligned} \frac{\partial L'_{ab}}{\partial U'_{ai}} &= \left(\frac{\partial p_k'}{\partial U'_{ai}} - S'_{ak}\frac{\partial U_k'}{\partial U'_{ai}}\right) \operatorname{cosec} (U_a' - U_b')_k \cos U'_{bk} \\ &= C(U_i')_a \operatorname{cosec} (U_a' - U_b')_k \cos U'_{bk} \qquad \text{......(15)} \end{aligned}$$

and

$$\frac{\partial H'_{ab}}{\partial U'_{ai}} = - C(U_i')_a \operatorname{cosec} (U_a' - U_b')_k \sin U'_{bk}. \qquad \text{......(16)}$$

Similarly, a change, dp_{ai}, made in the path of ray a at surface i will lead to the expressions

$$\frac{\partial L'_{ab}}{\partial p_{ai}} = C(p_i)_a \operatorname{cosec} (U_a' - U_b')_k \cos U'_{bk}, \qquad \text{......(17)}$$

$$\frac{\partial H'_{ab}}{\partial p_{ai}} = - C(p_i)_a \operatorname{cosec} (U_a' - U_b')_k \sin U'_{bk}. \qquad \text{......(18)}$$

Turning now to the effects of changes dU'_{bi}, dp_{bi}, made in the path of the ray b at surface i, we can write down the final expressions for the transfer coefficients by inspection, a glance at figure 4 being sufficient to confirm the change of sign which occurs. Thus we have,

$$\frac{\partial L'_{ab}}{\partial U'_{bi}} = - C(U_i')_b \operatorname{cosec} (U_a' - U_b')_k \cos U'_{ak}, \qquad \text{......(19)}$$

$$\frac{\partial H'_{ab}}{\partial U'_{bi}} = C(U_i')_b \operatorname{cosec} (U_a' - U_b')_k \sin U'_{ak}, \qquad \text{......(20)}$$

$$\frac{\partial L'_{ab}}{\partial p_{bi}} = - C(p_i)_b \operatorname{cosec} (U_a' - U_b')_k \cos U'_{ak}, \qquad \text{......(21)}$$

$$\frac{\partial H'_{ab}}{\partial p_{bi}} = C(p_i)_b \operatorname{cosec} (U_a' - U_b')_k \sin U'_{ak}. \qquad \text{......(22)}$$

The intersection points Pr, Prf. In figure 5, the traced path of the principal ray after leaving the last surface of the system is represented by R Pr, and the corresponding path after a change dU_i' has been made at surface i is represented by R′ Pr′. Relative to the traced path, the new emergent ray has an incidence-point displacement, $dp_k' = (\partial p_k'/\partial U_i')\, dU_i'$, and a direction change, $dU_k' = (\partial U_k'/\partial U_i')\, dU_i'$. Following the general lines of the previous cases, we have

$$\text{Pr Pr}' = \text{Pr Q} + \text{Q Pr}' = (dp_k' - S'_{prk} dU_k') \sec U'_{prk},$$

from which it follows that

$$\begin{aligned} \frac{\partial H'_{pr}}{\partial U_i'} &= \left(\frac{\partial p_k'}{\partial U_i'} - S_k'\frac{\partial U_k'}{\partial U_i'}\right)_{pr} \sec U'_{prk} \\ &= C(U_i')_{pr} \sec U'_{prk}. \qquad \text{......(23)} \end{aligned}$$

The corresponding expression for small *dp*-changes will be

$$\frac{\partial H'_{pr}}{\partial p_i} = C(p_i)_{pr} \sec U'_{prk}. \qquad \text{......(24)}$$

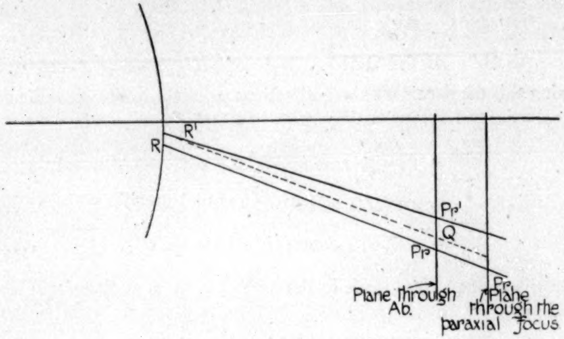

Figure 5.

The transfer coefficients for the point Prf with respect to the changes dU_i', dp_i made in the principal ray at surface *i* will obviously be,

$$\frac{\partial H'_{prf}}{\partial U_i'} = C(U_i')_{prf} \sec U'_{prk}, \qquad \text{......(25)}$$

$$\frac{\partial H'_{prf}}{\partial p_i} = C(p_i)_{prf} \sec U'_{prk}. \qquad \text{......(26)}$$

§ 5. THE INTERSECTION-POINT TRANSFER COEFFICIENTS FOR CHANGES OF CURVATURE, REFRACTIVE INDEX AND AXIAL SEPARATION

In the actual process of completing a design, the variables at the disposal of the designer are curvature, refractive index and the axial separation of successive surfaces. We now develop transfer coefficients for changes in these quantities.

Change of surface curvature. Suppose that a small curvature change, dc_i, is made at surface *i* of the system. To first order this leaves unchanged the incidence points of rays which strike the surface, and the total effect for any ray whose path has been traced through the original system is that after refraction the path of the ray will now be inclined to the traced path at an angle $dU_i' = (\partial U_i'/\partial c_i)\, dc_i$. Using the relations developed in the previous section, we can write down the new transfer coefficients at once.

For an axial ray, taking the marginal ray as typical, we have

$$\frac{\partial L_m'}{\partial c_i} = \frac{\partial L_m'}{\partial U_i'} \cdot \frac{\partial U_i'}{\partial c_i} = \frac{\partial U_i'}{\partial c_i} C(U_i')_m \operatorname{cosec} U'_{mk}$$

$$= C(c_i)_m \operatorname{cosec} U'_{mk}. \qquad \text{......(27)}$$

For the intersection point Ab it follows that since the *a* and *b* rays are affected by different amounts,

$$\frac{\partial L'_{ab}}{\partial c_i}dc_i = dL'_{ab} = (dL'_{ab})_a + (dL'_{ab})_b$$

$$= \frac{\partial L'_{ab}}{\partial U'_{ai}}\cdot\frac{\partial U'_{ai}}{\partial c_i}dc_i + \frac{\partial L'_{ab}}{\partial U'_{bi}}\cdot\frac{\partial U'_{bi}}{\partial c_i}dc_i,$$

which on combination with (15) and (19) gives

$$\frac{\partial L'_{ab}}{\partial c_i} = [C(c_i)_a \cos U'_{bk} - C(c_i)_b \cos U'_{ak}] \operatorname{cosec}(U_a' - U_b')_k, \quad \ldots\ldots(28)$$

while the corresponding expression for $\partial H'_{ab}/\partial c_i$ is

$$\frac{\partial H'_{ab}}{\partial c_i} = -[C(c_i)_a \sin U'_{bk} - C(c_i)_b \sin U'_{ak}] \operatorname{cosec}(U_a' - U_b')_k. \quad \ldots\ldots(29)$$

We note that the positions of the intersection points Pr, Prf will be affected both by the change in the path of the principal ray and by the shift along the axis of the plane through Ab or the plane through Px. Thus, for a small change dc_i, we have

$$dH'_{pr} = \frac{\partial H'_{pr}}{\partial U_i'}\frac{\partial U_i'}{\partial c_i}dc_i - \frac{\partial L'_{ab}}{\partial c_i}dc_i \tan U'_{prk},$$

whence

$$\frac{\partial H'_{pr}}{\partial c_i} = \frac{\partial H'_{pr}}{\partial U_i'}\frac{\partial U_i'}{\partial c_i} - \frac{\partial L'_{ab}}{\partial c_i}\tan U'_{prk}$$

$$= C(c_i)_{pr} \sec U'_{prk} - \frac{\partial L'_{ab}}{\partial c_i}\tan U'_{prk}, \quad \ldots\ldots(30)$$

while the corresponding expression for the point Prf is

$$\frac{\partial H'_{prf}}{\partial c_i} = C(c_i)_{prf} \sec U'_{prk} - \frac{\partial l'}{\partial c_i}\tan U'_{prk}. \quad \ldots\ldots(31)$$

Throughout these equations we have used the quantity $C(c_i)$ with the meaning defined by

$$C(c_i) = C(U_i')\frac{\partial U_i'}{\partial c_i}. \quad \ldots\ldots(32)$$

There remains only the ideal image point to consider. For an infinitely distant object point, for example, we have

$$H'_{id} = -f' \tan U_{pr} = -(y/u_k') \tan U_{pr},$$

whence

$$\frac{\partial H'_{id}}{\partial c_i} = (y/u_k'^2) \tan U_{pr}\frac{\partial u_k'}{\partial u_i'}\frac{\partial u_i'}{\partial c_i}. \quad \ldots\ldots(33)$$

The differential coefficients in (33) are those normally calculated for the paraxial ray, so that the point Id fits conveniently into the general scheme.

Changes in refractive index. If the relative refractive index, $n = N/N'$, is changed by an amount dn_i at surface *i*, the ray after refraction at this surface will undergo a direction change $dU_i' = (\partial U_i'/\partial n_i)dn_i$, relative to the traced ray path. The transfer coefficients for the intersection points with respect to *n*-changes may therefore be written down from the corresponding expressions for the curvature coefficients by replacing c everywhere by n. The C-quantity involved, $C(n_i)$, is given by

$$C(n_i) = C(U_i')\frac{\partial U_i'}{\partial n_i}. \qquad \ldots\ldots(34)$$

Changes in axial separation. The axial separation between the surfaces $(i-1)$ and i is specified by d_i. This quantity is essentially negative according to our sign convention, but it is more convenient than $d_i'{}_{-1}$ on account of the form of the final equations. In order to change the separation by an amount δd_i, we move the surface i and all succeeding surfaces through δd_i. Any ray incident on the surface i will meet the surface at a new incidence point after the change. Thus if the dotted arc in figure 6 represents the new position of the surface, the traced ray now meets the surface at a new incidence point given relative to the original by $dp_i = \sin U_i \, \delta d_i$. Hence the effect of a change in axial separation may be described in terms of incidence-point changes only. It follows that the expressions for the transfer coefficients for the intersection points with respect to d-changes can be obtained from those for the curvature changes by writing d everywhere in place of c. The C-quantity which occurs in these expressions is

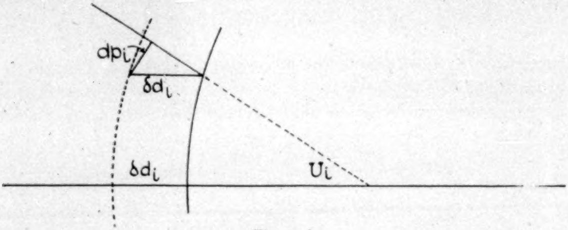

Figure 6.

$$C(d_i) = C(p_i)\frac{\partial p_i}{\partial d_i} = C(p_i)\sin U_i. \qquad \ldots\ldots(35)$$

§6. GLASS CHANGE FOR A COMPONENT OF A LENS SYSTEM

In treating the refractive index as one of the variables of the system we have derived transfer coefficients which measure the aberration changes per unit change of the relative refractive index at each surface. In practice, a change of glass affects the complete component and thus involves two surfaces. It is necessary to develop a transfer coefficient which takes account of the complete change.

Let us denote the successive components of the system by subscripts a, b, . . . h . . ., using subscript h for the general component. It will be sufficient to denote the first and second surfaces of this general component by subscripts 1 and 2. The refractive index of the component is N_h, while the refractive indices of the media preceding and following the component will be denoted by N_{h-1} and N_{h+1}. If the glass of the component is now changed, its new index being

$N_h + dN_h$, the change in the value of n at the first surface is

$$dn_1 = \frac{\partial}{\partial N_h}\left(\frac{N_{h-1}}{N_h}\right) dN_h = -\frac{N_{h-1}}{N_h^2} dN_h, \qquad \ldots\ldots(36)$$

while the change at the second surface is

$$dn_2 = \frac{\partial}{\partial N_h}\left(\frac{N_h}{N_{h+1}}\right) dN_h = dN_h / N_{h+1}. \qquad \ldots\ldots(37)$$

The monochromatic aberrations. Excluding the chromatic aberrations Lch' and Tch', which are treated separately, we can now write down the change in any aberration due to the glass change dN_h. Taking spherical aberration as typical, we have

$$dLA' = \frac{\partial LA'}{\partial N_h} dN_h = \frac{\partial LA'}{\partial n_1} dn_1 + \frac{\partial LA'}{\partial n_2} dn_2,$$

which, on combination with (36) and (37), gives

$$\frac{\partial LA'}{\partial N_h} = \frac{\partial LA'}{\partial n_2}\frac{1}{N_{h+1}} - \frac{\partial LA'}{\partial n_1}\frac{N_{h-1}}{N_h^2}, \qquad \ldots\ldots(38)$$

with corresponding expressions for the other aberrations.

The chromatic aberrations. It is usual to adjust the longitudinal chromatic aberration to zero for some zone of the system, often the 0·707 zone. Suppose that the system is to be achromatized for two colours r and v. We write down expressions for the final intersection lengths of rays of these colours, incident at the selected zone, in terms of the intersection length of a traced ray of an intermediate colour d. Using first-order terms only, we have,

$$L_r' = L_d' + \frac{\partial L_d'}{\partial N_a}(N_r - N_d)_a + \frac{\partial L_d'}{\partial N_b}(N_r - N_d)_b + \ldots,$$

the sum extending over all the components of the system. Similarly,

$$L_v' = L_d' + \frac{\partial L_d'}{\partial N_a}(N_v - N_d)_a + \frac{\partial L_d'}{\partial N_b}(N_v - N_d)_b + \ldots.$$

Hence $$L_r' - L_v' = -\frac{\partial L_d'}{\partial N_a}(N_v - N_r)_a - \frac{\partial L_d'}{\partial N_b}(N_v - N_r)_b - \ldots,$$

that is, $$Lch' = -\Sigma \frac{\partial L_d'}{\partial N_h} P_h, \qquad \ldots\ldots(39)$$

where P_h is the partial dispersion $(N_v - N_r)_h$. If we change some of the glasses of the system so that the glass constants are altered by small amounts, we have, to first order,

$$dLch' = -\Sigma \frac{\partial L_d'}{\partial N_h} dP_h, \qquad \ldots\ldots(40)$$

which means that the appropriate transfer coefficients for Lch' are of the type

$$\frac{\partial Lch'}{\partial P_h} = -\frac{\partial L_d'}{\partial N_h}. \qquad \ldots\ldots(41)$$

In a similar manner we can deduce a corresponding expression for the transverse chromatic aberration and appropriate transfer coefficients. A measure of the transverse chromatic aberration is provided by $H'_{prr} - H'_{prv}$, the intersection points concerned being those in which the principal rays for colours r and v cut a fixed plane perpendicular to the axis, which is either the paraxial image plane or the plane through Ab. Using the coefficients for the traced principal ray of intermediate colour d, we have

$$H'_{prv} = H'_{prd} + \left(\frac{\partial H'_{prd}}{\partial N_a}\right)_{L'} (N_v - N_d)_a + \left(\frac{\partial H'_{prd}}{\partial N_b}\right)_{L'} (N_v - N_d)_b + \ldots,$$

with a corresponding expression for H'_{prr}. The subscript L' indicates that the plane in which the intersection points occur remains fixed. Hence we have

$$H'_{prr} - H'_{prv} = -\left(\frac{\partial H'_{prd}}{\partial N_a}\right)_{L'} (N_v - N_r)_a - \left(\frac{\partial H'_{prd}}{\partial N_b}\right)_{L'} (N_v - N_r)_b - \ldots,$$

that is,

$$Tch' = -\Sigma\left(\frac{\partial H'_{prd}}{\partial N_h}\right)_{L'} P_h, \qquad \ldots\ldots(42)$$

whence, also,

$$\frac{\partial Tch'}{\partial P_h} = -\left(\frac{\partial H'_{prd}}{\partial N_h}\right)_{L'}. \qquad \ldots\ldots(43)$$

The expression for $\left(\frac{\partial H'_{prd}}{\partial N_h}\right)_{L'}$ follows fairly obviously from (30), (34), and (38). Equations (39) and (42) are of great value in practical designing. They provide a very rapid guide to glass changes which will improve the achromatism of the system, and permit an analysis of the distribution of the intersection lengths of rays of different colours without the labour of separate tracings. The order of accuracy is fairly high. As an example, the chromatic aberrations of a photographic lens of six components was calculated by (39) and (42), and checked by tracing, giving the following values:

	Lch_z'	lch	Tch'
From eqns. (39), (42)	0·429	0·393	0·00516
From trace	0·440	0·387	0·0059

the differences being insignificant when the uncertainty of the last figure in the five-figure trace is considered.

§7. THE TRANSFER COEFFICIENTS FOR SMALL CHANGES OF THE DIAPHRAGM POSITION

If the procedure developed for the alteration of the axial separation of successive surfaces is applied at the first surface of the system, there is no alteration in the spacings of the surfaces of the system. It remains, then, to interpret the meaning of the values of the transfer coefficients for d-changes which are obtained by the formal application of our equations at the first surface. Thinking of the incident traced rays in the space to the left of the first surface as fixed, a shift of the first surface will result in incidence-point changes for all rays except those incident parallel to the principal axis. In particular, the original principal ray of an oblique pencil will strike the first surface at a new incidence point, and will no longer pass through the centre of the diaphragm, but will intersect the principal axis at some neighbouring point. If the diaphragm is shifted so that its centre coincides with this point, the ray in its new course will be a principal ray for this new diaphragm position. The surface shift, made in the manner considered, is therefore equivalent to a change in the position of the diaphragm. The transfer coefficients associated with the surface shift must therefore give information as to the effect of the shift of the diaphragm on the aberrations.

Suppose that the diaphragm is placed between the surfaces i and $(i+1)$ of the system, its axial distance from the pole of the first surface being L'_{pr}. The principal ray in a pencil of the original trace is aimed at the centre of the entrance pupil, O, distant L_{pr} from the pole of the first surface, and passes through O′, the centre of the diaphragm. If the point O is shifted a distance dL_{pr} the point O′ will be displaced through dL'_{pr}, and the ratio of these two displacements is the longitudinal magnification. As an approximation let us assume that the longitudinal magnification is equal to the square of the lateral magnification, as in paraxial theory, and we may write

$$\frac{dL'_{pr}}{dL_{pr}} = M'^2 = \frac{\sin^2 U_{pr}}{\sin^2 U'_{pri}}. \qquad \ldots\ldots(44)$$

A shift of the first surface, carried out in the manner prescribed, is equivalent to an equal shift of the entrance pupil. Hence, for any aberration A,

$$\frac{\partial A}{\partial L'_{pr}} = \frac{\partial A}{\partial d_1} \cdot \frac{\partial L_{pr}}{\partial L'_{pr}} = \frac{\partial A}{\partial d_1} \frac{\sin^2 U'_{pri}}{\sin^2 U_{pr}}, \qquad \ldots\ldots(45)$$

giving a series of transfer coefficients for small displacements of the diaphragm.

Another useful feature incidental to the transfer coefficients of the principal ray at the first surface of the system is that the t-focus is readily available from them, thus eliminating the necessity of a trace for close tangential rays. If a small dp-change is made for the principal ray at the first surface, the resulting dp_k' and dU_k' specify the emergence point and direction of a ray close to the principal ray as it leaves the last surface of the system. It is immediately obvious that the intersection of this ray with the principal ray gives the t-focus, that is,

$$t_k' = \frac{\partial p_k' / \partial p_1}{\partial U_k' / \partial p_1}. \qquad \ldots\ldots(45\,a)$$

REFERENCES

Conrady, 1929. *Applied Optics and Optical Design* (Oxford : Clarendon Press).
M'Aulay and Cruickshank, 1945. *Proc. Phys. Soc.* **57,** 302.

A SYSTEM OF TRANSFER COEFFICIENTS FOR USE IN THE DESIGN OF LENS SYSTEMS: II. A SECOND-ORDER CORRECTION TERM

By F. D. CRUICKSHANK,

University of Tasmania

MS. received 25 *January* 1944; *in revised form* 26 *February* 1945

ABSTRACT. Expressions are derived for a second-order correction term for the differential transfer coefficients developed in Part I. Need for the correction term arises on account of the neglect of the effect of the small change in the direction of the emergent ray during the calculation of the transfer coefficients for the intersection points in the final image-space. The correction term is used when the effects of changes in the system beyond differential size are required with increased accuracy. For single changes of this kind in a system, the correction term frequently improves the accuracy from the order of 7 to 10 per cent to less than one per cent. The necessary modifications are given for the case in which a series of changes are made simultaneously within the system.

---

§ 1. INTRODUCTION

In the account of the transfer coefficients given in Part I we have considered only terms of first order, a procedure which is adequate for general designing needs as long as small changes only are made in the system. In the course of correcting a system it is frequently necessary to make curvature changes of the order of 0·001 mm.$^{-1}$, and thickness changes of the order of one millimetre. When such changes are made, especially in systems of large aperture, it is found that the shifts of the various intersection points in the final image space as predicted by the transfer coefficients may be in error by as much as twelve per cent. There is one second-order term associated with the final stage of the calculation of the transfer coefficients, the use of which will improve considerably the order of accuracy of such changes. It arises from the neglect of the effect of the small change, dU_k', in the final direction of the emergent ray, on the computation of the transfer coefficients for the intersection points from the corresponding C-quantities. It would seem that the wider problem of second-order terms affecting the fundamental transfer coefficients is such that the amount of computation involved is incommensurate with the results obtained therefrom.

§ 2. THE CORRECTION TERM FOR SINGLE CHANGES MADE WITHIN THE SYSTEM

In figure 7 we represent by R_1M a traced ray in the final image space which intersects the optical axis of the system at M. As a result of a change made within the system, let us say a curvature change, dc_i, at surface i, the emergent ray now follows the path R_2M'. The lines MP and MQ are drawn perpendicular to R_1M and R_2M' respectively. Then

$$\begin{aligned} \mathrm{MP} &= dp_k' - S_k' dU_k' = C(c_i)dc_i, \\ \mathrm{MQ} &= \mathrm{MP}\cos dU_k', \\ \mathrm{MM'} &= \mathrm{MQ}\,\mathrm{cosec}\,(U_k' + dU_k') \\ &= C(c_i)dc_i \cos dU_k' \left[\mathrm{cosec}\ U_k' + \frac{\partial}{\partial U_k'}(\mathrm{cosec}\ U_k')dU_k'\right]. \end{aligned}$$

It would be most unusual for dU_k' to be greater than about 2°, so that we may safely put its cosine $=1$. Writing $\mathrm{MM}'=\delta L_k'$, we have

$$\delta L_k' = C(c_i)dc_i \operatorname{cosec} U_k'(1-\cot U_k'\, dU_k') \qquad \ldots\ldots(46)$$

$$= C(c_i) \operatorname{cosec} U_k'\, dc_i - C(c_i) \operatorname{cosec} U_k' \cot U_k' \frac{\partial U_k'}{\partial c_i}(dc_i)^2. \qquad \ldots\ldots(47)$$

The first term on the right-hand side of (47) is the first-order term which we have used all along, while the second term now appears as a correction to be added to it. We write this correction term as $\lambda'(c_i)(dc_i)^2$, where

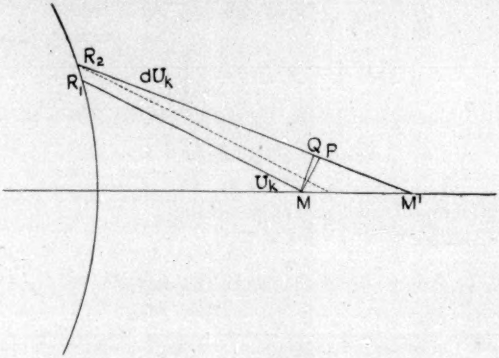

Figure 7.

$$\lambda'(c_i) = -C(c_i) \operatorname{cosec} U_k' \cot U_k' \frac{\partial U_k'}{\partial c_i}. \qquad \ldots\ldots(48)$$

In the next place we consider the intersection of a ray in the final image space with a fixed plane at right angles to the optical axis. Proceeding in a manner similar to the foregoing, it is easily seen that the change in the H'-coordinate of the intersection point is given by

$$\delta H_k' = C(c_i)dc_i \cos dU_k' \sec (U_k' + dU_k')$$

$$= C(c_i)dc_i \sec U_k'(1+\tan U_k'\, dU_k') \qquad \ldots\ldots(49)$$

$$= C(c_i) \sec U_k'\, dc_i + C(c_i) \sec U_k' \tan U_k' \frac{\partial U_k'}{\partial c_i}(dc_i)^2. \qquad \ldots\ldots(50)$$

The first term on the right-hand side of (50) is the usual first-order term, while the second is the correction term to be applied where greater accuracy is desired. Writing this in the form $\nu'(c_i)(dc_i)^2$, we have

$$\nu'(c_i) = C(c_i) \sec U_k' \tan U_k \frac{\partial U_k'}{\partial c_i}. \qquad \ldots\ldots(51)$$

There remains one further important case to consider, that in which the ray intersects a plane at right angles to the axis of the system, the plane being no longer fixed, but changing its position when an alteration is made within the system. Having in mind the use to be made in subsequent work of intersections of rays with the paraxial image plane, we will consider this case in detail. By analogy with equation (31), Part I, it follows that for any ray intersecting the paraxial image-plane

$$\frac{\partial H_k'}{\partial c_i}=C(c_i)\sec U_k'-\frac{\partial l_k'}{\partial c_i}\tan U_k'.$$

Extending this expression to take account of the effect of the change in U_k', it is fairly obvious that for the change in the H'-coordinate of the intersection point resulting from the curvature change, dc_i, we shall have

$$\begin{aligned}\delta H_k'&=C(c_i)dc_i\sec(U_k'+dU_k')\\&\quad-\left[\frac{\partial l_k'}{\partial c_i}dc_i+\lambda_0'(c_i)(dc_i)^2\right]\tan(U_k'+dU_k'),\end{aligned}\qquad\ldots\ldots(52)$$

where $\lambda_0'(c_i)$ is the λ' correction term for the paraxial ray, which, by analogy with (48), is seen to be

$$\lambda_0'(c_i)=-\frac{\partial l_k'}{\partial c_i}\frac{1}{u_k'}\frac{\partial u_k'}{\partial c_i}.\qquad\ldots\ldots(53)$$

Developing the terms of equation (52), we obtain

$$\begin{aligned}\delta H_k'&=C(c_i)dc_i\sec U_k'(1+\tan U_k'dU_k')\\&\quad-\left[\frac{\partial l_k'}{\partial c_i}dc_i+\lambda_0'(c_i)(dc_i)^2\right]\tan U_k'(1+\operatorname{cosec}U_k'\sec U_k'\,dU_k')\end{aligned}\qquad\ldots\ldots(54)$$

Multiplying out the bracketed expressions and neglecting the third-order term which occurs, we obtain

$$\delta H_k'=\text{first-order terms}+[\nu'(c_i)+\gamma'(c_i)+\rho'(c_i)](dc_i)^2$$

where we have written

$$\gamma'(c_i)=-\frac{\partial l_k'}{\partial c_i}\tan U_k'\operatorname{cosec}U_k'\sec U_k'\frac{\partial U_k'}{\partial c_i}\qquad\ldots\ldots(55)$$

and

$$\begin{aligned}\rho'(c_i)&=-\lambda_0'(c_i)\tan U_k'\\&=\frac{\partial l_k'}{\partial c_i}\tan U_k'\frac{1}{u_k'}\frac{\partial u_k'}{\partial c_i}.\end{aligned}\qquad\ldots\ldots(56)$$

We may now write the correction term which is to be applied for intersection points in the paraxial image-plane as $\mu'(c_i)\,(dc_i)^2$, where

$$\mu'(c_i)=\nu'(c_i)+\gamma'(c_i)+\rho'(c_i).\qquad\ldots\ldots(57)$$

In spite of the apparent complexity of these expressions, they are computed very easily on account of the fact that portions of each term have already been evaluated at an earlier stage in the general computation. Some examples taken at random from a computation are set out below, the system being an f/1·5 camera lens of focal length 106·5 mm. comprising ten surfaces. These examples will afford some idea of the effect of the use of the correction terms for single changes made within the system.

Example 1. The extreme marginal ray of the axial pencil of this lens had the following coefficients for curvature changes at the first surface:

$$\frac{\partial L_k'}{\partial c_1}=-9913{\cdot}0,\qquad\lambda'(c_1)=878530.$$

On making a change of curvature at the first surface of amount 0·001 mm.$^{-1}$, the radius thereby changing from +72·84 mm. to +67·89 mm., the following results are obtained:

Expected change in L_k' using first-order coefficient $= -9{\cdot}913$ mm.
Expected change corrected by second-order term $= -9{\cdot}034$ mm.
Change as calculated by trace $= -8{\cdot}838$ mm.

The use of the correction term in this case reduces the error of the predicted change from 12·16 per cent to 2·22 per cent.

Example 2. A paraxial ray traced through the same lens had the following coefficients at the first surface:

$$\frac{\partial l_k'}{\partial c_1} = -7447{\cdot}2, \qquad \lambda_0'(c_1) = 446350.$$

For the same change in curvature at the first surface we find:

Expected change in l_k' by first-order coefficient $= -7{\cdot}447$ mm.
Expected change, corrected $= -7{\cdot}001$ mm.
Change as given by trace $= -7{\cdot}031$ mm.

In this case the use of the correction term reduces the error of the predicted change from 6·35 per cent to 0·43 per cent.

Example 3. The principal ray of an oblique pencil incident on the same system at an angle of 17° to the principal axis had the following coefficients:

$$\frac{\partial H_k'}{\partial c_1} = 1764{\cdot}8, \qquad \mu'(c_1) = -117550.$$

For the same curvature change made at the first surface of the system we have:

Expected change in H_k' by first-order coefficient $= 1{\cdot}765$ mm.
Expected change, corrected $= 1{\cdot}647$ mm.
Change as calculated by trace $= 1{\cdot}637$ mm.

The error in the prediction is thus reduced from 7·82 to 0·61 per cent.

§ 3. THE CORRECTION TERM FOR SEVERAL SIMULTANEOUS CHANGES

In the course of an actual design it is usual to make several changes in the system at the same time and then to check the result either in full or in part by a new trace of the system. If the changes are such that a considerable alteration has been made in the positions of the intersection points, it will generally be desirable to use the dU_k' correction term to improve the accuracy of the expected changes. In order to do this we must alter the form of the expressions for these correction terms. In applying the first-order theory to several changes made simultaneously, we treat the change in position of an intersection point as a total differential. Thus, suppose that changes are made in the curvatures of surfaces $i, j, \dots r$, then for an intersection point on the principal axis

$$\begin{aligned} dL_k' &= \frac{\partial L_k'}{\partial c_i}\,dc_i + \frac{\partial L_k'}{\partial c_j}\,dc_j + \dots + \frac{\partial L_k'}{\partial c_r}\,dc_r \\ &= \sum_i^r \left(\frac{\partial p_k'}{\partial c_i} - S_k'\frac{\partial U_k'}{\partial c_i}\right) \operatorname{cosec} U_k'\,dc_i \\ &= (\Sigma dp_k' - S_k'\Sigma dU_k') \operatorname{cosec} U_k'. \qquad \dots\dots(58) \end{aligned}$$

The summation of the effects of the several differential changes is to be made, therefore, at the last surface of the system, so that the ray under consideration will emerge from the last surface with an incidence-point displacement, $\Sigma dp_k'$, and a direction change, $\Sigma dU_k'$, relative to the original traced path. For changes that are not differential in size we still obtain a useful tool for design by assuming that the summation property holds, and the order of accuracy can be improved by applying the correction term. The value of the small angle-change, dU_k', for which the correction is made, is of course the sum of the various dU_k' due to the several changes. The correction terms must therefore be written as factors which multiply the resultant angle change, $\Sigma dU_k'$, and not as factors multiplying $(dc_i)^2$, etc., as in the previous section. Anticipating the needs of subsequent methods, we consider the two main cases, the intersection point of the paraxial ray with the principal axis and the intersection point of any ray with the paraxial image-plane.

In the former case it is easily seen that by analogy with equation (46)

$$\begin{aligned}\delta l_k' &= \Sigma \frac{\partial l_k'}{\partial c_i} dc_i\Big(1 - \frac{1}{u_k'}\Sigma du_k'\Big)\\ &= \Sigma_i \frac{\partial l_k'}{\partial c_i} dc_i - \left(\Sigma \frac{\partial l_k'}{\partial c_i}\frac{1}{u_k'}\, dc_i\right)(\Sigma du_k'). \qquad \ldots\ldots(59)\end{aligned}$$

Hence the correction term to be applied for the paraxial intersection point is $(\Sigma\lambda_0(c_i)dc_i)(\Sigma du_k')$, where

$$\lambda_0(c_i) = -\frac{\partial l_k'}{\partial c}\,\frac{1}{u_k'} \qquad \ldots\ldots(60)$$

and

$$\Sigma du_k' = \Sigma \frac{\partial u_k'}{\partial c_i} dc_i. \qquad \ldots\ldots(61)$$

In the case of the intersection of any ray with the paraxial image-plane we have by analogy with equation (52)

$$\begin{aligned}\delta H_k' &= [\Sigma C(c_i)\, dc_i] \sec\,(U_k' + \Sigma dU_k')\\ &\quad - \left[\Sigma \frac{\partial l_k'}{\partial c_i} dc_i + \Sigma\lambda_0(c_i)\, dc_i\, \Sigma du_k'\right] \tan\,(U_k' + \Sigma dU_k')\\ &= \Sigma\left[C(c_i) \sec U_k' - \frac{\partial l_k'}{\partial c_i} \tan U_k'\right] dc_i\\ &\quad + \Sigma C(c_i) \sec U_k'\, dc_i \tan U_k' \,.\, \Sigma dU_k'\\ &\quad - \Sigma \frac{\partial l_k'}{\partial c_i} \tan U_k'\, dc_i \operatorname{cosec} U_k' \sec U_k' \,.\, \Sigma dU_k'\\ &\quad + \Sigma \frac{\partial l_k'}{\partial c_i} \tan U_k'\, dc_i \frac{1}{u_k'} \,.\, \Sigma du_k'\\ &= \text{first-order term} + \Sigma\nu(c_i)dc_i \,.\, \Sigma dU_k'\\ &\qquad\qquad + \Sigma\gamma(c_i)dc_i \,.\, \Sigma dU_k' + \Sigma\rho(c_i)dc_i \,.\, \Sigma du_k', \qquad \ldots\ldots(62)\end{aligned}$$

where

$$\nu(c_i) = C(c_i) \sec U_k' \tan U_k', \qquad \ldots\ldots(63)$$

$$\gamma(c_i) = -\frac{\partial l_k'}{\partial c_i} \tan U_k' \sec U_k' \operatorname{cosec} U_k', \qquad \ldots\ldots(64)$$

$$\rho(c_i) = \frac{\partial l_k'}{\partial c_i} \tan U_k' \frac{1}{u_k'}. \qquad \ldots\ldots(65)$$

Combining the first two of these terms by writing

$$\pi(c_i) = \nu(c_i) + \gamma(c_i), \qquad \ldots\ldots(66)$$

the correction term becomes

$$\Sigma\pi(c_i)dc_i \,.\, \Sigma dU_k' + \Sigma\rho(c_i)dc_i \,.\, \Sigma du_k'.$$

It will have been noted that the quantities corresponding to $\nu(c_i)$, $\gamma(c_i)$, $\rho(c_i)$ and $\lambda(c_i)$ used in the first section are distinguished from those of the present section by the addition of a dash. This serves to remind the computor that they relate to single changes only. It is to be stressed that the correction term for a series of changes is only of use when there is a considerable change of the intersection points in the image space. During the correction of a design it is not unusual to make up to eight or ten changes, the total result of which may be to displace the intersection points in general through quite small distances, although the small relative shifts of these points may alter the aberrations considerably. However, when the result of the series of changes shifts the intersection points through distances of the order of 10% of the focal length of the system, the effect of the correction term is worth while.

We have not considered the correction terms for changes of thickness or refractive index, as these may be written down by analogy with the curvature expressions.

REVIEWS OF BOOKS

The Measurement of Colour, by W. D. Wright. Pp. vii + 223. (London: Adam Hilger, Ltd., 1944.) 30*s*.

The main theme of this book is the trichromatic system of specifying colours, and the exposition of the principal facts and formulae of the system occupies about one-fifth of the whole. The emission, reflection and transmission of radiation and the response of the eye to light are dealt with in introductory chapters. The rest of the book is devoted to the practical methods of colorimetry and spectrophotometry, both visual and photo-electric, and to applications of colour measurement in industry, agriculture, medicine, etc.

Dr. Wright writes with authority in this field, and of the soundness of the treatment it need only be said that it is as expected. Great pains are taken to make the subject intelligible to those who are not familiar with linear transformation theory, projective and differential geometry, and the basic ideas are well illustrated by analogies and coloured diagrams. The result is an excellent elementary presentation of trichromatic colorimetry. Of the few points which may be criticized, the first is the author's discussion of the use of the visibility curve in fixing the distribution coefficients of the colorimetric observer. This was an expedient imposed by the fact that in neither of the fundamental determinations of the mixture data were measurements made of the energy in the spectrum. Wright's treatment here is a little confusing, as he links this unfortunate gap in our knowledge with the difficulty of designing a colorimeter incorporating the reference stimuli as instrumental stimuli. But had such a colorimeter been used and no energy measurements made, the visibility curve would still have been required, and conversely with the energy measurements made, the visibility curve could have been dispensed with, whatever the instrument stimuli. While variations of the colour matches of different observers are stressed in several places, no indication of their magnitude is given. A plot of the mixture curves through the spectrum for a group of observers and Wright's diagram showing how differences in retinal pigmentation scatter the "white points" in a chromaticity chart based on spectral primaries might have been included with advantage. In the chapter on colour atlases a brief explanation of the Oswald system, similar to the excellent summary of the Munsell system, would have been welcome.

Admirable features are the concise explanation of the principles underlying the many measuring instruments used in colour work, and the clear statement in simple language of colour problems in the dyeing and paint industries, in colour reproduction and in photo-elasticity. The book should be of particular value to those newly entering this field of work, while all concerned with colour questions will find it interesting reading. It is a pity the price is so high. W. S. S.

Tables of Elementary Functions, by F. Emde. Pp. xii + 181. (Leipzig: Teubner, 1940; photographic reprint published under licence by J. W. Edwards, Ann Arbor, Mich., U.S.A., 1945.) $3.20.

Most physicists will be familiar with "Jahnke und Emde"; many will remember that the third (1938) edition omitted the material of the first 76 pages of the second (1933) edition, and that an extended set of tables of the "elementary" functions was promised. The volume appeared in Germany in 1940, and this reprint makes it generally available.

We have the familiar mixture of letterpress and formulae, numerical tables and diagrams. The above-mentioned material has all been incorporated, but a larger page has been used, and all the numerical tables have been reset, using the "heads and tails" numerals, which make them so much easier to read. Four-figure accuracy is standard, and the tabular intervals are generally so chosen that it is attainable by linear interpolation (for which a slide-rule is advocated). Divided differences are given, and in some ranges where linear interpolation is not adequate they are printed in italics. Text and legends are in both German and English.

Space permits the mention of only the more important additions. We have x^2 and $1/x$, x^3 and $1/x^2$, and square and cube roots, in the section on powers. 100 multiples of

$M(=\log_{10} e)$, $1/M$, $\pi/2$ and $2/\pi$ are given to six decimals, and 10 multiples to 16 decimals. A factor table includes all composite odd numbers less than 10,000 not divisible by 3 or 5. There is a section, with numerical tables, on quadratic equations—in which a diagram similar to figure 11 for the cubic might with advantage have been included—and a long account of the quartic, with diagrams but no significant numerical material.

Probably the most important addition is the set of tables of circular, exponential, and hyperbolic functions. Sine, cosine, tangent and cotangent are given for angles in degrees. A comprehensive set of tables of the direct and inverse functions, in natural (radian) measure, is given. There is also a set of tables of the direct functions in terms of the quadrant as a unit, i.e., the circular, exponential and hyperbolic functions of the argument $\pi x/2$. There are also tables of a few functions such as $1-\cos x$, $\cosh x-1$, $\sqrt{2}\sin x$, $\sqrt{2}\cos x$.

Some special functions such as e^{-x^2}, $\coth x-1/x$, $\tan(x\sqrt{i})/x\sqrt{i}$ (pertinent to skin effect), and some Chebyshev polynomials, are included. A section near the end gives the coefficients in powers and roots of polynomials (truncated series). There is also a very useful few pages of advice on computing, and a bibliography.

The book will be of great use to that body of engineers and physicists who have frequent dealings with the " elementary " functions, but only rarely need the " higher " ones. The compiler of such a book is obviously dependent, in the main, upon extant computations, so that scrappiness and unevenness are inevitable. Much of the apparent disorder of the arrangement is due to the idiosyncrasies of the individual functions tabulated. The important thing is that the information is in the book, and that with the help of a detailed list of contents and a comprehensive index it is not difficult to find. W. G. B.

The Velocity of Light, by N. Ernest Dorsey. Pp. 110. (Trans. Amer. Phil. Soc. vol. xxiv, part 1, 1944.) $2.25.

If a list of physical quantities were made in the order of the time and attention devoted to their measurement, most physicists would place the velocity of light very high in that list. It will come as something of a shock to learn that many of these " standard " investigations leave a great deal to be desired in view of the accuracy claimed.

The author examines, in detail, the investigations, using the toothed wheel (Fizeau, Cornu, Perrotin-Prim), the rotating mirror (Foucault, Newcomb, Michelson, Michelson-Pearse-Pearson) and the Kerr-cell methods (Karolus-Mittelstaedt, Anderson, Hüttel). Particular care is devoted to the consideration of possible systematic errors, to the evidence of a search for systematic errors on the part of the investigators, and to the standard of the reporting of all relevant data. The author's conclusions are summarized in the following table, taken from the paper.

Summary of values for the velocity of light in a vacuum
(unit of $V=1$ megameter/second in vacuum)

Observer and date	Range for V	Centre V	Remarks
Cornu 1872	296·5–300·5	298·5	Preliminary
Cornu 1876	299·3–300·5	299·9	Uncertain
Perrotin and Prim 1908	299–301	300	Systematic error
Newcomb 1880–82	299·71–299·86	299·78	Systematic error
Michelson 1878	297–304	300	Preliminary
Michelson 1879	299·7–300·1	299·9	Systematic error
Michelson 1882	299·6–300·1	299·85	Systematic error
Michelson 1924	299·73–299·87	299·80	Report deficient
Michelson 1927	$299{\cdot}77_8$–$299{\cdot}81_8$	$299{\cdot}79_8$	Report deficient
Michelson, Pearse, Pearson 1935	$299{\cdot}76_4$–$299{\cdot}78_4$	$299{\cdot}77_4$	Little study of apparatus
Karolus and Mittelstaedt 1929	$299{\cdot}75_8$–$299{\cdot}79_8$	$299{\cdot}77_8$	Apparatus studied
Anderson 1937	$299{\cdot}75_6$–$299{\cdot}78_6$	$299{\cdot}77_1$	Apparatus studied
Anderson 1941	$299{\cdot}76_2$–$299{\cdot}79_0$	$299{\cdot}77_6$	Apparatus studied
Hüttel 1940	$299{\cdot}75_8$–$299{\cdot}77_8$	$299{\cdot}76_8$	Apparatus studied

The last five of these determinations are alone considered to have other than historical interest. The best value for the velocity of light is given as $299{,}77_3$ km./sec. in a vacuum, with a dubiety of ±10 km./sec. The possibility of a secular variation in the velocity of light is dealt with briefly, with the conclusion that the data give no indication of any variation.

The report forms a valuable study in critical examination ; it also contains a statement of the standard to which an accurate experimental investigation and its reporting ought to conform, which should be read once a year by every physicist for the good of his soul.

M. B.

School Physics, Part II, by T. M. YARWOOD. Pp. x+438. (London: Macmillan and Co., Ltd., 1945.) 7*s*. 6*d*. net.

To appraise the value of this School Physics, Part II, it is necessary to study it concurrently with Part I, since both books cover the same ground and form, as stated in the preface, " a four-year concentric school course in Physics whereby a certain amount of work in all branches of Physics is done in each year ". Thus the Section headings, with the exception of an additional one on *Molecular Forces* in Part II, are identical for both volumes. The author is concerned to apply physical principles to everyday life, and he includes numerous references to modern appliances. Especially is he anxious to encourage the future citizen to become more air-minded. The book makes interesting reading with its good and simple diagrams and its generally clear explanations of working principles. It is carefully produced, though the reader of p. 259 might conclude that the overtones of most vibrating systems, including bells, were harmonic.

The subject-matter includes those portions of physics which may best be studied at school by the average pupil, so that this publication, at a time when school, scholarship and university syllabuses are in the melting pot, is very welcome. For effective teaching, the book would need to be supplemented by a historical and biographical background.

M. D. W.

Sechsstellige trigonometrische Tafeln, by H. BRANDENBURG. Pp. xxiv+304 (Leipzig: Lorentz, 1932; photographic reprint published under licence by J. W. Edwards, Ann Arbor, Mich., U.S.A., 1945.) **$5.00.**

This is a reprint of a well-known table. It gives the sine, tangent, cotangent and cosine, for angles in a quadrant at interval 10 seconds, to six decimals (except for tangent and cotangent for a few degrees), with differences and proportional parts (pp. 30–299). Preliminary tables give the cotangent, for every second up to 3°, to at least seven figures (pp. 2–24), and sines and tangents, at interval 10 seconds up to 1°, to seven decimals (pp. 26–28). At the end are given the values of $n!$, $1/n!$, $(\pi/2)^n$ and $(\pi/2)^n/n!$ for $n=0(1)20$ (p. 300), tables for converting sidereal into mean solar time and vice versa (pp. 302–3), and for converting angles into time (p. 304).

The preface is given in seven languages.

Some errata (supplied by Dr. L. J. Comrie) are printed on p. iv. W. G. B.

CORRIGENDA

Page 231. The legend " Colours of sunlight and daylight " appearing under figure 5 should be transferred to p. 235, under figure 9.

Page 233. The point in figure 7 marked " SB(2) 20% Tm 24·1 " should be marked " SB(2) 20° c. Tm 24·1 ".